DEVELOPMENT AND APPLICATION OF "RESISTIVE PULSE SPECTROSCOPY"; STUDIES ON THE SIZE, FORM AND DEFORMABILITY OF RED BLOOD CELLS

James P. Yee
(Ph. D. thesis)

January 1979

DEVELOPMENT AND APPLICATION OF
"RESISTIVE PULSE SPECTROSCOPY"; STUDIES
ON THE SIZE, FORM AND DEFORMABILITY OF RED BLOOD CELLS

by

James P. Yee

Lawrence Berkeley Laboratory
University of California
Berkeley, California 94720

DEVELOPMENT AND APPLICATION OF "RESISTIVE PULSE SPECTROSCOPY";
STUDIES ON THE SIZE, FORM AND DEFORMABILITY OF RED BLOOD CELLS

JAMES P. YEE

ABSTRACT

"Resistive pulse spectroscopy" (RPS) was developed and applied to a variety of studies on the size, form and deformability of red blood cells. The RPS method is based on the "Coulter" principle, but differs from conventional electronic sizing systems in that RPS seeks to enhance and extract, in addition to size, information about other cellular properties, including deformability and shape.

In Chapter 1, studies on the cumulative spectra and individual pulse forms for rigid latex polymer spheres help to elucidate the electronic, electrical, and hydrodynamic phenomena involved in the "size-transduction" process. The analysis for these particles of known shape and rigidity serves as a foundation for the study of more complex biological cells. A bimodal RPS distribution for singlet spheres is attributable to the passage of the particles in two principal flow regions. This particular bimodality is unrelated to particle deformability. An effective "hydro-dynamic focussing," comparable to that of capillary guide systems, of the particles occurs with a reduction of the sample flow rate.

The acquisition and analysis of the RPS spectral data is controlled by a specially designed computer program (Chapter 2). The pulses corre-sponding to individual cells are electronically "structured" into ordered spectral arrays (pulse height distributions); each spectrum is recorded with the actual time during which the data was generated. Serial spectra thereby represent sequential time-dependent events or changes in the cell

sample properties. The RPS program includes a convolution operation subroutine serving to smooth and differentiate the spectra by polynominal curve fitting to least squares best fit criteria. This numerical analysis method is also adapted to create a "bimodality index" to quantitate the bimodal character of spectra. This spectral feature is shown to be associated with cellular deformability in Chapters 3 and 4.

The interaction of red blood cells with glutaraldehyde (GA) is studied in Chapter 3. A sequence of cell "volume" responses following exposure to GA is measured by RPS. The final volume depends on fixative solution osmolality. Cell-membrane deformability decreases continuously and monotonically with time. The rate of fixation is a direct function of GA concentration, in accordance with a derived empirical expression.

Various membrane properties of erythrocytes undergoing abrupt osmotic hemolysis are explored in Chapter 4. The drop in apparent volume for hemolysing cells, as measured by electronic "sizing" by RPS is ascribed primarily to a greatly increased, flow-induced, cell-membrane deformation and associated expulsion of ghost contents through a single circular rupture, rather than to an intrinsic event of hemolysis per se. The time and flow-rate dependence of the RPS spectra measure the rates of ghost formation and repair of the hemolytic lesion in the membrane. Membrane rather than cytoplasmic (internal viscosity) properties dominate deformability measured from RPS spectral shape.

In Chapter 5, the reversible effects of the binding of chlorpro-mazine·HCl (CPZ·HCl), at the red cell membrane surface was followed with

RPS and coordinated microscopic and microelectrophoretic studies. Low concencentrations of CPZ induced discocyte-stomatocyte transformations, and an associated RPS-measured increase in apparent size and decrease in the "normal" spectral bimodal character. These RPS changes are attributed to the morphological shape change and partial loss of cell deformability. The RPS measure of "dynamic osmotic hemolysis" of treated cells demonstrates the time dependent protective effects of CPZ•HCl against osmotic lysis.

The effects of a high cholesterol diet on the erythrocytes of guinea pigs are examined in Chapter 6. In comparison to control red cells, the "cholesterol-loaded" red cells are (a) more resistant to osmotic swelling and loss of biconcave discoidal form, (b) remained intact longer against osmotic swelling, and (c) appeared unable to repair or reseal after lysis. Control guinea pig red cells, for the most part, behaved as do normal human red cells. The "cholesterol-fed" red cells were detected to be more osmotically resistant as early as 24 hours after initiating a 1% cholesterol diet. A simple centrifugation in a sucrose medium (30% w/v) adequately separates intact cells from ghosts, if the cell suspension is pretreated with glutaraldehyde.

In Chapter 7, some applications of this methodology which also display the pitfalls and strengths of electronic sizing are exemplified. The cases include: (a) multi-population analysis for a mixture of fetal and maternal red cells; (b) developmental changes for phenylhydrazine-induced anemia in the rat; (c) in vitro aging changes in cell volume and deformability, and (d) the dynamic osmotic hemolysis of hereditary spherocytes.

ACKNOWLEDGMENTS

I wish to acknowledge my debt to Professor Howard C. Mel from whom I have learned much about biophysics and being a gentleman. Under his leadership and in his laboratory, along with the ideas and stimulation of his former students, Drs. T. Regimbal and D. Ross, assistance in computer programming by S. Akeson, and electronics support from F. Upham and P. Banchero, I evolved the substance of this dissertation. The many individuals associated with Donner Laboratory and the Group in Biophysics who also contributed are too numerous to be named here, but I would like to give thanks in particular to Professor Michael C. Williams and Professor Robert I. Macey for their interest and comments, as members of the thesis committee.

The final development and preparation of this work was done with a considerable sacrifice of personal "spare" time by Professor Mel and my wife, Lilley. To her I owe special gratitude for enduring this challenging situation together with me and our son, Benjamin.

TABLE OF CONTENTS

PREFACE

This dissertation consists of two interrelated themes: (a) the development of "resistive pulse spectroscopy" (RPS) as an effective form of automated cytology, and (b) the study of a variety of properties of red blood cells, using RPS and complementary methods.

In terms of technique and instrumentation, the goals of RPS are, in general, similar to the objectives of any effective automated cytology method. Specific aims include: (1) the ability to identify the "normal" specimen; (2) to uniquely characterize and display the distribution of cell types, both normal and pathological; and (3) to process the acquired information for efficient evaluation and interpretation. The RPS method takes to advantage the capabilities of (1) examining cells individually, under controlled flow stress conditions; (2) examining cells at very rapid and specific time intervals; and (3) correlating the RPS data with selected microscopic observations of parallel cell samples, often times preserved with glutaraldehyde fixatives.

In recent years, red blood cell rheology has been a subject of widespread interest, not only because of recognition of the clinically significant role of altered red cell deformability in various pathologies, but also because a comprehensive structural and functional model of the general mamallian cell membrane needs to account for its various visco-elastic properties. Generally speaking, the term "deformability" refers to the tendency of a body undergoing change in its form or shape by the action of stresses or forces. Herein, the RPS measurement of deform-ability and deformation is not a direct assessment of changes in precise

geometric dimensions, but rather the RPS measure of deformability is inferred from independently founded observations of basic changes in deformability. For example, it is well established that red cells are mechanically hardened by treatment with glutaraldehyde, as demonstrated by the inability to draw the fixed cell into the bore of a micropipette or through the pore of a nucleopore filter. We thereby infer that changes in the RPS spectra may reflect changes in cell deformability, when proper account is taken for fixative effects on other cell properties such as intrinsic volume and conductivity.

Three different kinds of cell "deformability" are considered here: (1) deformation assessed by the flow-stress-altered, effective shape factor, γ, of a cell of true volume, V_t, where the measured volume $V_a = \gamma \cdot V_t$; (2) in the case of red cell ghosts, the flow induced intracellular volume expulsion through a lesion in the membrane and associated deformation; and (3) the deformability of a cell population reflected by the tendency for those cells to yield a "bimodal" apparent volume distribution. The reader is alerted that these three separate kinds of measures of deformability are explored in various contexts during the course of the thesis.

CHAPTER 1

OUTLINE - STUDIES ON RIGID PARTICLES: RPS SPECTRA AND INDIVIDUAL PULSE FORMS

I. INTRODUCTION

   A. Purposes and advantages of studying rigid particles with RPS.

   B. Description of rigid particle studies undertaken.

II. MATERIALS AND METHODS

   A. Description of particles.

   B. Microscopic measurement of particle diameters.

   C. Suspension media, flow rate control, RPS system.

III. RESULTS

   A. Fig. 1. RPS "size" distributions for rigid spheres at four different flow rates (2.95 micron diameter latex particles): (a) 1.5 X; (b) 1.0 X; (c) 0.5 X; and (d) 0.2 X normal flow.

   B. Fig. 2. Summary of RPS spectral peak positions for rigid spheres at different flow rates (2.95 micron diameter latex particles).

   C. Fig. 3. Individual pulse tracings representative of rigid spheres at normal and slow flow rates.

   D. Fig. 4. Telefunken central stream electronic sizing.

   E. Table 1. Summary of individual pulse characteristics of rigid spheres.

   F. Table 2. Size calibration using rigid spheres.

IV. DISCUSSION

   Correlation and interpretation of individual pulse characteristics and cumulative spectra; physical, hydrodynamic, and electrical phenomena.

   A. Evidence of hydrodynamic "focussing" and boundary layer effects.

   B. Shape factor, and orientation effects on sizing.

   C. Discussion of the present work in relation to findings of other workers.

INTRODUCTION

In addition to sensing actual volume, Coulter-type electronic "sizing" of particles is influenced by several other properties including particle conductivity, orientation, trajectory, deformability, and shape while in the transducer aperture (1,2,6). Although our primary interest here is the study of biological cells, the investigation of standard polymer spheres is useful on several accounts:

1. the latex particles are relatively inert, stable and mechanically rigid;

2. the simple, symmetrical geometry of the spherical particles eliminates orientation effects; the doublets formed by the sticking together of two single spheres provide a means for comparison and analysis of the effects of shape and orientation on measured volume.

3. the particles have size distributions which are relatively sharp in comparison to biological cell populations; the size, in many instances, has been characterized by other methods, e.g., electron microscopy.

These combined features of commercially available polymer spheres make them suitable particles for "calibrating" the electronic sizing apparatus. The studies presented below attempt to define the relative roles of the different particle properties in influencing the RPS-measured, or apparent, volume of the particle. This analysis

involves studying cumulative pulse spectra at differing sample flow rates, and correlating these with the observations of individual pulse tracings.

MATERIALS AND METHODS

Particles

Polymer spheres of differing nominal diameters were supplied by Dow Chemical Company and others:

Composition	Nominal Diameter (Microns)	Std. Dev. (Microns)	Supplier No.
Polyvinyl-tolulene latex	2.95	0.015	E.P. 1356-38
" "	3.49	--	(Coulter Electronics)
Polystyrene divinylbenzene latex	6.14	--	642-19
" "	9.5	--	(Particle Infor. Service)
" "	10	--	(Dow Chemical Co.)
" "	11.8	--	6E-1
" "	10.5	--	(Particle Infor. Service)

Most of these samples were provided as concentrated suspensions of 10% solid content. These stock sources were diluted into the electrolytic suspension media to a final concentration of about 5×10^4 (particles/ml) for RPS sizing.

Suspension Media

The particles were dispersed into electrolytic solutions composed

of simple NaCl (normal saline = 0.9% NaCl), or Dulbecco's phosphate buffered saline. Hypertonic and hypotonic solutions were made by addition of NaCl or distilled water, respectively, to the stock normal saline solution.

Instrumentation

The instrumentation involved in RPS electronic sizing is given elsewhere (see Chapter 4 for details). Some basic aspects of the Coulter electronic sizing transducer principle upon which RPS is based will be given in the DISCUSSION.

Optical Sizing of Particles

The diameters of individual particles were measured by observation with a calibrated reticle eyepiece. For each sample, 100 or more particles were measured with a Zeiss Universal microscope using bright field illumination, a 100 X oil objective lens and a 10 X eyepiece.

RESULTS

The RPS spectra for the 2.95 micron spheres is given in Fig. 1c-d. Two, three, or four distinct subpopulation peaks are seen in Fig. 1 depending on the flow rate employed. This is a striking qualitative and quantitative heterogeneity and variation of size distributions for particles known to be relatively stable and inert. Microscopically, the particles are observed to be much more uniform in size and the majority are individually dispersed. Some particles

are viewed to be joined together as doublets and, more rarely, as higher order aggregates. From this visual evidence, the most accurate RPS spectral representation of the actual physical particle size distribution would be expected to show two major subpopulation peaks corresponding to singlet and doublet particles, with a peak channel ratio of 1.0 to 2.0. This result clearly is not obtained with ordinary or normal flow rate (Fig. 1b), but such an ideal distribution is approached at reduced flow (Fig. 1d). The exact ratio of 1.0:2.0 is never achieved, however, due to particle shape factor and orientation effects to be discussed below. In going from normal flow to slow flow, the calculated coefficient of variation (standard deviation/ mean), for each of the two main subpopulations decreases from 0.14 to 0.06 and from 0.2 to 0.03 for the singlet and doublet subpopulations, respectively.

To summarize the results of RPS measured size of the particles at the different flow rates, we plot the peak channel of each apparent subpopulation against the flow rate (Fig. 2).

As previously indicated for Fig. 1, a different number of distinct peaks is discernable depending on the flow rate (e.g., three peaks at 0.5X normal flow). With the curves of Fig. 2, the overall relationship of RPS-measured particle size to the flow rate is more readily apparent. At relatively slow flow (i.e., at about 0.2 X normal flow), there is only one peak corresponding to each of the two particle subpopulations: The upper corresponding to the doublet and the lower to the singlet spheres (as per Fig. 1d). With flow rate

increased to about 0.4 to 0.5 X normal flow, the doublet subpopulation peak diverges to form a pair of separate peaks. The singlet sphere peak does not diverge into two discernable peaks until flow is above 0.5 X normal flow. The divergence or splitting into two of each subpopulation tends to increase in the flow range between about 0.5 and 1.0 to 1.2 X normal flow; i.e., one of the pair decreases in size while its partner is stable, or increases in measured channel number. The range over which the peak positions are flow independent is very small for the doublets compared to the single spheres: 0.2 to 0.3 X, and 0.2 to 0.5 X normal flow, respectively. Both particle subpopulation peaks fall off in apparent size at flow rates below 0.2 X normal flow. Interpretation of these changes in apparent size resolution and the shifts in relative size are given in the DISCUSSION below.

Individual Pulse Forms

Examination of the individual pulse forms generated by the RPS transducer is helpful in analysis of the events underlying the flow rate dependent phenomena observed in the cumulative pulse spectra described in Fig. 1 and Fig. 2. Photographs of oscilloscope tracings of pulse forms corresponding to the passage of individual particles through the aperture are shown in Fig. 3.

Basically two pulse form shapes are observed with normal flow rate (Fig. 3a and 3b): (a) symmetrical bell shaped and (b) trapezoidal or nearly flat-topped forms. Each of these pulse forms occur in two amplitude ranges, the higher corresponding, of course, to the

doublets and the lower to the singlets. With the reduced ("slow")
flow rate of about 0.0016 ml/sec, the pulses observed may be classi-
fied by form as: (a) trapezoidal or flat-topped, or (b) "M" shaped
(Fig. 3c and 3d). Again two ranges of amplitude for these pulses
occurs, corresponding to singlet and doublet particles.

In addition to shape and amplitude, time duration and frequency
of occurrence are also used to characterize the pulses. The results
for such classification of about a hundred individual pulse forms
at each flow rate are given in Table 1. The pulse duration is taken
as the time over which each individual signal has an amplitude greater
than 0.25 volts.

Volume Calibration

Volumes of five nominally different sized spherical particles
were intercompared, using: (a) the manufacturer's nominal diameters,
(b) light microscopic estimates of particle diameter, and (c) RPS
measurements of relative peak size. The results are given in Table
2.

DISCUSSION

Overview

As originally formulated, the Coulter electronic sizing prin-
ciple does not take into account the effect of particle deformability.
With biological cells such as mammalian erythrocytes, rheological
properties are critical in determining the deformation, and hence,

TABLE 1

Rigid Spheres: Individual Pulse Characteristics

Latex spheres (2.95μ)	Pulse form	Relative frequency (%)	Relative amplitude (1.0 = mode)	Pulse duration (μsec)
Flow rate = 0.008 (ml/sec)	1. bell-shaped I	56	1.0	16
	2. trapezoidal I	21	1.4	27.5
	3. bell-shaped II	18	1.9	21.5
	4. trapezoidal II	5	2.6	30
Flow rate = 0.0016 (ml/sec)	1. flat-topped or trapezoidal	70	1.0	40-60
	2. "M" shaped	19	1.5	120
	3. "doublet"	22	2.0	60-70

TABLE 2

Rigid Spheres Volume Calibration: Nominal[*], Optical[**], and RPS Measured[§]

Diameter (μ)		Volume (μ^3)		Relative Volume between Spheres		
Nominal	Optical	Nominal	Optical	Nominal	Optical	RPS
2.95[+]	3.31	13.4	19.0	1.0	1.0	1.0
3.49[+]	3.94	22	32.0	1.66	1.7	1.33
9.5[‡]	10.7	449	641	33.4	34	39.1
10.5[‡]	10.8	606	657	45.1	34.6	42.7
11.8[‡]	11.14	860	723	63.9	38	42.7

[+]Current 6 gain 9, 48μ aperture (number C-341)

[‡]Current 2 gain 6, 48μ aperture (number C-341)

[*]The manufacturer's nominal values are based on measurements made with an electron microscope; the specimen preparation may induce artifactual shrinkage.
[**]The optical measurements of particle diameter are limited by physical contraints of maximal resolution of the microscope = ± 0.2 microns. (Con't under (a) below.)
[§]The RPS measurement is shown to be linear at the level of the signal amplifier by calibration with a voltage pulse generator.

(a) For the very heterogeneous, largest size particles, the optical measurements are also limited by small sample size.

the shape of the cell as it passes through the sensing aperture.
The RPS approach seeks to elucidate the role of deformability, and
therefore to use the same basic transducer principle not only for
sizing but also for measurement of deformability. Prior to focuss-
ing on the deformability information obtainable by electronic pulse
analysis (Chapter 4) it is helpful to study the phenomena of the trans-
ducer that are independent of particle deformability by evaluating
the results for latex polymer spheres which are essentially inert
and mechanically rigid. With the rigid particle studies described
above, conclusions may be drawn about:

1.   the role of particle transit time in relation to electrical
and electronic response times of the transducer system;

2.   the effects of shape, i.e., shape factor, on RPS-measured
size;

3.   the role of particle trajectory in the presence of apparent
inhomogenieties of aperture electric and hydrodynamic fields; and

4.   the operating conditions best suited to evaluate actual
particle volume properties.

The RPS System and the Coulter Principle

The Coulter principle is based on the change in resistance due
to the passage of a nonconducting particle through a current limiting
aperture. To a first approximation, this change may be calculated

from simple physical principles (3). In the absence of a particle,
the resistance of the electrode circuit, Ω (ohms), is limited by the
orifice and will depend upon the length L (cm) and cross-sectional
area A(cm^2) of the orifice as well as the specific resistivity of
the electrolyte, ρ_e (ohm-cm) as follows:

$$\Omega = \rho_e \frac{L}{A}$$

A nonconducting particle will displace its equivalent volume of con-
ducting solution. As modeled by Kubitschek, the incremental resis-
tance due to a particle having segment length $d\ell$ and effective
particle cross-section σ will be $dR = \rho_e \frac{d\ell}{(A-\sigma)}$. If A is much
greater than the maximum particle cross-section, the integration is
particularly simple, leading to the expression (3):

$$R = \Omega + \rho_e \frac{v}{A^2} \text{ , and}$$

$$= R - \Omega = \rho_e \frac{v}{A^2}$$

Thus, change in resistance ($\Delta\Omega$) is proportional to v, the volume,
of the particle, if $v \ll A\cdot L$. These concepts provide the basis for
the design of instrumentation to process and analyze the informa-
tional resistive, Ω , pulse. More complex considerations are
necessary to account for particle shape, orientation, trajectory,
and deformability properties, and the inhomogeneity of the elec-
trical and hydrodynamic fields of the sensing aperture.

Particle Transit Time and Electrical Response Characteristics of the Transducer

Independent of the other considerations discussed below, the RPS-measured size of a particle is dependent upon its transit time through the sensing aperture. The rise time of the electrical pulse is determined by the frequency response characteristics of the aperture-transducer and its associated circuitry; the pulse rise time must be faster than the transit time of the particle to allow the signal to reach a true peak value (4).

In Fig. 2, the curve segments labelled "a" and "b" represent a range of increasing flow over which the particle transit time is progressively shorter than the rise time. (The average transit time is directly proportional to flow rate, and calculated to be about 11.6 microseconds for normal flow rate.) Thus a linear decrease in measured size is observed with the increase in flow rate. In contrast, curve segments "c" and "d" do not follow this pattern because of other factors (to be discussed below) dominating over the transit time contribution. With sufficiently long transit time, the measured size is independent of flow rate if other phenomena, such as rotation of the particle, do not enter into play (i.e., curve segment "e" in Fig. 2). (See also footnote on page 22.)

To overcome the inherent frequency response limitations of the aperture-electrode circuit, some workers have taken the approach of separating the sensing electrodes from the power electrodes (5). A bridge circuit for potential or current sensing is used as the

pulse detector rather than using the primary power electrodes. When electronic response characteristics have been controlled in this manner, the basic conclusions made about importance of particle trajectory and field inhomogeineity discussed below have been further substantiated.

A basic physical explanation or interpretation of the cumulative pulse spectra and individual pulse forms requires modeling of the hydrodynamic and electric fields associated with the transducer aperture. With the singlet spheres, orientation and shape factor effects are known, thus the analysis of the fields is more straightforward. The hydrodynamic field has been theoretically and experimentally considered by various workers. Grover et al. (2) calculated a Reynolds number, R_e, for a typical Coulter aperture to be much less than 1000. ($R_e = R u\rho/\eta$; where R is the radius (cm) of the aperture, u the average velocity (cm/s), η the viscosity (poise), and ρ the density (g/cm^3) of the suspension medium). With this modeling, it is predicted that parabolic, laminar flow is not able to develop fully in the usual short length of the aperture. Instead, plug flow exists in the central core region, with a high shear gradient and lower velocity near the wall region of the aperture. Examination of individual pulse durations, or transit times experimentally confirms the general concept of differences in velocity at different radial trajectory positions. In addition, the method of particle director guides or "central-stream," hydrodynamic focussing to direct particles to selected radial positions of transit (Fig. 4) have demonstrated that particles traversing near the wall regions have transit times significant longer

than particles passing through the near axial region, (2,8,9). These
workers (2,8,9) have analyzed individual pulse forms similar to those
shown in Fig. 3. Particles traversing the central axial region, tend
to have signals that are not fully developed in amplitude, related
to the capacitance limitations of the transducer circuitry. The
minority of particles traversing in the off-axial trajectories have
longer transit times, and approach or achieve full development of
signal amplitude.

The electric field distribution has similarly been studied (2,7,8).
The electric field is calculated to be most dense near the entrance
and exit, as well as the wall regions of the aperture. Thus, particles
traversing axial pathways of the aperture cross section block rel-
atively less of the current than particles traversing near the edges.
This theoretical prediction has been tested both on scale models of
the aperture constructed in electrolytic tanks where the electric
field was mapped out corresponding to specific particle trajectories,
and with measurements of individual pulse forms for particles con-
trolled by director guide systems (7,9). In order to correct for,
or eliminate, effects of transit time as such, the aperture length
was increased or the sample flow rate decreased so that the signal
was fully developed for each radial trajectory. With such control
of the influence of particle transit time, it has been demonstrated
that the signal amplitude generated by a particle of constant size,
is greatest at the entrance and exit of the aperture, and the field
strength at the wall is greater than near the central axial region.
Thus a particle traversing in an off-axial position tends to give
a "M" shaped pulse.

Our observations and tabulation of individual pulse forms may be interpreted in terms of these hydrodynamic and electric field inhomogenities. Based on the above modeling, we may infer that at different bulk sample flow rates, the particles change in their distribution of positions in the aperture cross-section (Fig. 1 and 2). At relatively high flow rate, particles tend to traverse principally in two regions: the majority through the central core, presumably low shear gradient region; a smaller number through in the low velocity, high shear field, high electric field region. Because the coefficients of variation corresponding to the major pulse subpopulations (i.e., the singlet and doublet particles) decrease with decreased flow rate there appears to be a process of intrinsic hydrodynamic focussing of the particles. That is, the convergence of the minor "shoulder" subpopulation with the principal mode, major population upon decreasing flow rate is not due solely to the increasing transit time of the central-core trajectory particles. If only transit time limitations were operative at the higher flow rates, one would expect the principal peak simply to move upwards, with decreased flow rate, towards the shoulder population peak, as a consequence of increasing signal development. However, as demonstrated in Fig. 1 and 2, this does not happen. Instead the minor shoulder subpopulation peak positions actually converges down towards the upward moving principal peak population. One interpretation of this evidence is that the particles comprising the upper shoulder subpopulations are driven away from the wall region of maximal electric field towards the central axis at the lower flow rate.

Particle Shape and Orientation

The role of shape factor has been analyzed by various groups (2,4,7,9). The measure or apparent volume, V_a, is related to the actual volume, V_t, by the shape factor γ, where $V_a = \gamma V_t$. Based on our RPS data, a shape factor for the doublet relative to the singlets at different flow rates may be calculated.

The shape factor for a sphere has been taken as 1.5 (4). The shape factor of two spheres adjoined to one another and aligned with the direction of flow may be estimated from the electronically meas-ured doublet volume relative to that of singlets. The ratio of par-ticle shape factors then gives a correction factor for the ratio of measured electronic volumes (the ideal, true volume ratio for doublets compared to singlets is evidently 2.00). Using the peak channels found at normal flow, a ratio of 1.76 is calculated; at 0.2 X normal flow, the ratio of electronic volumes is 1.86. A shape factor for the doublet spheres of 1.44 would be consistent with the latter flow rate, whereas a shape factor of 1.34 is calculated for the normal flow rate electronic volume ratio. This may reflect a greater ten-dency for the doublets to be, on the average, located somewhat off-axis at the lower flow rate relative to the higher flow rate. This would be consistent with the effects of increased development of parabolic flow predicted by Grover et al. (10).

Translational movements of particles (that is movement from one radial position to another), and rotations rarely occur while the

particle is in the aperture. This conclusion is based on observations of individual pulse forms and laser flash photographs of particle in the aperture (7). This is probably due to the very unfavorable energy requirements for particles to rotate while in the aperture. Grover has argued that with decreasing sample flow rate, there should be a greater tendency for the particle to be rotated, because at the decreased flow rate, the velocity profile more closely approaches a Poisueille parabolic flow. That is, at low flow more shear gradient develops across the cross-section of the aperture, relative to that at the higher flow rate, when a greater proportion of the aperture has bulk plug flow without a shear gradient across it (10).

SUMMARY

These studies of resistive pulse spectra and individual pulses generated by latex particle spheres serve to extend the understanding of the interrelationships of particle properties (such as size, shape, transit time, trajectory and orientation), and the electrical response characteristics and inhomogeneous electrical and hydrodynamic fields associated with the aperture transducer. Our findings are consistent with and supported by previously reported investigations. In addition they go beyond, to provide a rationale for measuring particles in suspensions at several different flow rates. The RPS results show that repeated measurements at different flow rates are needed both to most accurately identify the true volume distributions and also serve to assess the "non-volume" properties of particles, as mentioned previously.

With this groundwork done on rigid spheres, the analysis of more complex biological cells is considerably facilitated. In earlier studies of red cells, in which the flow-dependent phenomena were not recognized, rather gross misinterpretations of the observed electronic size spectra have been reported (11). Resistive pulse spectroscopy studies of red blood cells are reported in Chapters 2 through 5.

REFERENCES

1. Coulter, W. H. High speed automatic blood cell counter and cell size analysis. Proc. Nat. Electron. Conf. 12, 1014, 1956.

2. Grover, N. B., Naaman, J., Ben-Sasson, S. and Doljanski F. Electrical sizing of particles in suspensions. I. Theory. II. Experiments with rigid spheres. Biophys. J. 9, 1398-1425, 1969.

3. Kubitschek, H. E. Electronic measurement of particle size. Research (London) 13, 128-135, 1960.

4. Gregg, E. C., Steidley, K.D. Electrical counting and sizing of mammalian cells in suspension. Biophys. J. 5, 393-405, 1965.

5. Thomas, R. Cameron, B.F., and Leif, R. C. Computer-based electronic volume analysis with the AMAC II transducer. J. Histochem. Cytochem. 22, 626-641, 1974.

6. Shank, H. B., Adams, R. B., Steidley, K. D., and Murphy, J. R. A physical explanation of the bimodal distribution obtained by electronic sizing of erythrocytes. J. Lab. Clin. Med. 74, 630-641, 1969.

7. Thom, R., Hampe. E., and Saurbrey G. Die elektronische Volumenbestimmung von Blutkö rperchen und ihre Fehlerquellen. Z. ges. exp. Med. 151, 331-349, 1969.

8. Adams, R. B. and Gregg, E.C. Pulse shapes from particles tra-
    versing Coulter orifice fields. Phys. Med. Biol. 17, 830-842,
    1972.

9. Metzger, H., Kachel, V., and Ruhenstroth-Bauer, G. Einfluss
    von Partikelgrosse form und konsistenz auf Rechtsschiefe Coulter-
    Volumenverteilungskurven. Blut 23, 143-154, 1971.

10. Grover, N. B., Naaman, J., Ben-Sasson, S. and Doljanski, F.
    Electrical sizing of particles in suspensions. III. Rigid
    spheroids and red blood cells. Biophys. J. 12, 1099-1117, 1972.

11. Lushbaugh, C. C. Electronic measurement of cellular volumes
    II. Blood 20, 241, 1962.

Footnote for pg. 14.

It is well known that overheating and boiling can, under certain
circumstances, be induced by high current in "Coulter-type" orifices.
The drop in apparent size for the small particles of Fig. 2, for the
longest residence times (relative flow rates < 0.2), is most likely
an artifact resulting from this cause.

FIGURE CAPTIONS

Figure 1

RPS "size" distributions for rigid spheres. Latex particles (2.95 μ nominal diameter) were measured by RPS at four different sample suspension flow rates (1.0 = normal flow of 0.008 ml/sec). The relative number of particles (ordinate) is plotted against the relative pulse size (channel no.). (48 micron diameter X 48 micron length aperture, 400 μamp current.)

Figure 2

Rigid Particle Sizes. Peak channel values taken from spectra such as those represented in Fig. 1, are plotted against sample flow rate (normal flow is 0.008 ml/sec). The particle sample and the aperture and current specifications are the same as those described with the results in Fig. 1.

Figure 3

Individual Pulse Forms. In Figs. 3a and 3b, the pulses are representative of particles sized at normal flow rate. The pulses shown in Fig. 3c and 3d are representative of results obtained with reduced flow rate (about 0.2 X normal flow). The particles and instrumentation are the same as those described with the results of Fig. 1 and 2 above. The pulses were displayed with a Tektronix 545A oscilloscope and recorded on Polaroid film using a Tektronix oscilloscope camera as detailed in Chapter 4.

Figure 4

Electronic size distribution using Telefunken "central-stream" hydro-dynamic focussing guide. Comparison of focussed and unfocussed par-ticle volume distributions, adapted from the data of Thom, et al. (7), using their symbol, ϕ for diameters. For the total stream (unfocussed) spectrum the "shoulders" for both the singlet and doublet subpopulations arise from the near-wall, oversize pulses.

(a) Flow rate = 1.5 X

(b) 1.0 X

(c) 0.5 X

(d) 0.2 X

Relative number of particles

Channel no. (relative size)

25   50   75   100
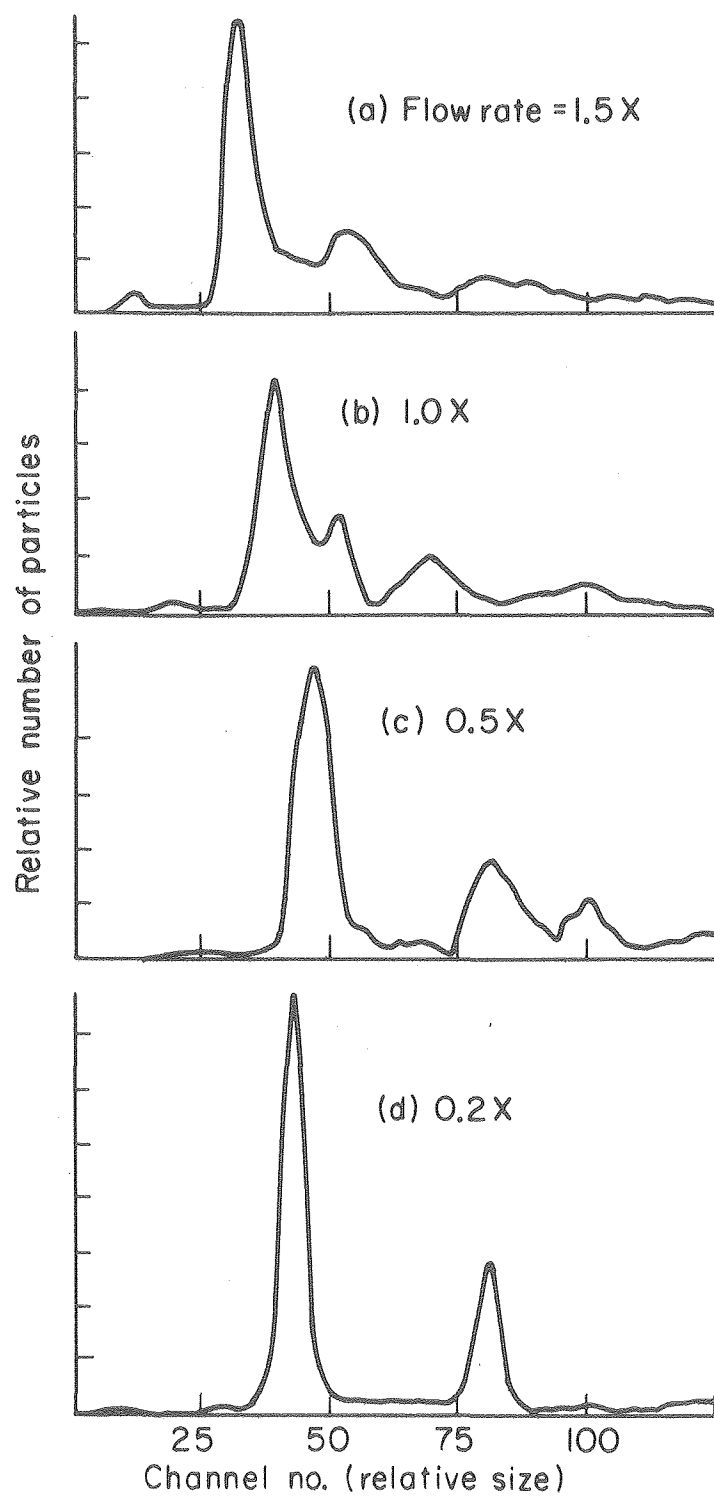
XBL 787-3320

Fig. 1
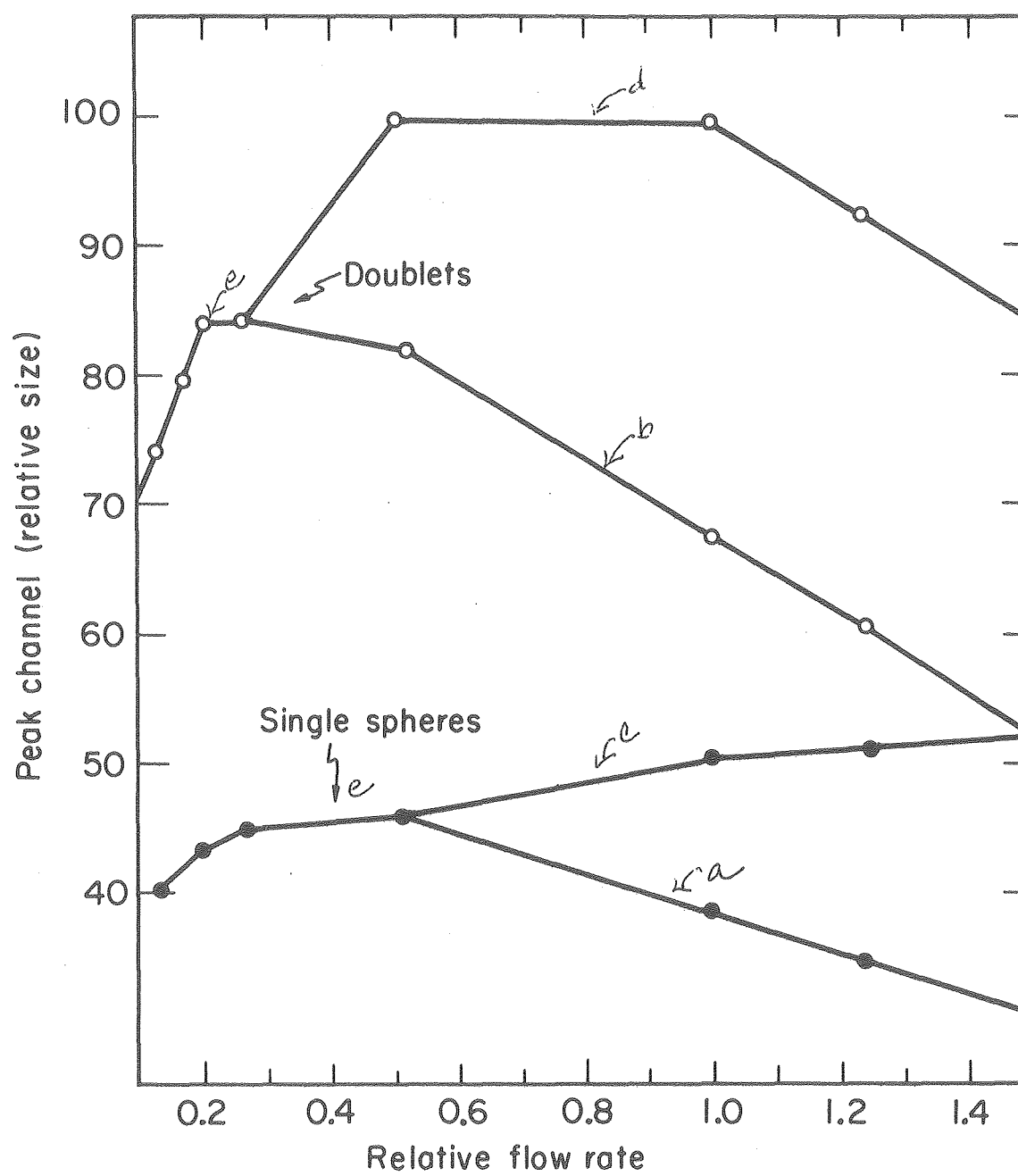
XBL 787-3321

Fig. 2
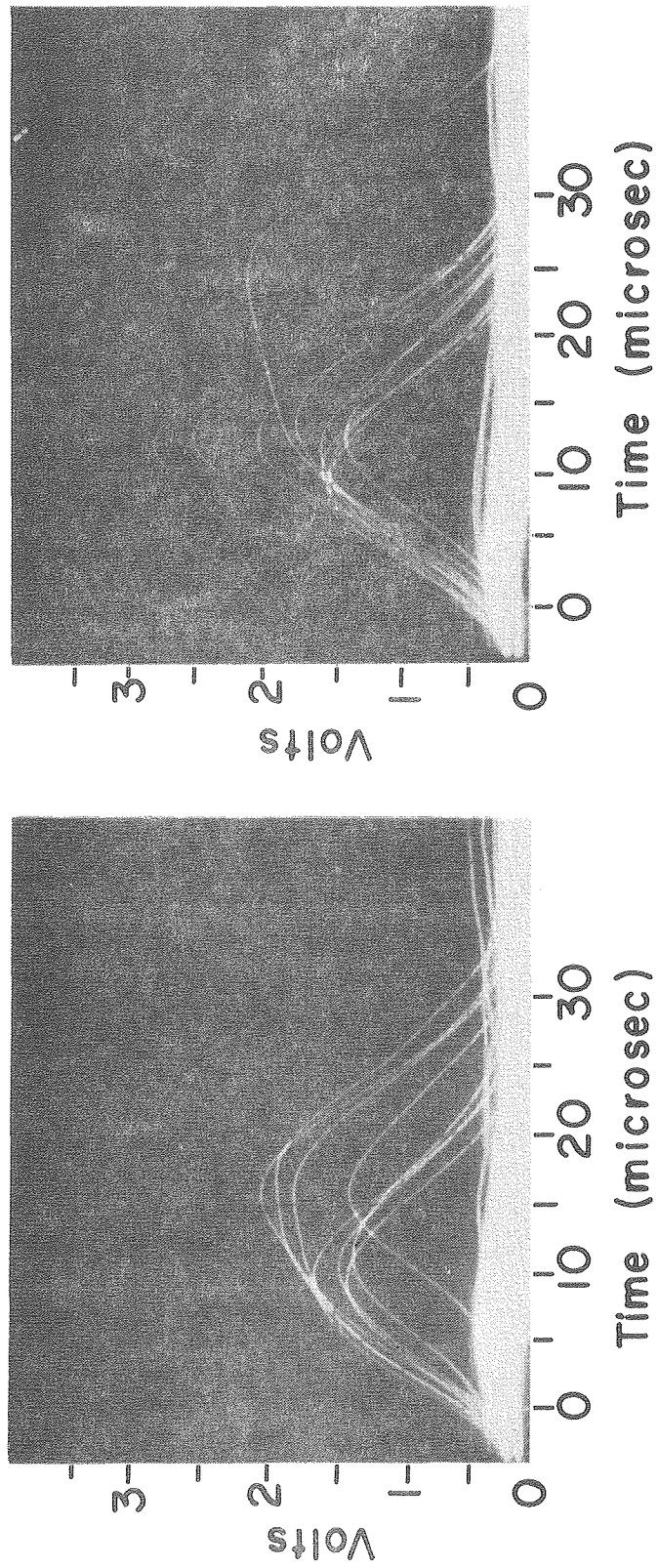
XBB 780-15691

Fig. 3A
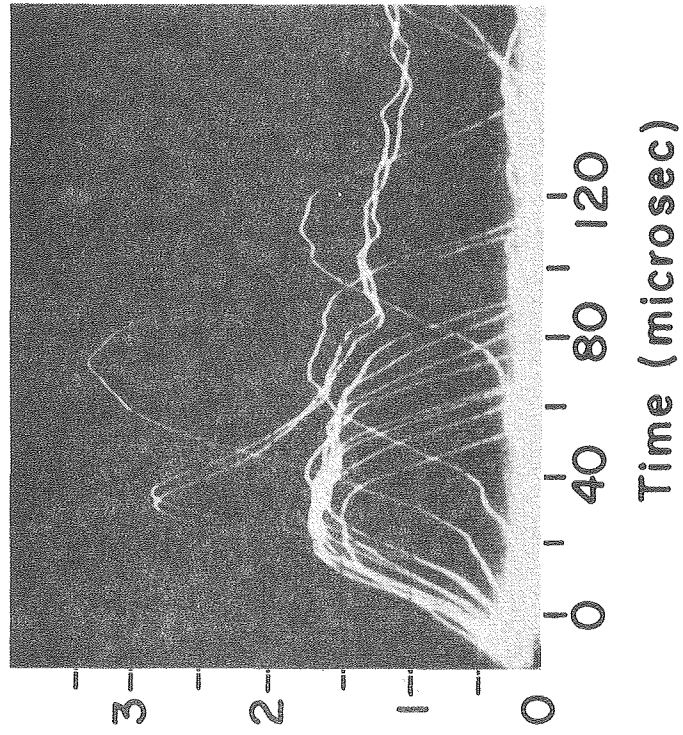
XBB 780-15692
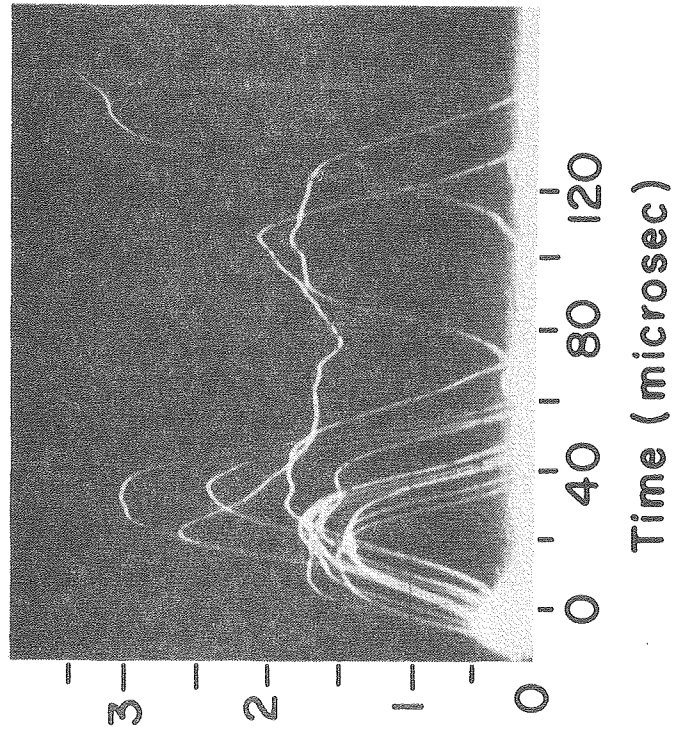
Fig. 3B
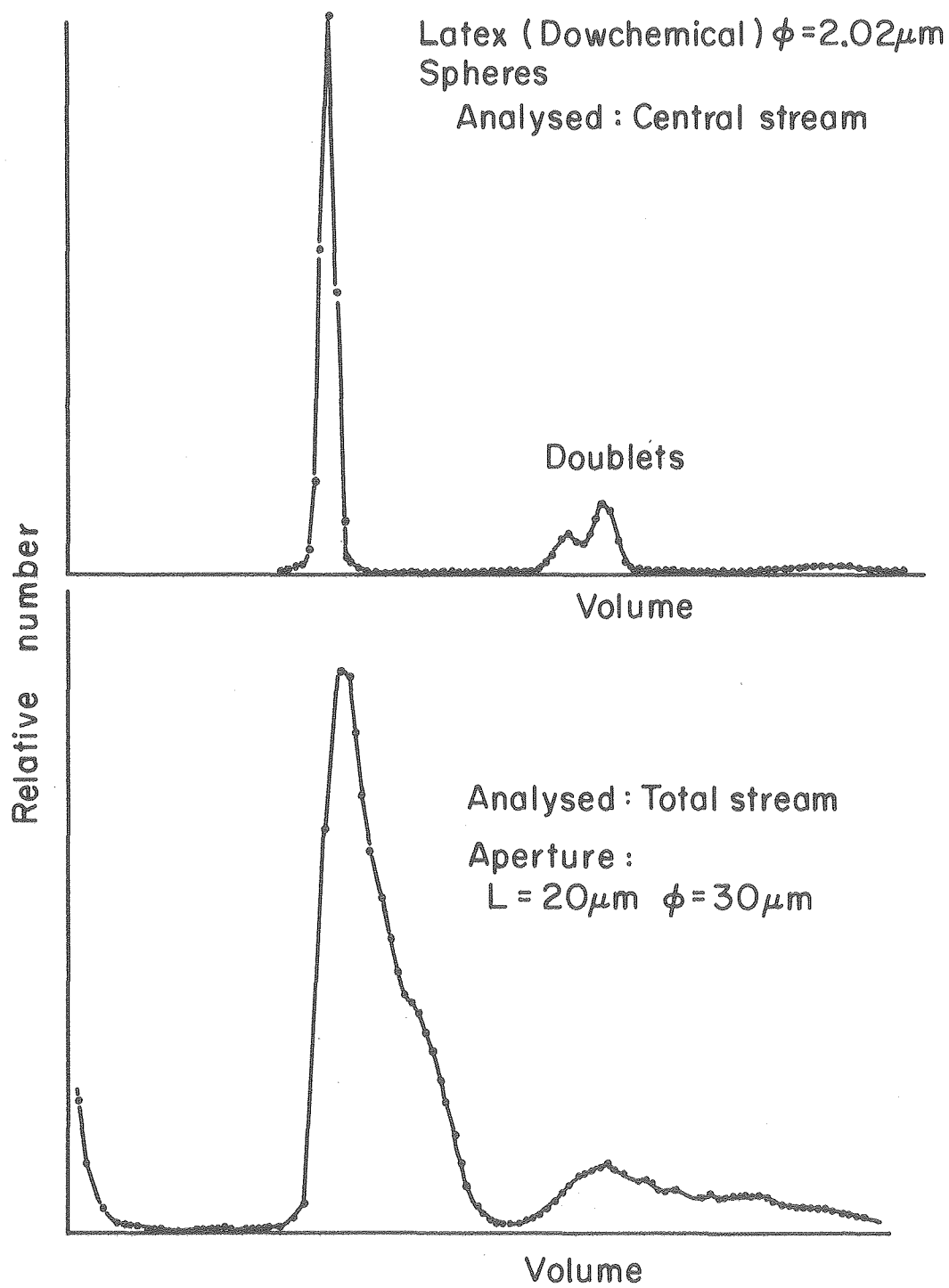
Fig. 4

XBL787-3317

CHAPTER 2

OUTLINE - NUMERICAL ANALYSIS OF RPS SPECTRA
AND THE RPS "BIMODALITY" INDEX

I.   INTRODUCTION

Purpose and basis of numerical analysis of RPS data and
the development of an RPS index.

II. METHOD

Description of n-polynomial best fit smoothing program
with references.

III. RESULTS

Examples of applications of RPS index:

A.   Fig. 1. RPS spectra; smoothing of data and differ-
entiation.

Fig. 2. RPS index parameters with bimodal and uni-
modal RPS spectra.

B.   Fig. 3. Examples of applications of RPS index:

(a) human red cells at different flow rates;
(b) hypotonically swollen human red cells,
(c) glutaraldehyde-treated human red cells.

IV. DISCUSSION

Applicability of index as a measure of deformability.

A.   Sensitivity and specificity.

B.   Relation of index and bimodality to individual
pulse characteristics.

INTRODUCTION

In attempting to use a digital computer to analyze the pulse height spectral data generated by the RPS system, various numerical methods were considered (1, 2). As with the primary output of any experiment, the phenomenon under observation has both quantitative information of interest and, superimposed upon and indistinguishable from this information, random errors. A fundamental goal of data analysis is therefore to remove as much "noise" as possible without significantly degrading the underlying information. Another major goal in the numerical analysis of the digitalized RPS spectra is to parameterize the curvature characteristics of the spectra. This curvature, specifically bimodality, is demonstrated to be a new kind of measure of the deformability properties of red cells.

Convolution Operations

Essentially, each RPS spectrum may be thought of as a two column data table: cell number (ordinate) vs pulse height (abscissa). The concept of a convolution operation (1) is conveniently applicable to such a data array. The mathematical description of this process is:

$$Y_j^\star = \sum_{i=-m}^{i=m} \frac{C_i \, Y_{j+i}}{N}$$

Where Y_j* is the new jth data point (ordinate) C_i the convoluting

integer, N the number of convoluting integers; and $2m + 1 = N$.

In the general case C represents any set of convoluting integers.

As a specific example, for a moving average convolution, each C_i is

equal to one.

Method of Least Squares

The experimenter presented with a plot of RPS spectral data

points would tend to draw a line through these points which, by eye,

best fits them. For a systematic best fit, the most common numerical

method used is that of least squares.

The method is as follows: A set of points is to be fitted to

some curve, e.g., the polynomial $a_3 X^3 + a_2 X^2 + a_1 X + a_0 = Y$. The

a's are to be selected such that when each abscissa point is substituted

into this equation, the square of the differences between the computed

numbers, y, and the observed numbers is a minimum for the total of

the observations used in determining the coefficients. It turns out

that a set of convolution integers is derivable which will give ex-

act fitting by least squares criteria. These sets of convolution

integers are available in tabular form for n-order polynomials (1)

(e.g., cubic or quadratic) fitting with N point convolution (e.g.,

5, 7, or 9 etc.). The first and second derivatives of the least

squares best-fit function may be derived from another set of convo-

lution integers. For our 64 channel spectra, a five point cubic

polynomial fit was chosen because it appeared to give no significant curve distortion while providing adequate "smoothing" and ability to calculate derivatives.

RESULTS

The initial RPS spectra are composed of a two dimensional array of information: (a) the abscissa, which consists of 64 channels corresponding to linear pulse height; and (b) the ordinate which may contain counts up to a maximum of 4095 per channel. In Fig. 1, each curve is from a line drawn through the 64 data points resulting from smoothing of raw data by convolution with a five-point cubic polynomial least squares fit. The first column, spectra (f), shows the smoothed data; the middle (f') and right (f") columns are the first and second derivatives, respectively, corresponding to the original data spectra (f).

Details of the relations between derivative curves, f', and original data "volume" distribution, f, curves are shown in Fig. 2. The small 0's mark the maxima and minima of the initial curves, f. These extrema, as expected, occur at the same channel values as the "zero" cross-over points of the first derivative (f'). The inflection points of the initial curve are marked with the x's; these correspond to the maxima and minima of the first derivative.

The above numerical parameters may be utilized as follows:

1. The "zero" cross-overs of the f' curve serve as criteria for automatic computer detection of multiple maxima and minima of the f curve. A simpler peak selecting algorithm cannot accomplish such identification of multiple extrema nor can it smooth out spurious noise fluctuations.

2. An index may be constructed to characterize the bimodality of the curve f.

Empirically two RPS indices have been developed, as defined in Fig. 3. The indices are intended to give a value of roughly 1.0 for normal "bimodality" and to progress monotonically towards zero with loss of bimodality. As developed further elsewhere (3), the bimodality is a sample-flow-rate-related manifestation of the normal deformability of native erythrocytes. Some specific examples of indices resulting from alteration of the deformability and deformation of RBCs are also included in Fig. 3. One observes that: (a) decreased sample flow rate leads to a decrease in spectral bimodal curvature; (b) mild to moderate osmotic swelling of the red cell causes a measurable loss of bimodality; and (c) exposure of native RBCs to low concentrations of GA (about 0.025% w/v) causes bimodality loss which increases with time of exposure.

DISCUSSION

The physical interpretation of the bimodal shape of the electronic "size" distribution of native erythrocytes has been presented elsewhere (3). Here the focus has been on techniques of numerical analysis of the RPS spectra to give objective measures of bimodality, or bimodality indexes. With continuing experience with two such indexes, the i_1 parameter has appeared to be more consistent than i_2 as a measure of bimodality, and therefore has been used more extensively in ongoing work. The i_1 index is relatively independent of the exact cell size (i.e., the mean channel number) or amplifier gain employed.

Incidental to the primary goal of parameterizing the bimodal character of the spectra, effective means of smoothing and differentiating the digital arrays of data were developed. This allowed for automated identification of maxima and minima of the distributions. The numerical analysis operations described here have been incorporated into a pre-existing larger, conventional statistical analysis program (detailed in Chapter 4.)

Several examples of RPS series were presented for cell specimens subjected to varying perturbations of their initial deformability properties including (a) cells decreasingly deformed by decreasing sample flow rates through the sensing aperture; (b) cells rendered less deformable by swelling induced by increasingly hypotonic suspension media; and (c) cells rigidified over time following exposure

to glutaraldehyde fixative solution. Each of these physical perturbations has qualitatively predictable effects on cell deformability and deformation; each has been studied in greater detail elsewhere (flow and osmotic effects in Chapter 4; glutaraldehyde effects in Chapter 6).

The role of the RPS bimodality index is to give a consistent, reproducible, quantitative measure of the visually apparent changes in spectral bimodality. In principle, the index value should allow quantitative intercomparison of cells whose deformability is altered by different causes, e.g., membrane aging vs GA fixation.

Such interpretation of the physical meaning of the changes in the bimodality index for any given experimental sequence requires confirmation and support by theoretical postulates (e.g., progressive hardening of the cell membrane secondary to the cross-linking of its protein contents by the glutaraldehyde), and selected independent measurements of cell deformability (e.g., the microhematocrit method of measuring mean cell volume). When these independent, supporting considerations are available, the RPS index can serve as a very sensitive, rapid, and convenient method of quantitatively measuring one deformability property of erythrocytes. The physical basis of this kind of "bimodality"-related deformability property, as well as other kinds of cellular deformability, is discussed in Chapter 4.

REFERENCES

1. Savitzky, A., and Golay, M. J. Smoothing and differentiation of data by simplified least squares procedures. Analyt. Chem. 36: 1627, 1964.

2. Mateosian, E. D. On-line small computer data handling in pulse height analysis and two parameter multichannel coincidence data storage. Nucl. Instrum. Methods 73: 77, 1969.

3. Yee, J. P., and Mel, H. C. Cell-membrane and rheological mechanisms: dynamic osmotic hemolysis of human erythrocytes and repair of ghosts, as studied by resistive pulse spectroscopy. Biorheology 15: 321-339, 1978.

FIGURE CAPTIONS

Figure 1

RPS spectra, smoothing and differentiation. Fresh human erythrocytes

measured by RPS at three representative sample flow rates results

in three basic spectral shapes. At sufficiently high flow (i.e.,

about 0.008 ml/sec) the curve is clearly bimodal ("Class I"); with

reduction of flow, there is reduction of the distinct second peak

to a shoulder ("Class II"), and with flow below about 0.004 ml/sec,

the curve approaches a symmetrical unimodal distribution ("Class III").

Figure 2

RPS index parameters. Detailed parameters of the first derivative

curves are defined as follows: a_1 and a_2 give the maximal upward

and downward slopes of the principal peak, and e and c the correspond-

ing values for the second peak of the f curve. For a "Class III"

curve, no e and c values exist.

Figure 3

RPS bimodality index. Indices i_1 and i_2 are defined at the upper

right. Tabulations show the calculated results for RPS spectra of

fresh human erythrocytes in (a) isotonic phosphate buffered saline,

(b) suspended in hypotonic saline solution as designated, and (c)

treated with GA at time zero, and evaluated at designated subsequent

times.

RPS ANALYSIS: SMOOTHING, DIFFERENTIATION

RPS = f   f'   f''

Class I

Class II

Class III

Fig. 1

DBL 745-4793
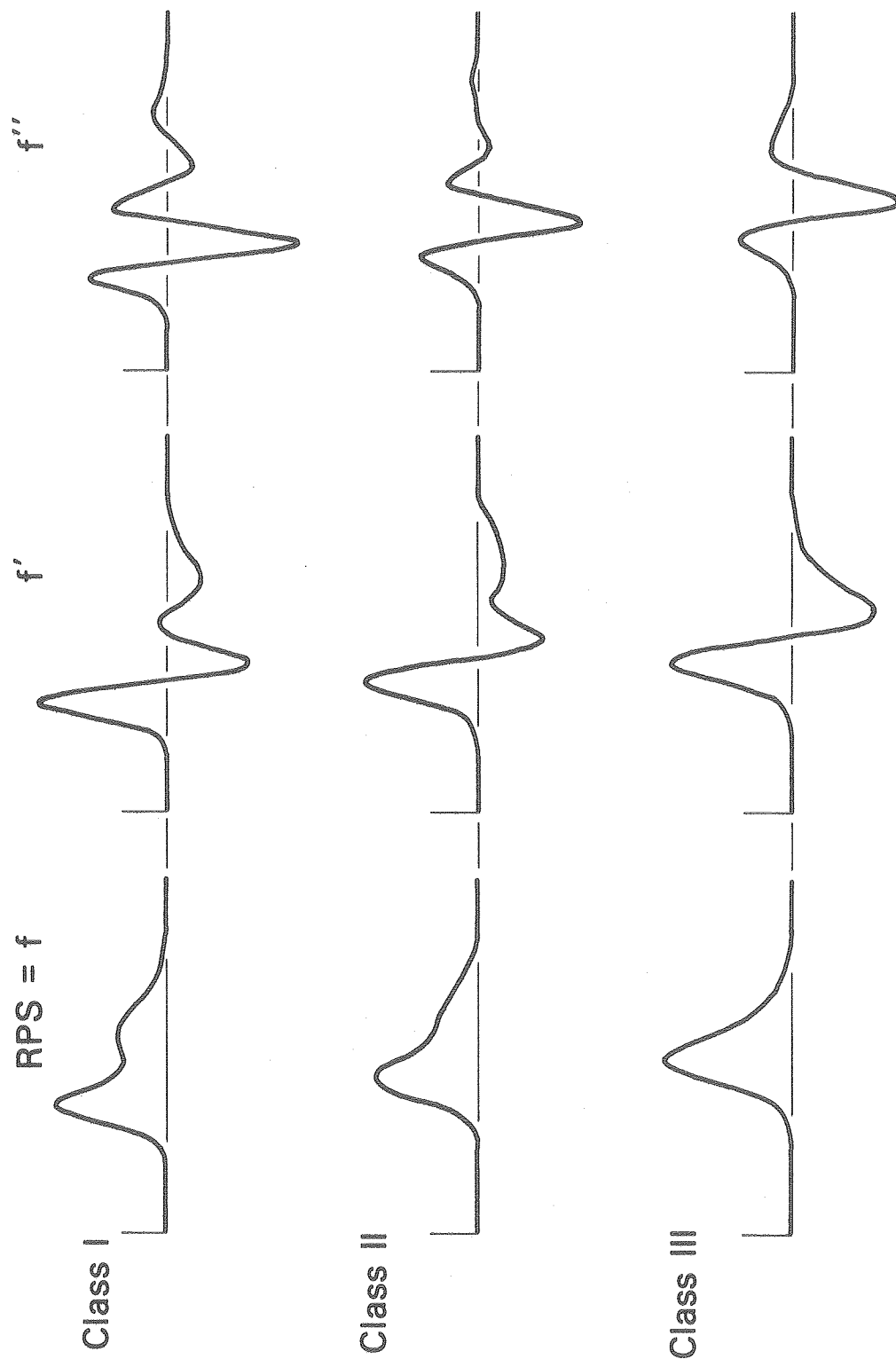
RPS INDEX PARAMETERS
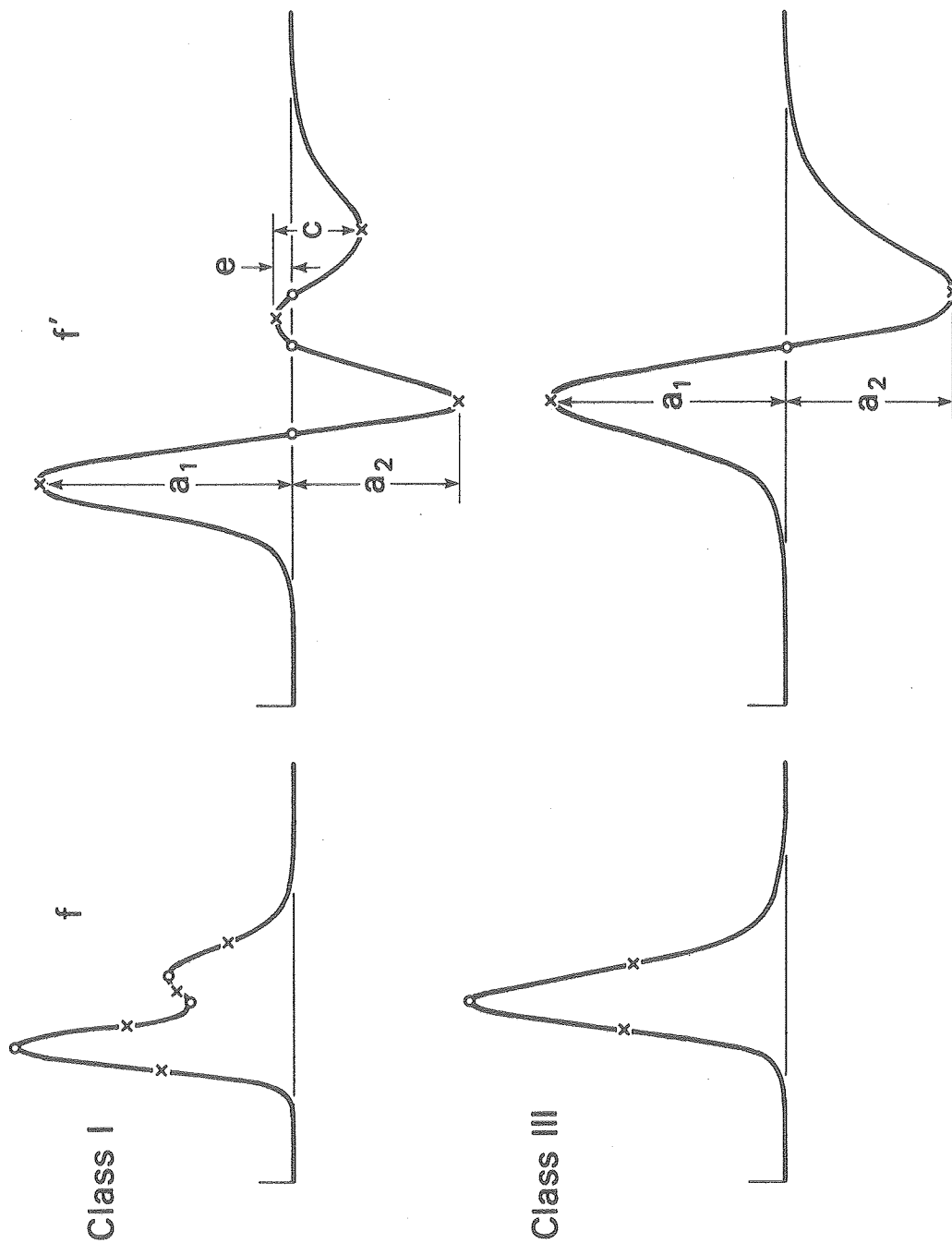
Fig. 2

DBL 746-4799
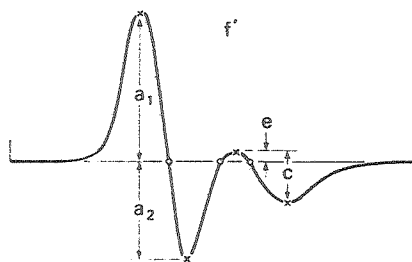
$$i_1 \equiv \frac{|a_2| + |c| + e}{a_1 - e}$$

$$i_2 \equiv |c| \times \text{peak ratio}$$

Flow rate	i_1	i_2
I (Norm.)	1.15	0.85
II (Int'med.)	0.52	0.26
III (Slow)	(0.34)	0.0

OSMOTIC			FIXATION		
mosm	i_1	i_2	t(sec)	i_1	i_2
308	1.25	0.91	0	1.58	1.17
277	1.21	0.88	20	0.95	0.62
246	1.02	0.74	70	0.72	0.24
215	0.73	0.59	120	0.34	0.12

XBL7812-12399

Fig. 3

CHAPTER 3

OUTLINE: KINETICS OF GLUTARALDEHYDE FIXATION OF ERYTHROCYTES

I.   ABSTRACT

II. INTRODUCTION

A.   Chemical nature of glutaraldehyde and its application to histological fixation.

B.   Concepts of "ideal fixation."

1.   Physico-chemical criteria for stability of fixation.

2.   Role of glutaraldehyde concentration, osmolarity of the fixative media, and the stability and purity of glutaraldehyde.

III. MATERIALS AND METHODS

A.   Preparation of glutaraldehyde fixative solutions.

B.   Application of RPS to study changes in cell size and deformability: "kinetics of fixation."

C.   Observations of cell morphology with light and electron microscope.

IV. RESULTS

A.   Glutaraldehyde kinetics followed by RPS spectral changes.

1.   Fig. 1: Examples of sequential RPS spectra.

B.   Rate of glutaraldehyde fixation: role of glutaraldehyde concentration.

1.   Fig. 2: Plot of RPS peak channel vs time with variation in glutaraldehyde concentration.

C.   Changes in volume with glutaraldehyde fixation: role of fixative medium osmolarity.

1.   Fig. 3: Plot of RPS peak size vs time with variation in medium osmolarity.

D. Shape, size and osmotic resistance of erythrocytes treated with GA.

    1. Fig. 4: Morphology of GA-treated cells after osmotic stress.

    2. Fig. 5: RPS peak volume of cells treated with GA, before and after treatment with distilled water.

E. GA fixation of cells in different stages of hemolysis.

    1. Fig. 6: Morphology of red cells, with competition between hemoglobin cross-linking and osmotic lysis.

ABSTRACT

Red blood cells interact with glutaraldehyde (GA) in a complex kinetic pattern. At a given GA concentration in phosphate buffered saline (PBS), the sequence of cell "volume" response, as measured by resistive pulse spectroscopy, (RPS) includes: (1) an early response to the overall solution osmolality; (2) a constant volume, latent phase; (3) a rapid swelling phase; (4) an intermediate constant volume phase; and (5) a shrinkage phase to a final steady state volume. The final volume depends on fixative solution osmolality; for GA concentrations between 0.05% and 0.25% w/v, fixative osmolalities of greater or less than 355 mOsm, including "isotonic", lead to a final cell volume less or greater than native, respectively. Cell-membrane deformability decreases continuously and monotonically with time, as assessed by RPS. The rate of fixation is a direct function of GA concentration, in accordance with a derived empirical expression. The measured kinetics responses are related to considerations of cell size, deformability and form and applied to situations of osmotic hemolysis.

INTRODUCTION

Glutaraldehyde (GA), or pentadialdeyde, is a bifunctional protein crosslinking reagent widely used in red cell and other histologic fixative procedures (1), yet surprisingly little information is available on the kinetic details of the fixation process at the cellular level. The goal of "fixation" is to preserve or maintain cells in their original condition with respect to: (a) geometric properties such as size, morphology, and spatial relationships of internal organelles and macro-molecules; and (b) functional properties such as enzymic activity and membrane semipermeability. Along with preserving the native properties of the cell, the ideal fixative should stabilize the cell against mechanical deforming forces, decomposition with aging or autolysis, and the effects of dehydration in preparation of specimens for electron microscopy. Although no single agent or combination of agents has fulfilled all the criteria of the ideal fixative, GA has been found to possess a number of advantageous qualities.

Sabitini, et al. demonstrated that many enzymes maintain activity after GA treatment (7). Vassar, et al. studied changes of several physico-chemical properties of red blood cells after treatment with GA and other aldehydes. They reported that cells treated with 1.65% w/v GA were stabilized against osmotic hemolysis, but displayed intracellular leakage of potassium (10). We have recently reported on the preservation of drug binding characteristics and native cell electrophoretic mobility subsequent to fixation with 0.25% GA (8).

Numerous studies have focussed on changes in cell size and morphology in relationship to the composition of the GA fixative medium (e.g., 6, 1, 2), but these have been characterized by relatively slow, indirect or quantitatively imprecise means of measurement. For example, neither packed cell hematocrit nor electronic cell-sizing measures are interpretable simply as volume changes in response to GA because of the concomitant effects of decreased cell deformability.

Corry and Meiselman have recently reported on the changes in selected cellular properties of erythrocytes resulting from the uptake of small quantities of pure monomeric GA. One of their conclusions was that cells fixed with 4 mM GA in an isotonic phosphate buffered saline solution underwent no volume change as assessed by packed cell hematocrit and electronic particle sizing methods (2). We have previously reported that a hypertonic fixative medium is required for such "isovolume" fixation (8). In a Commentary, we have taken exception to the conclusion of Corry and Meiselman, and analyzed the probable basis for the discrepancy in results (5).

Here we report further "resistive pulse spectroscopy" (RPS) and other studies on interactions of low levels of GA with human red cells, with emphasis on early-time kinetic responses. Measurements include: (a) the rate of induction of volume and rigidification changes with GA penetration in the cells; (b) the effect of osmolality of fixative medium on the volume of treated cells; (c) the relationship between GA concentration and the stability of cell shape, volume, and hemoglobin

retention against osmotic stress; and (d) the use of low levels of GA to selectively fix cells in various stages of hemolysis and deformation.

MATERIALS AND METHODS

Stock Suspension Medium.

Phosphate buffered saline following Dulbecco's formula (11) was adjusted with NaCl to 306 mOsm, nominally "isotonic" medium, at pH 7.3. A series of hypotonic and hypertonic solutions was made by addition of distilled water or NaCl, respectively, in different proportions to the stock PBS. The osmolality of each solution was measured by the freezing point depression method (Fiske osmometer).

Normal whole blood from a finger lancet prick wound was directly and immediately diluted ($\geq$ 1:200) into isotonic stock PBS. This suspension served as stock for subsequent preparations of fixed cells. Stock cells were kept at 23-25° C and used within 3 hours.

Glutaraldehyde Solutions.

GA used in these experiments was supplied by Polysciences, Inc., Rydal, Pa., as a nominal 8% (w/v) electron microscope grade solution in 10 ml ampules sealed under nitrogen. A nominal 2.5% w/v GA solution was made from this stock source by addition of 15 ml distilled water and 7 ml of stock PBS to 10 ml of the stock 8% solution. This 2.5% GA solution was mixed in varying proportions with the PBS suspension media,

either prior to or after the addition of cells to the mixture, as detailed in each specific procedure.

Microscopic Observations.

A Zeiss Universal light microscope was used with both bright field and phase contrast optics to examine morphology of cells before and after fixation.

Resistive Pulse Spectroscopy (RPS).

The RPS methods of this thesis, using controlled variations of fluid flow rate, and computer control of acquisition and analysis of the pulses and spectra, were applied to yield measures of size, cell-membrane deformability, form, and membrane disruption and recovery processes. The details of the method and instrumentation are given in Chapter 4.

RESULTS

As previously reported, (4, 11), native, discoid, deformable erythrocytes have a bimodal electronic size distribution using a 48 x 48 micron diameter aperture at the "normal" flow rate (0.008 ml/sec). The sequence of spectra of Fig. 1, shows the gradual qualitative change in the pulse height distribution over time from bimodal to unimodal, as deformability is gradually lost following exposure to GA. Another kind of change observed in the RPS curves during fixation is the shift in

modal, or peak, position. Over the range of times shown in Fig. 1, the modal channel gradually increases by about 20%.

Rate of Fixation: Role of GA-Concentration.

Using methodology similar to that employed in obtaining the spectral data of Fig. 1, a series of experiments was conducted varying only the GA concentration of the suspension media. The resulting RPS spectral data are summarized by plotting the spectral peak positions versus time elapsed for each of the GA concentrations tested (Fig. 2).

The response of red cells to GA-fixation, as reflected by the modal size changes summarized in Fig. 2, follows a qualitatively similar pattern over the range of GA-concentrations studied. These qualitative sequences may be described as follows: (a) an initial, latent phase without significant changes in RPS peak size or spectral bimodality; (b) a phase of apparent volume increase during which (about midway through the phase) the bimodal shape of the distribution is lost; (c) a phase of relative size stability (plateau); and (d) a phase of apparent volume decrease to a final "steady-state" volume.

The rate of reaction is evidently accelerated with increasing GA concentration. Empirically, the expression:

$$t = 500 \exp (1.25 \, (GA\%/0.01\%)),$$

predicts for a given GA concentration (in w/v %), the time (in sec.) required from the initial mixing of cells into the fixative until the achievement of the midway point of the volume-increase phase.

In each case, the amplitude of the volume <u>increase</u> phase quantitatively exceeds the later volume <u>decrease</u>. The final, "steady-state" volume, therefore, is larger than the initial native volume. At the higher GA concentrations, the percentage of increase relative to the native volume is the greater, the smaller the amount of GA (e.g., volume increases of about 11% and 30% for 0.045 and 0.00125% (w/v) GA, respectively). For the three lowest GA concentrations, the long-time volumes are essentially identical. A sample with GA = 0.01% was measured both at normal and reduced sample flow rates, in order to differentiate the relative contributions of cell deformability and actual changes in cell volume, from the apparent, RPS, size increases observed. Size increases of 33% and 16% at normal and reduced flow rates, respectively, are seen in Fig. 2 during the volume growth phase. The physico-chemical interpretation of these various spectral changes is given in the <u>DISCUSSION</u>.

<u>Role of Osmolality of the Fixative Suspension Medium.</u>

The total percentage of RPS volume increase and the absolute "steady-state" volume are related to the osmolality of the fixative suspension medium as shown in Fig. 3.

The general pattern of response shown in Fig. 3, is similar to that described with variation of GA concentration in Fig. 2. Here, the concentration of GA remains constant, and as expected, the time of occurrence of each of the phases of RPS response is about the same, e.g., the volume increase phase occurs at between 10 and 20 seconds in

each case. The key difference between the curves at the different osmolalities is in the absolute and relative volumes at all stages of the fixation. As expected from considerations of osmotic driving forces, the higher the fixative osmotic pressure the lower the measured volume of the cells.

The fixative medium osmolality determines the early-time baseline level of cell volume. The action of fixation, per se, is reflected by the temporal changes, or dynamic activity, in the peak position curves of Fig. 3. It turns out that the combination of these effects leads in general to a final "steady-state" volume significantly different from the early "latent" phase volume. We have previously reported, based in part on data such as that presented in Figs. 2 and 3, that red cells fixed under conventional (including nominal "isotonic") conditions have end volumes different from the native volume. We further reported that to fix the cells at a volume equal to the initial native volume using low GA concentrations required the relatively hypertonic fixative medium of 355 mOsm. Fig. 3 shows that at "isotonic" conditions (or other osmolalities $<$ 355 mOsm), final fixed volumes are greater than native, whereas for osmolalities $>$ 355 mOsm, the reverse is true.

Shape, Size and Osmotic Resistance of Erythrocytes Treated With GA.

Erythrocytes treated with various low levels of GA were subsequently observed, prior to and after, osmotic stress with distilled

water, according to the following protocol. Stock cells (0.1 ml) were
added to a series of fixative solutions (10 ml each) composed of stock
PBS and GA diluted to final concentrations in the range between 0.5 and
.0008% w/v GA. The suspensions were incubated at room temperature in
the fixative solutions for 20 minutes and then observed by light micro-
scopy and RPS analysis. Finally, the cells were sedimented by desk-top
centrifugation, the supernatant removed, the cells resuspended in dis-
tilled water and then reexamined under the microscope. The cells were
also reanalyzed with RPS, which required readjusting the distilled water
suspension medium to 150 mOsm, to provide adequate conductivity for the
transducer to function properly.

Photomicrographs of representative cells are shown in Fig. 4.

The RPS volumes of the GA traeated cells prior to and after osmotic
challenge with distilled water are summarized in Fig. 5.

The findings displayed in Fig. 5 may be correlated with those in
Fig. 4: at GA concentrations of 0.007% and higher, the cells tend to
retain both their basic biconcave discoidal shape and, roughly, their
native volume, both before and after distilled water stress. (The
larger apparent fixed-cell volume results from the isotonic fixation
conditions). At about 0.0035% GA, cells are somewhat swollen, both by
observation and RPS measurement, even before distilled water treatment;
they tend to become larger with the osmotic stress, but nevertheless, do
not hemolyze. With 0.0018% GA, the cells are microscopically normal,
and prior to stress by distilled water have a bimodal RPS distribution

and peak size similar to those of native untreated cells. After dis-
tilled water stress, the cells are observed to retain a generally intact
spherical shape, but to have lost most of their hemoglobin. They are
significantly decreased in RPS size, and have lost their RPS bimodality.

GA Fixation of Cells in Various Stages of Hemolysis.

We have previously reported on the appearance of cells fixed by
optimum concentrations of GA in the process of expulsion of hemoglobin
induced by osmotic hemolysis (11). Here we present further aspects of
the application of selected low concentrations of GA to observe cells in
differing stages of hemolysis. Basically, the method consists of adding
native red cells to fixative solutions composed of hypotonic PBS in the
hemolytic range, with differing amounts of GA added. Three key stages
are shown in Fig. 6.

The cells in Fig. 6a have been described previously (11); they are
believed to represent the normal lesion of abrupt osmotic hemolysis
rather than a GA-induced artefact. With somewhat lower GA (0.125%) the
critical balance of Hb crosslinking achieved with 0.25% GA is lost; the
cells are able to reseal the membrane lesion while apparently retaining
most of their hemoglobin (Fig. 6b). With further reduction of GA to
0.0625% most of the hemoglobin has escaped the cells before adequate GA
crosslinking of remaining intracellular hemoglobin has had time to
occur. We know from earlier-described studies that 0.0625% GA is more
than adequate to stabilize cells against even distilled water challenge,
if adequate time of fixation is given prior to the osmotic stress.

Hence, we have good evidence, as previously argued, that the semipermeability properties of red cells are well retained after treatment with low levels of GA, although the cells may become rigid due to gelation of intracellular hemoglobin by the crosslinking action of the fixative.

Flow Induced Deformation of Ghosts.

GA was used to fix cells (ghosts) in a state of deformation induced by their passage at high velocity through the RPS sensing aperture as follows: stock red cells were mixed into 10 ml of hemolytic medium composed of 104 mOsm PBS, and the suspension directly passed through the transducer aperture (48 micron diameter and length) at a sample flow rate of about 0.008 ml/sec (about 4.4 m/sec linear velocity). Immediately prior to the pumping of the cells through the aperture, the inner or "exit" compartment of the aperture was filled with a solution of .25% GA in 104 mOsm PBS. The cells were subsequently collected from the inner compartment, and observed by phase contrast microscopy. For a control comparison, a repeat experiment was run in which the osmotically hemolysing cells were fixed in a 0.25% GA solution of 104 mOsm PBS without passing through any aperture. The results indicated clearly that the cells fixed upon passage through the aperture were considerably distorted and flattened, in comparison with those fixed without the hydrodynamic flow stresses.

DISCUSSION

Interpretation of RPS Spectral Measurement of GA Effects on Cells.

We have previously reported on certain differences in the RPS spectral characteristics of GA treated cells compared to native cells. The bimodal shape of the pulse height distribution was demonstrated to be the result of the unique tendency for native, deformable, discocytic cells to traverse the aperture cross section in two principal flow regions. Cells rigidified with GA were shown to have a reduced tendency to traverse in the longer transit time, higher electric field wall region, resulting in spectra unimodal rather than bimodal in shape (4, 11).

We have also discussed the role of cell form, or "shape factor," on the measured pulse amplitude. Thom et al. has shown that cells flowing at a typical normal flow rate through the transducer aperture were deformed to a prolate ellipsoidal form (9). In principle, a decrease in the degree of deformation will always accompany a reduction in the deforming shearing forces. As we also reported previously, the native cell should be no more deformed than the GA rigidified cell, if the bulk fluid flow is sufficiently reduced. To our knowledge, there have been no systematic studies of differential deformation of cells with reduction of bulk fluid flow rate through the aperture other than our own (11).

The RPS spectral changes demonstrated in Figures 1, 2 and 3, thus represent shifts originating in a combination of actual volume change, cell-membrane deformability, and changes in cell shape factor. The contribution of deformability-associated shape factor changes is assessed by comparing the RPS measurements at normal and reduced sample flow rates (when the amount of flow-induced deformation is minimized). For example, in Fig. 2, the peak channel responses of cells to 0.025% GA in the volume increase phase of the fixation process were 32% and 16% at the normal and slow sample flow rates, respectively. We conclude that at normal flow, an apparent size increase of about 16% occurs due to rigidification and the associated increase in cell shape factor, and that the additional 16% represents actual volume increase. The increase of 16% observed at the slow flow rate, thus represents an actual volume increase. This is evidently contrary to the "no volume change" proposal of Corry and Meiselman (2), as previously discussed (5).

The entire complex pattern of RPS peak changes would also be difficult and unreasonable to explain solely in terms of changes in shape factor due to cell rigidification. Specifically, the late fixation phase of apparent volume decrease is more plausibly explained as an actual volume decrease than as a decrease, at that time period, in cell rigidity. Two possible explanations for an actual late shrinkage phase include: (a) coagulation or precipitation of the intracellular contents by a critical degree of crosslinking; or (b) a net outward leakage of intracellular ions, or decreased internal colloidal concentration due to the crosslinking, resulting in an osmotic outflow of water and shrinkage of the cell.

Regardless of the exact chemical reaction occurring between the
cell constituents and GA, the data presented provide strong evidence
that the ultimate fixed volume of the cells is highly dependent on the
concentration of the fixative, and more importantly, on the overall
osmolality of the fixative solution. To sum up our previous abbreviated
report (4), as elaborated herein: isotonic fixative solution leaves the
cells in a relative swollen state; a hypertonic fixative solution of
about 355 mOsm is required to fix the cells with low GA concentrations
at a volume equal to the native (at about 306 mOsm).

The other experiments described in this report tend to substantiate
our previous findings suggesting that the hemoglobin crosslinking action
of GA is separable from its effects on membrane function, specifically
on membrane semipermeability properties. At the critical concentration
of (0.0035%) GA, the cells were stabilized against osmotic lysis but
were still able to swell, perhaps due to a perturbation of the membrane-
intracellular contents relationship. In the experiment adding intact
cells to hemolytic solutions containing decreasing amounts of GA, it was
demonstrated that a competition occurs between the rates of intra-
cellular hemoglobin crosslinking, and of osmotic swelling and lysis.
At least a 0.25% concentration of GA is required to fix the intrac-
ellular contents faster than the cell can burst osmotically.

With the lower concentrations of GA, some stabilization of the intra-
cellular hemoglobin occurs, but most of it is expelled, and the membrane
proceeds to reseal in a gross fashion, before the GA fixation activity
has been able to take maximal effect.

The experiment of GA fixation of ghosts upon rapid passage through the aperture further supports the concept that significant shearing-force-induced deformation occurs during flow of the cell through the aperture.

REFERENCES

1. Arborgh, B., Bell, P., Brunk, U. and Collins, V. P., The osmotic effect of glutaraldehyde during fixation. A transmission electron microscopy, scanning electron microscopy and cytochemical study, J., Ultrastruct. Res., 56, 339-350, 1976.

2. Corry, W. D. and Meiselman, H. J., Modification of erythrocyte physico-chemical properties by millimolar concentrations of GA, Blood Cells, In Press, 1979.

3. Hopwood, D., Theoretical and practical aspects of glutaraldehyde fixation, Histochem. J. 4, 267-303, 1972.

4. Mel, H. C. and Yee, J. P., Erythrocyte size and deformability studies by resistive pulse spectroscopy, Blood Cells, 1, 391-399, 1975.

5. Mel, H. C. and Yee, J. P., Commentary on the Corry and Meiselman paper on glutaraldehyde effects, Blood Cells, In Press, 1979.

6. Morel, F. M., Baker, R. F. and Wayland, H., Quantitation of human red blood cell fixation by glutaraldehyde, J. Cell Biol., 48, 91-100, 1971.

7. Sabitini, D. D., Bensch, K. and Barnnett, R. J., Cytochemistry and electron microscopy. The preservation of cellular ultrastructure and enzymatic activity by aldehyde fixation, J. Cell Biol., 19-58, 1963.

8. Tenforde, T., Yee, J. P. and Mel, H. C., Electrophoretic detection of reversible chlorpromazine·HCl binding at the human erythrocyte surface, Biochem. Biophys. Acta., 511, 152-162, 1978.

9. Thom, R., Hampe, A. and Sauerbrey, G., Die elektronische Volumenbestimmung von Blutkörperchen und ihre Fehlerquellen, Z. Gesamte Exp. Med., 151, 331-339, 1969.

10. Vassar, P. S., Hards, J. M., Brooks, D. E., Hagenberger, B. and Seaman, G. F., Physico-chemical effects of aldehydes on the human erythrocyte, J. Cell Biol., 53, 809-818, 1972.

11. Yee, J. P. and Mel, H. C., Cell membrane and rheological mechanisms: dynamic osmotic hemolysis of human erythrocytes and repair of ghosts, as studied by resistive pulse spectroscopy, Biorheology, 15, 321-339, 1978.

Fig. 1 - GA Kinetics Spectral Sequence: RPS spectra of RBCs (0.10 ml of stock cell suspension) mixed at time t = 0 seconds, into a fixative solution composed of 0.1 ml of 2.5% GA and 10 ml of stock PBS (final GA concentration about 0.025%). Each curve represents a 64-channel spectrum resulting from the accumulation of pulses generated during a 10 second interval of cell sampling, with the relative number of cells, or pulses (ordinate), plotted against pulse size (channel number). The net elapsed time at the end of each collection interval is indicated for each spectrum. The sample flow rate was 0.008 ml/sec. with a 48 micron diameter aperture, and 200 microamp current source.

Fig. 2 - Rate of GA-Fixation: The RPS spectral peak channel (Modal size) is followed over elapsed time (semilogarithmic plot) for fresh stock red blood cells added at t = 0 to fixative solutions of nearly constant (isotonic) osmolality but of differing GA concentrations. The solutions consisted of stock PBS (10 ml) with appropriate amounts of 2.5% GA added to give final concentrations of 0.045, 0.01, 0.005, 0.0025 and 0.00125% w/v GA, respectively. Except for the uppermost, dashed curve, which resulted from use of a slower sample flow rate, about 0.0025 ml/sec, all other curves were obtained with a normal flow rate of about 0.008 ml/sec. The small horizontal arrows indicates the time point and apparent size at which the spectral bimodality is essentially lost. (For sequence of Fig. 1, this occurs at about 100 sec.)

Fig. 3 - RPS Volume Kinetics as a Function of Fixative Medium Osmolality:
Fresh red blood cells (0.1 ml of stock solution) were added at time
t = 0, to 10 ml of each fixative solution with a final GA concentration
of 0.045%. The osmolality of each solution is denoted to the right of
each curve. The RPS spectral peak channels are plotted on a logarith-
mically compressed time scale. Point C represents the initial native
unfixed RBC volume, C' the equivalant rigidified-cell volume, as deter-
mined from slow flow measurements (8). (Normal sample flow rate, 48 x 48
micron aperture.)

Fig. 4 - Morphology of Erythrocytes Treated With GA and then Challenged
With Distilled Water: Cells preincubated (a) in 0.007%; (b) 0.0035% and
(c) 0.0018% w/v GA, then suspended in distilled water. (Phase contrast
optics.)

Fig. 5 - RPS Volume of Cells Pretreated With GA Before and After Sub-
sequently Being Subjected to Distilled Water Stress.

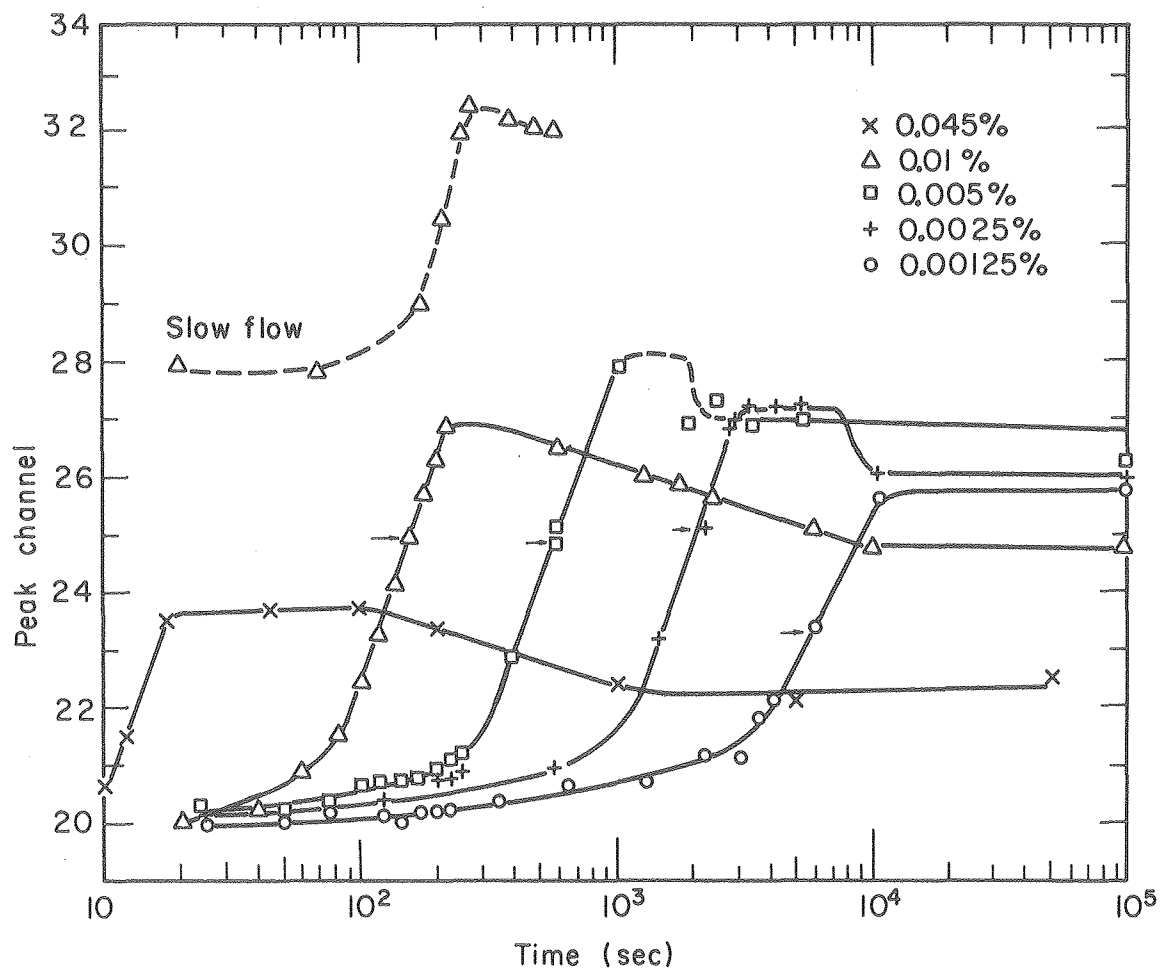Fig. 6 - Morphology of Cells Fixed With Differing Amounts of GA During
the Hemolytic Process: Fresh native cells (0.1 ml) were added into
hypotonic (104 mOsm PBS) fixative solutions containing: (a) 0.25%;
(b) 0.125%; and (c) 0.0625% w/v GA.

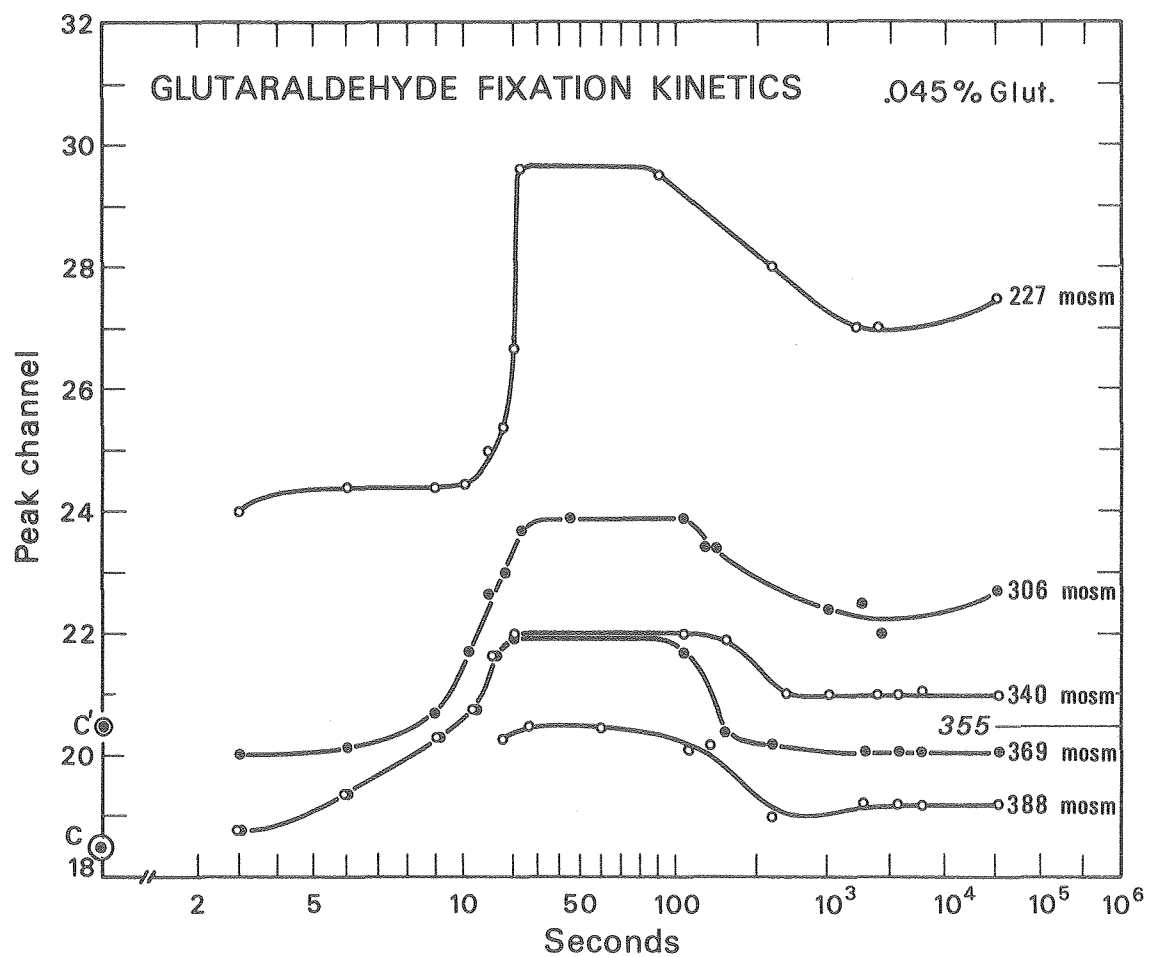## KINETIC SEQUENCE - 10 sec intervals
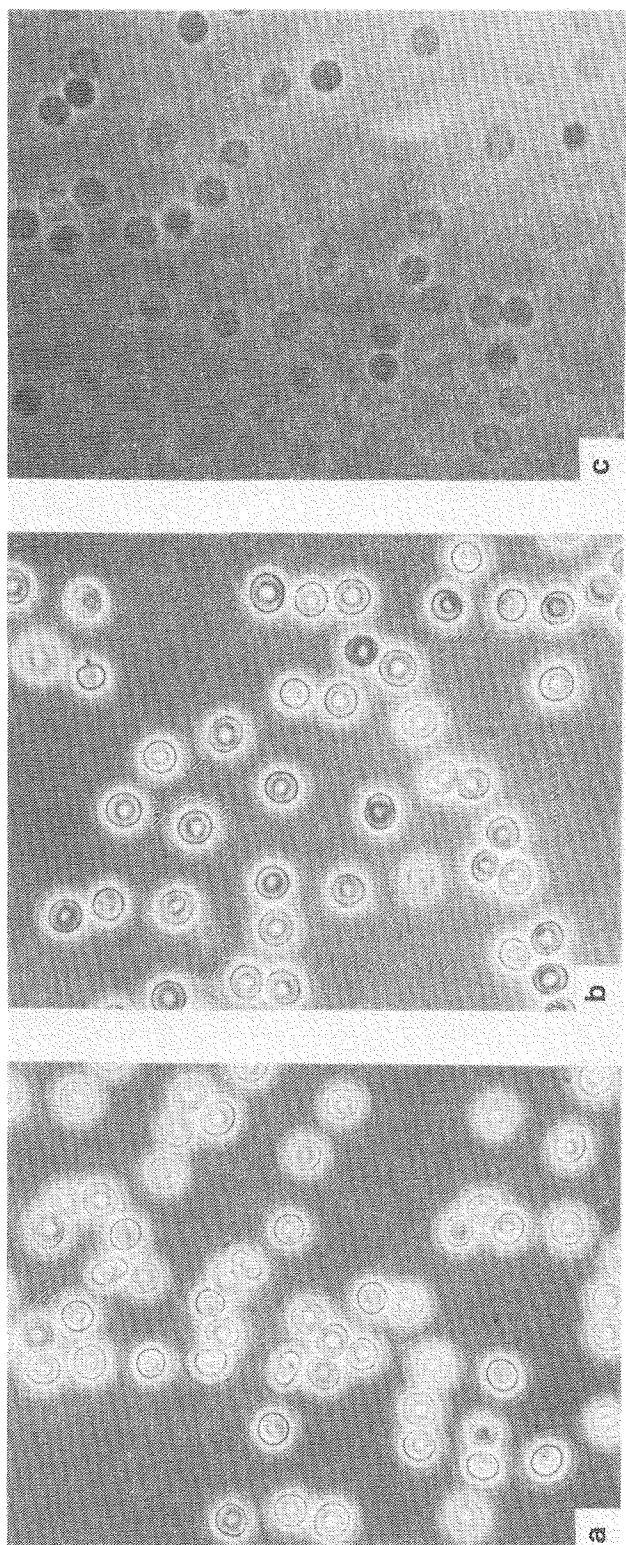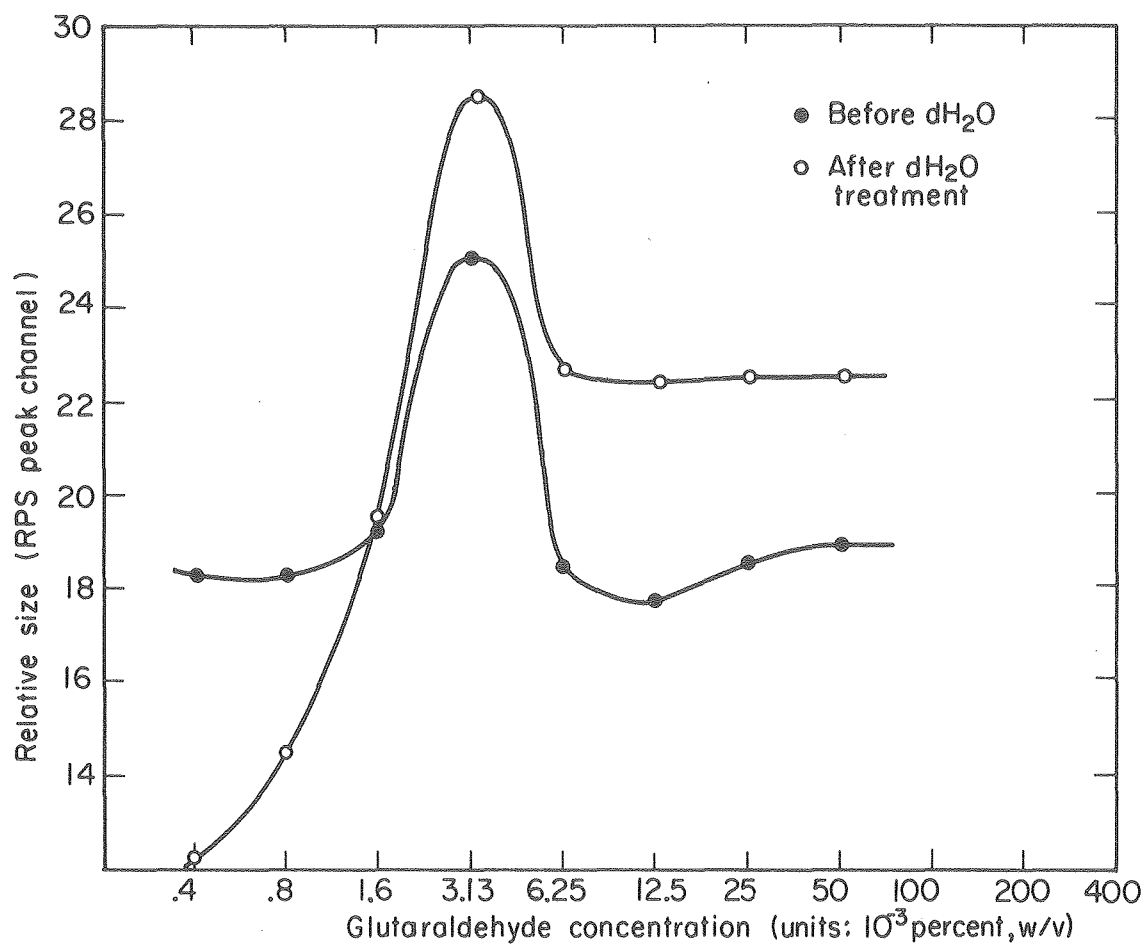### (Glutaraldehyde fixation)
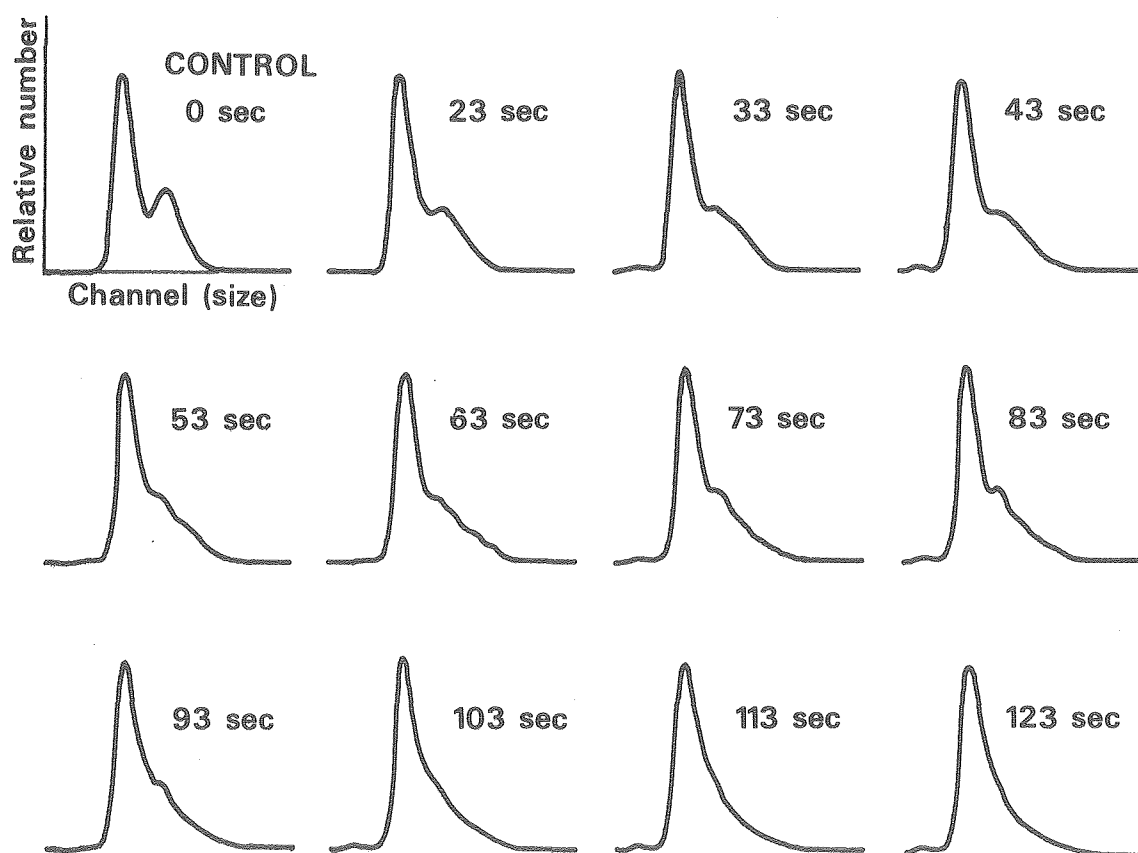
DBL 745-4792A

Fig. 1
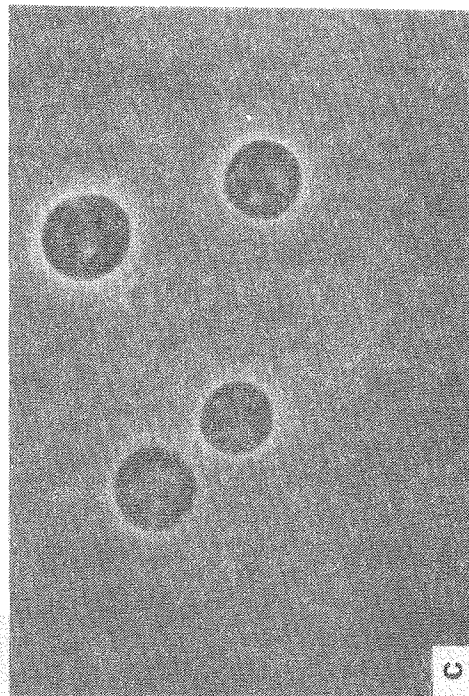
Fig. 2

XBL762-5180

Fig. 3

DBL 745-4790A
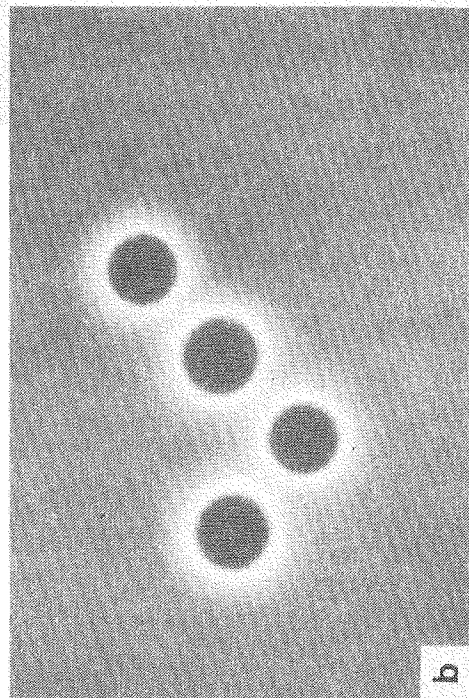
Fig. 4

Fig. 5
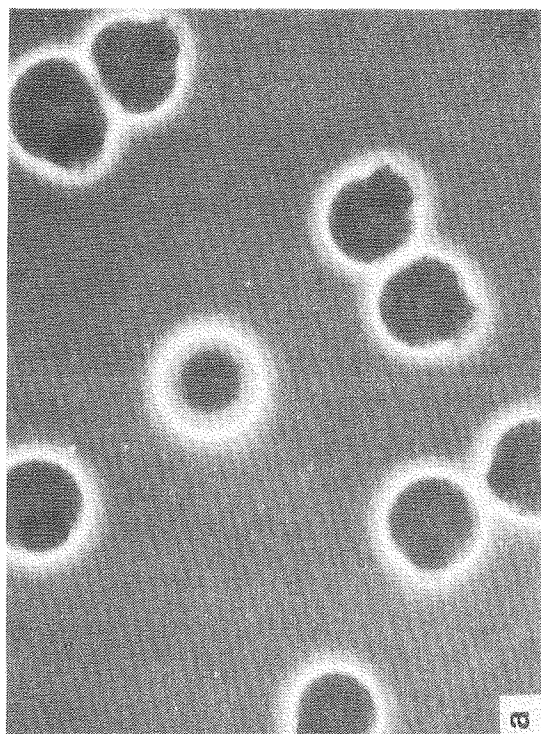
Fig. 6

CHAPTER 4

OUTLINE: CELL-MEMBRANE AND RHEOLOGICAL MECHANISMS: DYNAMIC
OSMOTIC HEMOLYSIS OF HUMAN ERYTHROCYTES AND REPAIR OF GHOSTS

I.   ABSTRACT

II. INTRODUCTION

    A.   Review of previous investigations of hemolysis.

    B.   Overview of the "resistive pulse spectroscopy" (RPS) method
        of studying hemolysis.

III. MATERIALS AND METHODS

    A.   Preparation of red cells, ghosts, glutaraldehyde and the
        suspension media.

    B.   Instrumentation: Fig. 1: Schematic of the RPS system.

    C.   RPS kinetics: data collection and analysis.

IV. RESULTS

    A.   Hemolytic lesion and critical volume.

        1.   Fig. 2: Views of hemolysing red cells.

        2.   Fig. 3: Prehemolytic swelling of red cells.

    B.   Kinetic studies on intact cells and ghosts.

        1.   Fig. 4: Pulse subpopulation analysis.

        2.   Fig. 5: Rate of hemolysis.

        3.   Table 1: Rate of ghost formation.

        4.   Fig. 6: Rate of ghost repair.

        5.   Size and deformability of intact cells and ghosts.
            Fig. 7: RPS-measured size dependence on flow rate.

        6.   Fig. 8: RPS spectra of restored ghosts and intact cells.

        7.   Analysis of individual pulse forms.

            a.   Fig. 9: Oscilloscope pulse tracings.

            b.   Table 3: Summary of pulse characteristics.

V. DISCUSSION

    A. The hemolytic lesion and action of glutaraldehyde.

    B. Dynamic osmotic hemolysis.

    C. Repair of the osmotic lesion.

    D. Relative size and deformability of ghosts compared to intact cells.

    E. Cell shape and deformability.

    F. Intrinsic membrane and internal viscosity properties and deformability.

    G. Rehemolysis.

    H. Summary

ABSTRACT

Normal human erythrocytes undergoing abrupt osmotic hemolysis display a single, transient, localized circular rupture over 15 to 20% of their total surface area. An immediate and striking drop in apparent volume for such cells, as measured by electronic "sizing" using resistive pulse spectroscopy (RPS), is ascribed primarily to a greatly increased, flow-induced, cell-membrane deformation and associated expulsion of ghost contents rather than to an intrinsic property of hemolysis per se. The time and flow-rate dependence of the RPS spectra measure the rates of ghost formation and repair of the hemolytic lesion in the membrane. Restored ghosts rehemolyze at a critical volume and lesion size similar to those of the original lysing cells. Membrane rather than cytoplasmic (internal viscosity) properties dominate deformability measured from RPS spectral shape.

INTRODUCTION

Mechanisms involved in the failure of the red blood cell membrane
under osmotic stress, and in its recovery, are of interest in a
variety of pure and applied biomedical areas. Although such osmotic
hemolysis has long been studied (1), many aspects of the phenomenon
have remained unclear. Cells subjected to osmotic hemolysis have
been variously reported to leak selectively (2-4), to burst suddenly
(5,6) or to do both (7). The different experimental conditions used
by different observers render any simple generalization of mechanism
difficult. In a recent review, Seeman leaned toward a local-lesion
interpretation but indicated that the question was still not settled
(8). Baker and Gillis (9) used glutaraldehyde treatment to trap
up to 80% of cells in a state of local hemolysis. Although their
microscopic pictures could be taken as evidence of a local-lesion
event occurring during normal osmotic hemolysis, these investigators
believed instead that these observations represent a glutaraldehyde-
chemical artifact.

The technique of resistive pulse spectroscopy (RPS) (10) offers
new opportunities to study hemolytic mechanisms and membrane properties
per se (11). We report herein new results on the following: (a)
the nature and size of the lesion in abrupt osmotic hemolysis; (b)
the kinetics of formation of ghosts from intact cells swollen to
critical volume; (c) the dynamics of ghost-membrane lesion recovery
and repair; and (d) the osmotic, rheological, and rehemolyzing properties
of isotonically restored ghosts. In all of this work, glutaraldehyde

(GA) responses of both intact cells and ghosts play an important role.

RPS is based on the extension of conventional Coulter-type electronic-sizing principles (12). An individual cell, as it traverses a current-limiting aperture in a dilute suspension, generates a single resistive pulse. The height or magnitude of the pulse is commonly taken as proportional to the volume of the nonconductive cell, and hence is used as a measure of cell size. The pulse height distributions, or spectra, accumulated from the sampling of thousands of cells require only a few seconds of time. These spectra have been widely interpreted as representative of cell population volume distributions (13).

This interpretation is now recognized to be oversimplified, for the pulse height also depends in a complex way on cell deformability and shape (10, 14-17). The role of these factors is elaborated upon in the DISCUSSION. Unlike other electronic sizing systems which attempt to suppress or eliminate factors not related to cell size, RPS analysis focuses on such features to evaluate cell deformability and shape, in addition to more clearly interpreting the actual size distribution. This requires intercomparison of RPS spectra obtained with controlled variations in sample flow rate and in rigidification procedures using GA.

MATERIALS AND METHODS

Sample Preparations

Erythrocytes and suspending media. Phosphate buffered saline
(PBS) following Dulbecco's formula (in mg/l: 100 $CaCl_2$, 200 KCl,
200 KH_2PO_4, 100 $MgCl_2 \cdot 6H_2O$, 8000 NaCl, 1150 $NaH_2PO_4 \cdot 2H_2O$) was adjusted
with NaCl to a 300 mOsm, nominal "isotonicity" at pH 7.3. Normal
whole blood from a finger lancet prick wound was directly and immedi-
ately diluted ($\geq$ 1:200) into the isotonic PBS. This blood suspension
served as stock for subsequent preparations of hemolysing cells and
ghosts. Except for specific in vitro aging studies, stock cells were
kept at 23-25°C and used within 3 hours. A series of hypotonic buf-
fered saline solutions was made by addition of distilled water to
different proportions of stock PBS. The osmolality of each solution
was measured by the freezing point depression method (Fiske osmometer).

Ghosts. Restored, or "reconstituted," ghosts are the spontaneously
self-repaired membranes derived from red blood cells that have lost
most of their hemoglobin during hemolysis and have been subsequently
returned to isotonicity (18, 19). To prepare such restored ghosts
we added 0.10 ml of intact stock cells, concentrated by centrifugation,
to 10 ml of 120 mOsm PBS. After 10 minutes at 23°C, 0.10 ml of this
ghost suspension was returned into an excess (10 ml) of isotonic PBS.
To create "rigid" restored ghosts, glutaraldehyde was added to the
restored ghosts, as described below.

Glutaraldehyde. A nominal 2.5% w/v glutaraldehyde (GA) solution
was made by the addition of 15 ml distilled water and 7 ml of stock
PBS to 10 ml of 8% w/v glutaraldehyde. The 8% electron microscope
grade glutaraldehyde solution was supplied by Polysciences, Inc. in
10 ml ampules sealed under nitrogen. The 2.5% GA solution was mixed
.(1:10) with the various tonicity buffered saline solutions to achieve
a net 0.25% w/v GA in the final fixative media. The addition of the
GA was done either prior to or after mixing cells into the PBS, as
is detailed in each specific procedure.

Instrumentation

The RPS system is shown schematically in Fig. 1, and consists
basically of the following:

Transducer and signal generation. The aperture (nominal 48 micron
diameter, and 48 micron length, Particle Data Inc.) is formed by a
circular right cylindrical bore through a ruby jewel. This jewel
is embedded in the wall of a glass tube so that the aperture is the
sole pathway connecting the fluid compartments on either side of the
glass tube. The aperture is also the sole current pathway between
a pair of platinum electrodes.

Flow rate control and calibration. A pressure drop across the
aperture forces a dilute cell suspension through the aperture. A
vacuum (pump) source controls the negative pressure. For a uniform
suspension of constant cell concentration, we find that the fluid
flow rate is linearly proportional to the pressure gradient across

the aperture. (Number of cells counted/time is equal to K x ΔP, where K is a constant dependent upon the cell concentration, and ΔP is the pressure drop determined by a mercury manometer.)

The cell concentration is determined by counting the number of cells in a known volume, using a volumetric manometer. The cell suspension is then counted for a specified time interval (e.g., 10 sec) at a constant flow rate, and the absolute volume flow rate calculated: (ml/sec) = (cells/sec)/(cells/ml). The flow rates used in these studies include the range between a normal flow of 0.008 ml/sec and "slow flow" of 0.0025 ml/sec. The designation "normal flow" for the higher flow rate is chosen because this corresponds closely to the single fixed rate used in conventional Coulter-type electronic counting apparatus. Using the calculated flow rate and the geometric dimensions of the aperture, we compute the mean linear velocity $\bar{v}$ (cm/sec) = volume flow rate (cm^3/sec)/cross-sectional area of the aperture (cm^2) = 442 (cm/sec). The average transit time τ = geometric length l(cm)/$\bar{v}$ (cm/sec) = 11.7 x 10^{-6} (sec), for the 48 micron aperture and the normal flow rate.

Constant current source. The calibrated current supply has seven steps between 13 and 1450 microamps. A current of 200 microamps was used for these studies on red blood cells. A zero-input impedence amplifier detects the small current displaced by the passage of the nonconductive particle through the current-limiting aperture. A current change of 1 microamp results in a 12.1 mV output from the pre-amplifier.

Pulse height analysis. The voltage signal is further amplified
to appropriately scale the signal for peak (height) detection and
for analog to digital conversion. A voltage threshold control sup-
presses low amplitude noise signals. For each pulse height over
the discriminator threshold, the digitalized value corresponding to
cell "size" is read into the memory of an on-line computer (PDP 8/I,
Digital Equipment Corporation) under program control. A series of
pulse heights corresponding to cells passing through the aperture
is collected over a specified time interval to create a cell population
"volume" distribution or spectrum.

Individual pulse forms. The individual pulses corresponding
to single cells traversing the aperture were observed with a Tektronix
oscilloscope, Model 545A with 53/52 L amplifier, displaying signal
voltage versus time. In order to study the detailed characteristics
of these pulses, the tracings were photographically recorded with
a Tektronix C-12 oscilloscope camera, using Polaroid Type 107 3000
ASA speed film.

Computer program control. In brief, the RPS program is an original,
real-time pulse height analysis program providing flexible computer-
controlled acquisition of sequential pulse height data generated by
the electronic sizing apparatus. Preselected time intervals of data
collection are regulated by referencing a crystal oscillator time
clock. As data accumulate, the resultant corresponding pulse height
spectrum is displayed on an oscilloscope.

The data analysis capabilities of the RPS program are manifold. The more or less standard statistical analysis parameters include computation of RPS spectral mean, mode, standard deviation, coefficient of variation, and third moment. Integral numbers in populations or subpopulations are also available on user command. A specially adapted numerical analysis subroutine which gives a polynomial best-fit to the raw data points has been incorporated in order to provide: (a) spectral data "smoothed" by best-fit criteria, (b) computation of spectral maxima and minima based on the first derivative of the curve, and (c) an index based on parameters derived from the first derivative of the spectrum, which characterizes the degree of "bimodality" of the spectrum.

The entire RPS program requires about 8000 bytes (with 12 bits/byte) in the PDP 8/I computer. Currently, an additional 24,000 bytes of memory are being used for data storage.

Input and output devices. The user primarily designs and modifies the collection and analysis of data by entering, via a teletype keyboard, control parameters into the program (e.g., the time interval over which data is to be collected and the number of consecutive spectra to be accumulated.) A Hewlett-Packard X-Y plotter is employed to print out spectra such as those seen in Fig. 4. Permanent tape records are made by a high-speed paper tape punch. For subsequent analysis, these tapes may be re-read into the computer memory by a high-speed paper tape reader.

RPS Kinetics

The kinetics of hemolysis were studied by combining cells, hypotonic salines, and glutaraldehyde fixative in differing time sequences. For example, we rapidly mix a 0.10 ml aliquot of the stock red blood cell suspension into a 10 ml 125 mOsm hypotonic solution. While this mixture is reacting, representative cells are continuously sampled by the aperture-transducer. The pulses thus collected into the first data region, e.g., over the first 5 seconds, comprise a "volume" spectrum representative of the cell population for that initial time interval; successive sequential volume spectra represent corresponding subsequent time intervals. Repeat cell samples, using variations of sample flow rate through the transducer and/or with addition of glutaraldehyde fixative, produce series of spectra useful in interpreting temporal changes in cell and ghost volume and deformability.

RESULTS

Hemolytic Lesion and Critical Volume

We present here a simple procedure to effectively arrest red blood cell populations in predictable stages of swelling and lysis, including up to 100% undergoing lysis. Cells added to a 104 mOsm PBS solution, containing 0.25% glutaraldehyde are captured in the act of local lysis (0.1 ml stock cell suspension was added to 10 ml of fixative solution made up of 1 ml of 2.5% GA and 9 ml of 104 mOsm PBS; Fig. 2).

Microscopic measurements made on 33 of the "neonate" ghosts (see Fig. 2A) indicate that the lunar surface areas corresponding to the hemolytic lesion occupy about 19% of the total surface area, i.e., a lesion area of 27 ± 6μ^2(s.d.), based on an initial total surface estimated to be 140 μ^2 (20)

An independent measure of volume of these swollen, GA-fixed hemolyzing cells is obtained from RPS. These cells are found to be equal in RPS-measured, or apparent, size to maximally swollen intact cells just prior to hemolysis. Another comparison shows that the critically swollen cells have an RPS volume that is 2.3 times larger than the apparent volume of biconcave native cells in isotonic solution. As indicated in the DISCUSSION, the RPS apparent volume must be corrected with cell shape factor considerations. When this is done, the corrected volume of critically swollen cells is 1.67 rather than 2.3 times that of native cells. (Herein, it is understood that RPS volume is a raw, uncorrected, experimental volume, unless otherwise specified.)

Fig. 3 depicts cells exposed to prehemolytic, hypotonic solutions containing GA. These show no microscopically observable lesion or evidence of hemoglobin leakage, and no observable differences in swelling or surface morphology, from cells not treated with GA.

Kinetic Studies on Intact Cells and Ghosts

Subpopulation analysis. The dynamic behavior of the cell and
ghost subpopulations is shown in the selected spectra of Fig. 4.
A dramatic and nearly instantaneously induced size drop of neonate
ghosts, compared to critically swollen intact cells, is clearly seen
in Fig. 4A. Microscopic counts on these sample suspensions and on
others prepared with compositions ranging from 0 to 100% in ghosts
confirm that the "smaller" of the two subpopulations, as measured
by RPS, corresponds to ghosts (most distinct in Fig. 4A-C).

Rate of ghost formation. The fraction of lysed cells (ghosts)
in the whole population is determined from estimates of the relative
numbers of counts ("cells") in the two RPS subpopulations. The pro-
portion of ghosts at a given elapsed time is dependent upon the initial
condition of the cells and on the osmolality of the lytic solution.
For fresh cells added to 125 mOsm PBS at time zero, the fraction of
ghosts at subsequent time intervals is given in Table 1.

TABLE 1

Initial Rate of Ghost Formation

Elapsed time (sec)	Percent ghosts
16	35
24	44
32	52
40	55
48	58
56	61
64	62
72	63

Over this early time interval the percentage of ghosts is seen to be leveling off at about 54%. That is, about 64% of the total cell population is susceptible to early hemolysis, with 36% of the population being relatively resistant. The percentage of ghosts, at any instant, is found to be independent of flow rate.

For the susceptible subpopulation (64% of the total) the data from Table 1 have geen recalculated as shown in Fig. 5. The early hemolysis evidently follows a first order reaction mechanism, with a half life of 14 seconds.

Ghost size and recovery rate. We determined ghost recovery from the time change of the RPS-measured ghost peak. The ghost peak was seen to move upwards toward the intact cell peak with increasing time (e.g., Fig. 4A-D). The ratio of apparent volumes, V_a(ghost)/V_a(critically swollen cell) was minimal early in the posthemolytic period (about 0.60, based on the subpopulation peaks given in Fig. 4a). The repeat preparation using a reduced sample flow rate shows a substantially reduced apparent volume loss for the ghosts (Fig. 4a-d). A physical interpretation of the ghost recovery process in terms of volume expulsion and membrane lesion considerations is given in the DISCUSSION.

The flow rate dependence of apparent ghost recovery is conveniently summarized by plotting the peak, or modal, volume of the ghosts vs time (Fig. 6). At the reduced flow stress, the ghost recovery reaches a plateau in about 150 seconds, while at the higher flow rate, greater than 400 seconds are required for such stabilization.

Ghost osmotic repair. The osmotic volume responsiveness of the
ghosts was evaluated by challenging them osmotically at different
posthemolytic times (Table 2). The ghosts were prepared by mixing
fresh cells into an excess of 100 mOsm PBS solution at time zero.
Small aliquots of the resultant ghost preparation were taken sequentially
and returned to an excess of 300 mOsm PBS. Each of these samples
was allowed an additional 10 minutes subsequent to the osmotic challenge
prior to RPS sizing. This delay was provided in order to minimize
effects of ongoing mechanical repair, as reflected in Fig. 5.

TABLE 2

Osmotic Volume Responsiveness of Ghosts

Time elapsed posthemolysis (sec)	Percent decrease of relative volume[b] following osmotic challenge ("ideal" decrease = 67%)
15	66
93	71
410	73
60[a]	50

[a]Ghosts fixed with 0.25% GA, as per Fig. 4B (dashed line).

[b]Uncorrected for shape factors.

Assuming that the intracellular contents of the initial ghost
rapidly achieve a diffusion equilibrium with the external lytic medium
(18), the "ideal" osmotic volume response of a completely resealed
ghost may be simply calculated as $V_1/V_2 = \pi_2/\pi_1$, where where V_1 and

π_1 are the initial ghost volume and external osmotic pressure, respectively, and V_2 is the final ghost volume in response to the external osmotic pressure π_2. Here, $\pi_2/\pi_1 = 0.33$, implying a 67% volume decrease of the ghosts for a change in external medium from 100 mOsm to 300 mOsm. We see that the RPS-measured unfixed ghost volume is not far from the ideal at any posthemolytic time. The differences in response may be related to incomplete diffusion equilibration at very early times. Other RPS measurements show that GA-fixed ghosts retain significant osmotic responsiveness (last line in Table 2).

Relative size and deformability of intact cells and ghosts. As noted earlier, ghosts are most susceptible to deformation early after hemolysis. The high deformability of young ghosts (e.g., at 24 seconds posthemolysis) in comparison to intact swollen cells is demonstrated by examining the apparent size of each over a range of flow rates (Fig. 7).

The fixed vs unfixed ghost apparent sizes (Fig. 4B and b) provide additional evidence for the large deformability of early ghosts. When the cell-membrane deformability was greatly reduced with GA, the ghost population at normal flow appeared to be much closer in size to the intact cell population.

Restored ghosts. Fig. 8A provides a comparison of "fresh" restored ghosts to glutaraldehyde rigidified ghosts prepared as described in MATERIALS AND METHODS above. When observed microscopically, both kinds of ghosts are biconcave discoids which are low in hemoglobin

content, as microscopically evaluated by their markedly reduced absorption of light in the Soret band wavelength (~415 nm). For comparison, Fig. 8B shows the RPS spectra for intact native cells.

Individual pulse forms. Representative pulse forms generated from the passage at normal flow rate of fresh native and GA-fixed cells are shown in Fig. 9. The predominant form in both samples is bell shaped. The most striking difference between the samples is the presence of some relatively large, flat-topped forms for native deformable cells, and the complete absence of these for the GA-rigidified cells. Slow-flow pulse forms (not shown in Fig. 9) for both samples are similar, and tend to be all flat-topped with greater than 30 to 40 microsecond duration.

A summary of the characteristics of such pulse oscillographs is given in Table 3. The average amplitude of the long flat-topped pulses is about 1.5 times greater than the mode amplitude of bell shaped pulses. This ratio corresponds to the ratio of peak positions of the bimodal curve seen in Fig. 8B, for fresh intact native cells. The time duration of the modal pulse form for both native and GA-fixed cells is roughly 16 to 20 microseconds. This is longer than the calculated physical transit time of about 10 microseconds because the cell is detected electrically while it is still outside of the geometric borders of the aperture.

TABLE 3

Summary of Pulse Trace Characteristics[a]

	Pulse form	Percent	(Average amplitude)/ (modal amplitude[b])	Pulse duration (μsec)
Native red cells	flat-top	5-10	1.5	30-40
	bell	90-95	1.0	16-20
GA-fixed red cells	bell	100	1.05	16-20

[a] Average values based on more than 100 pulses.

[b] Modal amplitude of bell-shaped pulses from native cells.

DISCUSSION

An integrated analysis of the above described experimental findings gives a fairly complete view of the sequence of events associated with the process of osmotic hemolysis.

The Hemolytic Lesion and Action of Glutaraldehyde

The initial localized lesion is relatively large, but very transient. It was by use of an appropriate glutaraldehyde concentration and time sequence that we were able to capture the cells in the act of hemolysis. The expulsion of intracellular contents through the membrane lesion site (Fig. 1) is arrested by the transformation of the free hemoglobin solution to a GA-crosslinked gel. Glutaraldehyde, or pentadialdehyde, is a bifunctional protein crosslinking reagent widely

used in histological fixation procedures. GA-treated red cells are mechanically rigidified by the formation of covalent amide bridges with the lysinyl or 3-amino groups of valine in the intracellular hemoglobin, and in the membrane-associated proteins. Another example of the use of GA to capture red cells in a normally transient state is its recent application to "freeze" the cells in the temporary state of deformation induced by turbulent shear flow (21).

Several important cell membrane properties are unaltered by GA treatment, as shown by the present work and other studies. Considered all together, these findings not only help to define the action of GA, but they also provide convincing evidence that the localized circular lesion is real rather than an artifact of GA. Evidence for the mild action of GA includes the following:

1. Preservation of semipermeability. The GA-arrested hemolysing cells (Fig. 2) have RPS and microscopically measured volumes equal to the maximal critical volume achieved by untreated cells prior to hemolysis. This implies that the influx of osmotically driven water in the GA-treated cell was not impaired. Further, the ghosts retain osmotic responsiveness subsequent to GA-treatment, i.e., they shrink and swell in response to changes in salt concentration in the external medium (Table 2). Though GA-treated intact cells, such as seen in Fig. 3, by inference probably also retain membrane semipermeability, their shape and volume are firmly fixed due to the much higher concentration of intracellular hemoglobin serving as substrate for the GA. Semipermeability may not be completely retained

under all conditions of GA-fixation; Vassar et al. have reported

leakage of intracellular potassium by intact cells about 1 hour after

fixation with 1.65% GA (22).

2. RPS evidence for an abrupt lesion. The initial presence of a

large hemolytic lesion is independently evidenced by the RPS spectra

of neonate ghosts. The observed spectrum (Fig. 4A) is consistent

with the expected reaction to compressional forces of a membrane-

bounded sphere with a large surface lesion. A large opening would

allow expulsion of volume with associated deformation, and would

thus explain the small apparent size of the neonate ghosts. The

critically swollen intact cell is unable to deform without volume

expulsion because the surface to volume ratio of a sphere is already

at a minimum, and the membrane is essentially inextensible (23).

Furthermore, we have also collected ghosts which passed through the

aperture directly into a fixative solution. Microscopically they

appear flattened and deformed in comparison to ghosts left in free

suspension.

3. Noninterference of GA with drug binding and surface charge.

Tenforde, Yee, and Mel have recently reported that neither pre- nor

postfixation of red cells with GA affected the reversible binding

of the drug chlorpromazine HCl (24). The GA also had no effect on

the electrophoretic mobilities either for the native cells, or for

the reduced-mobility drug-treated cells. (Chlorpromazine·HCl is

a cationic phenothiazine agent which can induce a reversible stomato-

cytic morphological change in the red cell.)

Dynamic Osmotic Hemolysis

The large difference in RPS-size between early ghosts and swollen intact cells, at normal flow rate, allows the computation of a rate of hemolysis as shown in Table 1 and Fig. 5. The percentage of hemolysed cells calculated from the RPS spectra is consistent with the values obtained by conventional spectrophotometric osmotic fragility methods, e.g., both methods show that for normal cells 50% hemolysis occurs with hypotonicities of about 130 to 140 mOsm. In addition to estimating the steady state level of hemolysis, the RPS method can characterize the initial rate of hemolysis or "dynamic" osmotic fragility of the cell sample. A parameter such as the half life of the most labile subpopulation may serve as a sensitive measure of cell-membrane condition, not evident from studies of steady state levels of hemolysis. Other advantages of the RPS dynamic osmotic hemolysis method include, (a) speed: the measurement requires only a few minutes; (b) simplicity: determination of the percentage of lysis does not require an exact dilution, and less than 1 microliter of blood is sufficient sample; (c) rates of recovery can also be followed, as discussed below.

Repair of the Lesion

It has been known since at least 1952 (25), that erythrocyte ghosts reseal after the hemolytic event and then behave as osmometers. Studies of the repair process, however, have been limited by the general complexity, indirectness, or cumbersomeness of the methodologies

employed. Seeman et al. estimated that the lesion remains open for
10 to 180 seconds after the exposure of the cells to the hypotonic
medium. These values were the limits of the time interval over which
relatively large solutes such as ferritin, were able to diffuse into
the posthemolytic cells (26). Bodemann and Passow evaluated membrane
resealing by following the permeability of small labelled alkali
ions, such as ^{86}Rb (19). They found that for most of the ghosts,
the membrane leakiness to the ions decreased as early as 1 minute
posthemolysis, but that a significant subfraction did not achieve
resealing until as late as 30 minutes posthemolysis.

We believe that new insights on effective repair mechanisms
are to be gained by following the increase in apparent ghost peak
volume after hemolysis (Fig. 6). Our interpretation is that as ghosts
progressively repair or reseal, they become less deformable in response
to external flow stresses encountered during RPS sampling. In support
of this explanation are the RPS observations on ghosts at reduced
flow rate and with GA-fixation: (a) with a reduction in the deforming
stresses associated with the reduction in flow rate, the relative
extent of ghost size reduction is decreased, and the rate of recovery
is accelerated (Fig. 6); and (b) when the ghosts are fixed with GA
at 60 seconds elapsed time (Fig. 4B), the flow stress no longer
induces volume expulsion and deformation. (As discussed earlier,
however, GA-fixed ghosts are not so rigid that all osmotic responsiveness
is lost.)

The minimum size for the ghost subpopulation occurs at about 25 seconds elapsed time rather than near zero time (Fig. 6). The delayed minimum may occur because of one or more of the following: (a) the lesion is present near zero time, but has not become maximally enlarged or weakened until about 25 seconds; (b) the earliest cells to lyse have a somewhat smaller lesion than cells lysing subsequently; (c) the subfraction of cells lysing prior to 25 seconds is volumetrically larger than cells lysing subsequently. Regardless, the repair process is well under way by no later than 30 seconds, as reflected by the increasing apparent size of the ghosts. The repair progresses most rapidly initially, and then gradually approaches a relative plateau of recovery.

Although the repairing lesion appears to be vulnerable to the mechanical deforming stresses encountered during flow through the aperture for at least 400 seconds posthemolysis, an effective osmotic barrier of the neonate ghosts seems to re-establish much more quickly, i.e., within 10 to 60 seconds following the lytic event. This was demonstrated by testing volume responses of ghosts exposed at specific times to changes in external salt concentration. As was shown in Table 2, both early ghosts (15 sec posthemolysis), and older ghosts (> 400 sec posthemolysis), behaved functionally as osmometers when challenged with changes in external osmotic concentration. Furthermore, when ghosts are treated immediately after hemolysis with addition of GA, no gross membrane lesion is microscopically observable. Together, these findings suggest that a mechanically weak, but osmotically functional resealing process occurs within about 15 seconds posthemolysis,

whereas the effective mechanical strength of the resealing membrane increases progressively for at least 400 seconds.

Our explanation is contrary to several other previous interpretations of the electronically measured repair events. Based on the limited technical capabilities then available, Weed and Bowdler reported that the ghost volume becomes intrinsically small due to the collapse of the cell following hemolysis (27). The subsequent ghost volume increase was attributed to osmotic reswelling due to colloidal effects of residual intracellular hemoglobin. Our measurements would attribute a loss of intrinsic (i.e., nonflow-induced) volume to be limited to 5 to 10%. (This is based on the RPS size of young ghosts treated with GA and measured at slow flow rate. The GA-fixation is required, because as discussed below and in Fig. 7, native ghosts are significantly deformed even at slow flow.)

Seeman et al. proposed that the small electronic size of ghosts was the result of a temporary electrical short-circuit caused by hemolysis. During repair, the cell membrane would regain its electrical resistive properties and thus appear to reswell in size (28). This electrical, or more properly, dielectrical, breakdown of the membrane has been recently demonstrated experimentally at very high current densities (29), but not at the lower current, such as we have used here. Gear has proposed that the lower electrical resistance of ghosts manifested above the critical current density provides a suitable method for electronically measuring osmotic fragility (30). Interestingly, ghosts which are presumably well repaired after 30 minutes, do not

show any reduction in their tendency for dielectric breakdown, suggesting that this measurement is insensitive to the repair processes we have demonstrated.

Repair evidently has many varieties and is of many facets. In addition to a more detailed understanding of its structural aspects, the individual roles of relevant metabolic species such as Ca^{++}, Mg^{++}, and ATP also remain to be established.

Relative Deformability and Size of Ghosts Compared to Intact Cells

In electronic particle sizing methods, the measured, or apparent, size of the cell is dependent not only on the actual volume of the cell, but also on the transit time, trajectory, and shape of the cell in the aperture (14-17, 31). As given in MATERIALS AND METHODS, with normal sample flow rate, the cell has a mean physical transit time of 10 to 15 microseconds. Empirically, our findings (Fig. 9) indicate that the electrical capacitance associated with the transducer requires the cell transit time to be about 30 microseconds or more for the corresponding electrical signal to develop completely. Thus at normal flow the sizing signal is not fully developed. As the flow rate is reduced, the electrical cutoff of signal amplitude diminishes, and the measured modal size increases (Fig. 7).

However, not all cells traverse the aperture with the same trajectory. Cell trajectory and associated orientation are important because of the irregularities of hydrodynamic and electrical fields associated with a short aperture of about 50 micron length and diameter

(14-16). Differences in cell trajectories help to provide an under-lying physical explanation for the bimodal "size" distribution of native intact red cells obtained with normal flow rate (Fig. 8Ba).

The true volume distribution of the cells is known by microscopic measurements to be unimodal. The bimodal distribution obtained at the normal sample flow rate results from the unique tendency for deformable, biconcave (at rest) cells to travel in two principal flow regions of the aperture cross section. The majority of cells traverse in the central, high-velocity low shear gradient, lower electrical field region of the hydrodynamic flow stream. These cells with shorter transit times are of smaller "size" due to the electrical cut off of signal size and also to the lower electric field strength (principle peak in Fig. 8Ba).

A smaller number of cells traverses in the low velocity, high shear gradient, higher electric field, wall region of the aperture. These cells with longer transit times have fully developed, larger signals, thus accounting for the second peak at channel 28, Fig. 8Ba. In contrast, red cells rigidified by GA lose the tendency to traverse in the longer transit time wall region, with the result that the bimodal shape of the cumulative pulse spectra is lost (Fig. 8Ba).

These interpretations of the origin of the bimodal cumulative spectra are directly supported by the results of the individual pulse analysis presented in Fig. 9 and Table 3.

Cell Shape and Deformability

Independent of these electrical features, the shape of the cell while in the aperture also influences the size of the signal generated (14, 31). At a given flow rate, the true cell volume, V_t, is related to the measured, or apparent volume, V_a, by a correcting shape factor, γ, which is defined by the orientation and shape of the cell while in the sensing field of the transducer, $(V_a = \gamma \cdot V_t)$. For example, the shape factor is 1.5 for a sphere, 1.2 for a biconcave discoid, and 1.0 for an elongated propate ellipsoid, each with its major axis aligned in the direction of fluid flow. By laser-flash photography, Thom has shown that native biconcave red cells are deformed into prolate ellipsoids aligned with the direction of flow, as they pass through an aperture similar to ours (14). With decreased flow stress, less deformation should occur, and the shape factor γ should increase from about 1 towards 1.2, and the apparent volume would accordingly increase.

With the above considerations at hand, we surmise that Coulter-type electronic size can be independent of flow rate only if: (a) the transit time of the cell is adequately long for complete development of the electrical signal; (b) the shape factor, γ, of the cell is constant; and (c) the trajectory of the cell through the aperture does not vary significantly with flow rate. These conditions are evidently met by intact cells in the flow range between 0.004 and 0.0025 ml/sec, as reflected by the plateau region seen in Fig. 7.

Ghosts, in contrast, do not satisfy all of these requirements at any flow rate in the range we have studied. Since the transducer electrical cutoff characteristics are the same as for intact cells, the steeper linear dependence of ghost size on flow rate must be primarily caused by significant deformation continuing in the low flow range, below 0.004 ml/sec. This is consistent with the existence of a minimally repaired lesion that we have postulated at 24 seconds elapsed time. Such deformation is also reasonable, considering that the absolute flow stress, even at 20% of normal flow, is still quite high.

In Table 4 we summarize the deformability and shape information derived from examining relative peak position shifts, with change from normal flow to slow flow. The relative contributions to peak shift of electrical response time and cell deformation factors can be separated in the case of completely rigid particles such as the GA-fixed intact biconcave RBC. Since the true size and shape of these fixed cells does not change with flow rate, the observed upward peak shift of about 15% must be attributed entirely to the longer time, allowing for complete signal development at reduced flow. The electrical response conditions remain constant for all the specimens measured. Peak shifts in excess of 15% are therefore attributable to increases in cell shape factor, associated with decreased cell deformation or, in the case of ghosts, with decreased volume expulsion.

Some conclusions that may be drawn from Table 4 include: (a) critically swollen intact cells behave as rigid particles; i.e.,

TABLE 4

Deformability: Change in Shape Factor with Decreasing Flow Rate

	Total upward peak shift (%)	Electrical contribution (%)	Contribution of shape factor (%)	Shape Factor	
				normal flow	slow flow
(a) GA-fixed biconcave RBCs	15	15	0	1.2	no change
(b) Critically swollen RBCs	15	15	0	1.5	no change
(c) Native RBCs	28	15	13	1.1	increases
(d) Restored repaired ghosts	35-42	15	20-27	1.0	increases
(e) GA-fixed restored ghosts	20-25	15	5-10	1.0	increases
(f) Unrestored neonate ghosts	83-88	15	68-73	1.0	increases
(g) "Repaired" unrestored ghosts	50-55	15	35-40	1.0	increases

(a) from Fig. 8B; (b) from Fig. 7; (c) from Fig. 8B; (d) from Fig. 8A;

(e) from Fig. 8A; (f) from Fig. 6; (g) from Fig. 6.

they undergo no shape changes with flow rate; (b) young ghosts are

by far the most deformable of all specimens tested; (c) repaired

ghosts continue to be significantly more deformable than intact cell

specimens; and (d) GA-fixed restored ghosts, shown in Table 2 to

be osmotically responsive, also appear to change shape with reduced
flow rate. However, as discussed below, other measurements indicate
that significant membrane rigidification does exist in the GA-fixed
ghost.

Intrinsic Membrane and Internal Viscosity Properties, and Deformability

The deformation of a red cell undergoing surface shearing forces
is dependent on both the intrinsic deformability of the membrane
and on the fluidity of the internal contents. For steady state
viscometric evaluations of RBC deformation, the viscosity of intracellular
contents relative to that of the external medium has been reported
to be the dominant factor (32). Our RPS evidence is that for the
two kinds of spectral changes we measure that can be directly linked
to changes in deformability, one is determined primarily by membrane
properties, the other by internal viscosity properties.

The most evident qualitative RPS feature associated with deforma-
bility is the "bimodal" shape of the spectra. In earlier discussion,
a physical explanation was presented for this bimodal RPS size distri-
bution, for native intact cells at normal flow. For restored ghosts,
the dependences of the RPS volume distribution on flow rate and on
GA-fixation are very similar to those of the native intact cells
(compare Figs. 8A and 8B.) The similarity of the bimodality spectral
feature, shown to be dependent on deformability, holds despite an
approximately sevenfold greater internal viscosity in the intact
cells than in the ghosts. (An intact cell containing 34 g% hemoglobin
has an internal viscosity of about 7 cp compared to about 1 cp for

the restored ghost in the PBS suspending medium (33).) This implies
that, of the two deformability factors, it is the intrinsic membrane
properties (similar in the two samples) that dominate over the relative
viscosity.

The restored ghosts not only behave in this same manner as do
hemoglobin-filled intact cells in the native state, but they are
also seen to become similarly "rigidified" by GA-treatment, as evaluated
by RPS-spectral shape changes (Figure 8A). Presumably, therefore,
the membrane-associated proteins, such as spectrin (perhaps aided
by the small amounts of residual hemoglobin in the restored ghosts)
provide adequate substrate for the crosslinking action of GA to result
in the conversion of the RPS bimodal spectral shape to a unimodal
one, just as occurs with intact cells. We infer from this that the
configuration of membrane-associated structural proteins plays a
major role in the deformability of the cell as a whole. This finding
is entirely consistent with the report on local membrane deformability,
as measured by the micropipette technique, that as litle as 0.009%
w/v GA causes a doubling of the elastic shear modulus of ghost as
well as intact red cell membranes (34).

In contrast to this membrane related result, there is evidence
of a different kind of deformability effect in the "peak-shift" data
in Table 4. Both GA-treated and untreated restored ghosts are seen
to have greater shape-factor associated peak shifts with decreased
flow rate than do intact cells. The larger value of this kind of
deformability measure for the ghosts is most reasonably attributed

to their considerably reduced internal viscosity in comparison to that of intact cells.

To obtain a bimodal RPS-spectral shape at normal flow rate, the overall biconcave discoidal shape of the unstressed intact cell or restored ghost seems to be required, in addition to the local deformability of the membrane substance. For example, although the hemolysing cells discussed in Figure 4 have been argued to be highly deformable because of the surface hemolytic lesion, the RPS spectral shape of the ghost subpopulation is unimodal. Furthermore, as intact cells approach a more spherical form due to swelling in a hypotonic solution (e.g., Fig. 3B), they too tend to lose the bimodality feature of RPS-spectral shape. Such partially swollen cells would not be expected to have a significant increase in local intrinsic membrane rigidity, and the lowering of internal viscosity by the dilution of intracellular hemoglobin should increase the deformability rather than decrease it.

Rehemolysis

In further investigations of the posthemolytic repair processes, we have used RPS to follow the response of isotonically restored ghosts when they are subsequently re-exposed to hypotonic solutions. We find that as the external salt concentration is reduced below the original lytic osmotic composition, the repaired ghosts reach a critical volume very nearly the same as the original intact cell critical volume, and then they lyse again. The ensuing "neonate II" ghosts have a flow-induced volume drop measured by RPS comparable

to the original volume difference between swollen cell and ghost seen in Fig. 4A. Based on the equivalence of the initial and secondary critical volumes, we infer that the original hemolysis and repair of the membrane lesion occurred without significant change in membrane surface area. The similarity of the early, minimum volumes may also be considered evidence of the similarity in size of the lesion in the two instances. The rate of repair of the hemolysis is, however, observed to be slower in the second recovery series.

Summary

We have presented new findings on the events involved in the hemolytic process for osmotically stressed normal red blood cells. The RPS techniques used to characterize the rates of ghost formation, the flow rate and glutaraldehyde dependence of spectral size and shape, and the rates of repair of the lesion are currently being applied to studies of changes in cell-membrane properties associated with various pathophysiologic conditions and with the effects of exogenous chemical agents, including pharmaceutical products and environmental pollutants.

REFERENCES

1. PONDER, E. Hemolysis and Related Phenomena. New York: Grune and Stratton, 1948, reprinted 1971.

2. HEEDMAN, D. A. Hemolysis of individual red blood cells. An interferometer microscopic investigation. Exp. Cell Res. 14, 9-22, 1953.

3. KATCHALSKY, A., KEDEM, O., KLIBANSKY, C., and DEVRIES, A. Rheological considerations of the haemolysing red blood cell. In: Flow Properties of Blood, pp. 155-171. Oxford: Pergamon Press, 1960.

4. MACGREGOR, R. D. and TOBIAS, C. A. Molecular sieving of red cell membranes during gradual osmotic hemolysis. J. Membr. Biol. 10, 345-356, 1972.

5. COMANDON, J. and DE FONBRUNE, P. Contribution à l'étude du mecanisme de l'hémolyse. Arch. Anat. Micros. Morphol. Exp. 25, 555-570, 1929.

6. KOCHEN, J. A. Structural disturbances during red cell lysis. Am. J. Dis. Child. 104, 537-538, 1962.

7. DANON, D. Osmotic hemolysis by a gradual decrease in the ionic strength of the surrounding medium. J. Cell. Comp. Physiol. 57, 111-117, 1961.

8. SEEMAN, P. Ultrastructure of membrane lesions in immune lysis, osmotic lysis and drug-induced lysis. Fed. Proc. 33, 2116-2124, 1974.

9. BAKER, R. G. and GILLIS, N. R. Osmotic hemolysis of chemically modified red blood cells. Semin. Hematol. 5, 170-178, 1968.

10. MEL, H. C. and YEE, J. P. Erythrocyte size and deformability studies by resistive pulse spectroscopy. Blood Cells 1, 391-399, 1975.

11. YEE, J. P. and MEL, H. C. Cell membrane responses during dynamic osmotic hemolysis. Biophys. J. 16, 219a, 1976.

12. COULTER, W. H. High speed automatic blood cell counter and cell size analyses. Proc. Nat. Electron. Conf. 12, 1034, 1956.

13. BRECHER, G., JAKOBEK, E. F., SCHNEIDERMAN, M. A., WILLIAMS, G. Z., and SCHMIDT, P. J. Size distributions of erythrocytes. Ann. N. Y. Acad. Sci. 99, 242-261, 1962.

14. THOM, R., HAMPE, A., and SAUERBREY, G. Die elektronische Volumenbestimmung von Blutkörperchen und ihre Fehlerquellen. Z. Gesamte Exp. Med. 151, 331-349, 1969.

15. GROVER, N. B., NAAMAN, J., BEN-SASSON, S., and DOLJANSKI, F.
     Electrical sizing of particles in suspensions. III. Rigid spheroids
     and red blood cells. Biophys. J. 12, 1099-1117, 1972.

16. SHANK, B. B., ADAMS, R. B., STEIDLEY, K. E., and MURPHY, J. R.
     A physical explanation of the bimodal distribution obtained by
     electronic sizing of erythrocytes. J. Lab. Clin. Med. 74, 630-
     641, 1969.

17. GREGG, E. C. and STEIDLEY, K. D. Electrical counting and sizing
     of mammalian cells in suspension. Biophys. J. 5, 393-405, 1965.

18. HOFFMAN, J. F., EDEN, M., BARR, J. S., and DEDELL, R. Hemolytic
     volume of human erythrocytes. J. Cell Comp. Physiol. 51, 405-
     414, 1958.

19. BODEMANN, H. and PASSOW, H. Factors controlling the resealing
     of the membrane of human erythrocyte ghosts after hypotonic
     hemolysis. J. Membr. Biol. 8, 1-26, 1972.

20. CANHAM, P. B. and BURTON, A. C. Distribution of size and shape
     in populations of normal red cells. Circ. Res. 22, 405-422,
     1968.

21. SUTERA, S. P. and MEHRJARDI, M. H. Deformation and fragmentation
     of human red blood cells in turbulent shear flow. Biophys. J.
     15, 1-10, 1975.

22. VASSAR, P. S., HARDS, J. M., BROOKS, D. E., HAGENBERGER, B., and SEAMAN, G.V.F. Physiochemical effects of aldehydes on the human erythrocyte. J. Cell Biol. 53, 809-818, 1972.

23. LACELLE, P. L., EVANS, E. A., and HOCHMUTH, R. M. Erythrocyte membrane elasticity, fragmentation, and lysis. Blood Cells 3, 335-350, 1977.

24. TENFORDE, T., YEE, J. P., and MEL, H. C. Electrophoretic detection of reversible chloropromazine•HCl binding at the human erythrocyte surface. Biochim. Biophys. Acta 511, 152-162, 1978.

25. TEORELL, T. Permeability properties of erythrocyte ghosts. J. Gen. Physiol. 35, 699, 1952.

26. SEEMAN, P. Transient holes in the erythrocyte membrane during hypotonic hemolysis and stable holes in the membrane after lysis by saponin and lysolecithin. J. Cell Biol. 32, 55-70, 1967.

27. WEED, R. I. and BOWDLER, A. J. Metabolic dependence of the critical volume of human erythrocytes: Relationship to osmotic fragility and autohemolysis in hereditary sperocytosis and normal red cells. J. Clin. Invest. 45, 1137-1149, 1966.

28. SEEMAN, P., SAUKS, T., ARGENT, W., and KWANT, W. O. The effect of membrane-strain rate and of temperature on erythrocyte fragility and critical hemolytic volume. Biochim. Biophys. Acta 183, 476-489, 1969.

29. ZIMMERMAN, U., PILWAT, G., and RIEMANN, F. Dielectric breakdown of cell membranes. Biophys. J. 14, 881-899, 1974.

30. GEAR, A.R.L. Erythrocyte osmotic fragility: Micromethod based on resistive-particle counting. J. Lab. Clin. Med. 90, 914-928, 1977.

31. KACHEL, V. Basic principles of electrical sizing of cells and particles and their realization in the new instrument "Metricell." J. Histochem. Cytochem. 24, 211-230, 1976.

32. BESSIS, M. and MOHANDAS, N. Deformability of normal, shape-altered and pathological red cells. Blood Cells 1, 315-321, 1975.

33. CHIEN, S., USAMI, S., DELLENBACK, R. J., and GREGERSON, M. I. Shear-dependent deformation of erythrocytes in rheology of human blood. Am. J. Physiol. 219, 136-142, 1970.

34. HEUSINKVELD, R. S., GOLDSTEIN, D. A., WEED, R. I., and LACELLE, P. L. Effect of protein modification on erythrocyte membrane mechanical properties. Blood Cells 3, 175-182, 1977.

FIGURE LEGENDS

Figure 1

Schematic representation of RPS system.

Figure 2

Views of hemolysing red blood cells.

2A. Hemolysing RBCs, phase-contrast photomicrographs (about x 1850). This composite of segments from three fields of hemolyzing RBCs is chosen to display different aspects of the hemolytic lesion. A single, localized, circular rupture is seen for all hemolyzing cells. Essentially all cells in the fields observed were in the erupting condition. The mean cell volume estimated from optical measurements of diameters is about 150 μ^3.

2B. Scanning electron microscope (SEM) views, composite of three SEM fields taken from similar samples, selected to include some intact cells. Considerable shrinkage occurs during the dehydration and critical-point drying, but the localized rupture is clearly preserved. The "wrinkled skin" appearance of the hemolyzing cells can be contrasted with the "taut skin" appearance of the critically swollen intact cells, attributable to the greater (artifactual) shrinkage of the ghosts.

Figure 3

Prehemolytic swelling of RBCs.

RBCs were added to solutions composed of 0.25% glutaraldehyde and

(a) 300 mOsm or (b) 210 mOsm phosphate buffered saline (0.1 ml stock
cell suspension added to 10 ml of 0.25% GA, hypotonic saline.) The
classical biconcave morphology is most evident at 300 mOsm. With
increasing hypotonicity the cells approach a more spherical shape.
Note the degree of uniformity in shape between individual cells in
each preparation, and the absence of membrane surface lesions.

Figure 4

Kinetics of hemolysis.

Fresh stock RBCs mixed at zero time with hypotonic PBS (5×10^5 cells/ml,
140 mOsm, pH 7.3) were followed by RPS spectra taken in a continuous
sequence of 5 second measurement intervals under automatic program
control. These separate intact-cell and ghost subpopulations are
identified in Fig. 4A. The dynamic behavior of the subpopulations
is more evident with normal sample flow rate (0.008 ml/sec) as shown
in the selected specta, A-D. The end-interval times (in seconds)
and peak "size" positions are indicated for each of the 64 channel
spectra. Both the number and the apparent size of the ghosts increase
with time (see A-D). The strong dependence of the spectra on flow
stress is seen in the lower sequence a-d, from a repeat preparation
using a reduced sample flow (0.0024 ml/sec). The subpopulations at
this lower flow rate are much less separated in apparent size. As
with normal flow, the ghost subpopulation appears to blend upward
into the intact cell population with increasing time.

In separate, repeat experiments, glutaraldehyde was rapidly added
at elapsed time t = 60 seconds (final GA concentration = 0.25%).

These fixed cells (dashed curves B and b) correspond to the unfixed cells at this time interval (solid curves B and b).

Figure 5

Rate of hemolysis.

Semilogarithmic plot of the lysis of the early-time susceptible sub-population vs the time elapsed since exposure to the lytic medium. The RPS data were collected at 8 second time intervals and with a normal sample flow rate.

Figure 6

Rate of ghost repair.

The RPS size (modal channel) of the ghost subpopulation is plotted vs time, for normal and slow sample flow rates (lower and upper curves, respectively). In this particular example, cells were added to 140 mOsm PBS after being stored for 24 hours in isotonic PBS at room temperature. Qualitatively similar results are seen for fresh blood, however.

Figure 7

RPS-measured size dependence on flow rate.

The apparent modal sizes of swollen intact cells (upper curve) and 24 sec old ghosts (lower curve) are plotted vs relative sample flow rate (1.0 = normal flow). The apparent volume of intact cells is linearly dependent upon flow rate until reaching a flow-independent

RPS size, at about 50% of normal flow. Ghost volumes, in comparison, have a greater dependence on flow between 100% and 50% of normal flow, and they continue to be linearly dependent down to 20% of normal flow rate or lower. These data are based on RPS spectra for cells exposed to 125 mOsm PBS.

Figure 8

RPS spectra of ghosts and intact cells.

8A. Restored ghosts. The RPS-spectra are given for "native" restored ghosts at normal and slow flow (a) and (a'), and comparable fixed restored ghosts (b) and (b'). (Peak channels and mean values are designated.)

8B. Native, intact RBCs. The same qualitative spectral forms as seen in Fig. 7A have previously been observed for native and GA-fixed biconcave erythrocytes (10) (reprinted by permission from Blood Cells 1, 39, 1975).

Figure 9

Oscilloscope pulse tracings.

9A. Native RBCs. Fresh cells were suspended in 300 mOsm stock PBS, with final cell concentration about 5×10^6 cells/ml.

9B. GA-fixed RBCs. Stock fresh cell suspension (0.1 ml) was added to 10 ml of fixative solution made up of 1 ml of 2.5% GA and 9 ml of 355 mOsm PBS.
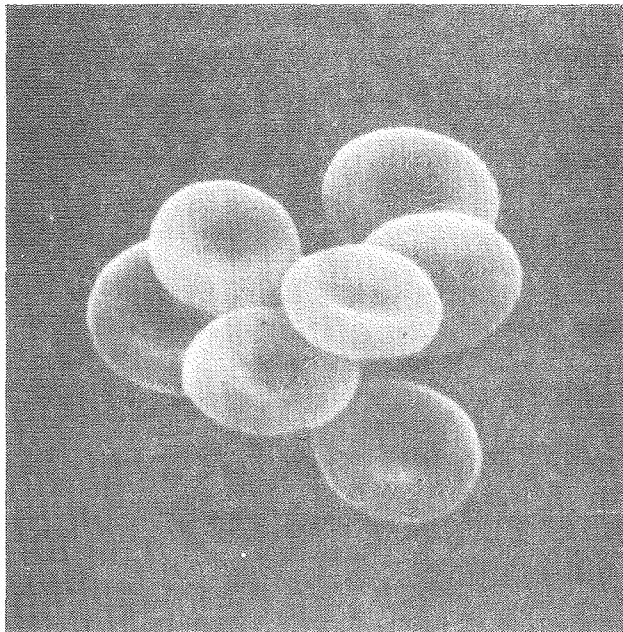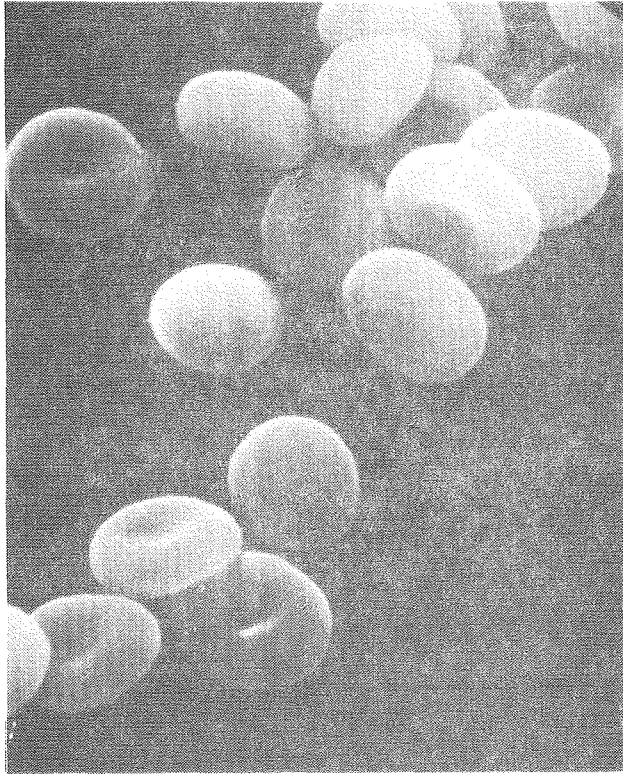
TRANSDUCER   PULSE HEIGHT ANALYSIS   COMPUTER CONTROL

| Flow rate control | | Threshold control | | Oscilloscope: individual pulse forms | | | Input/ output devices |

| Cell Suspension | | Aperture | | Signal Amplifier | | Analog-Digital Converter | | PDP 8/I Computer |

| Constant current source | | | Peak detector | | | | Oscilloscope display of RPS spectra |
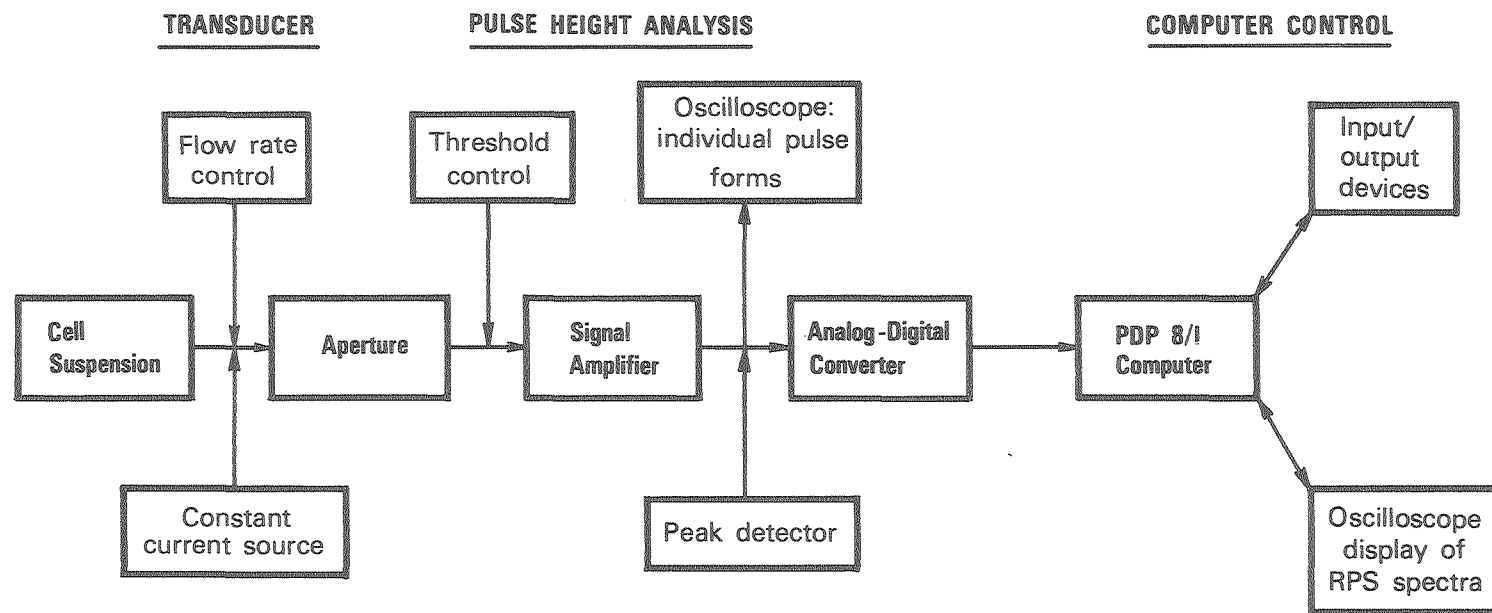
XBL785-3187

Fig. 1
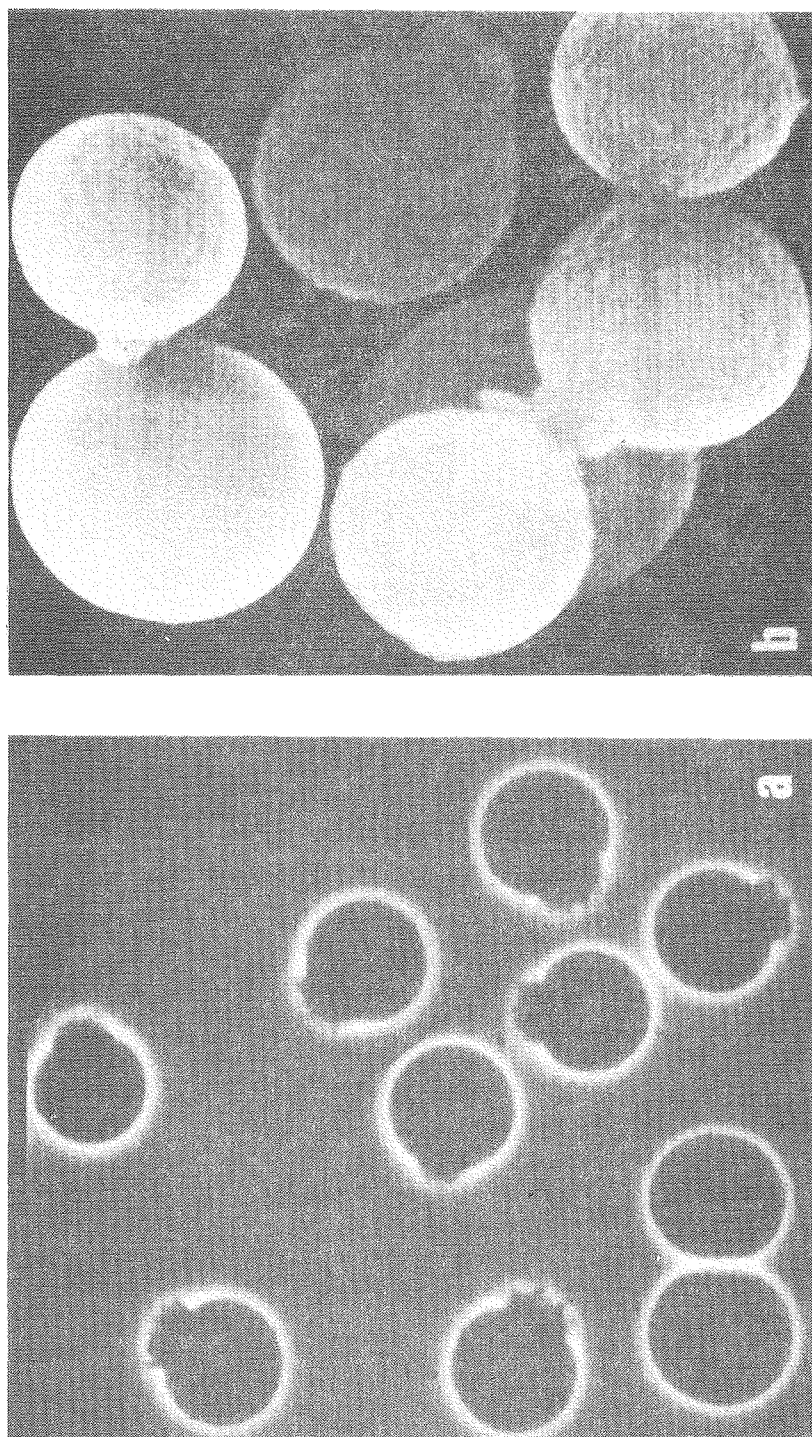
XBB 768-7784

Fig. 2

(a)
300 MOSM
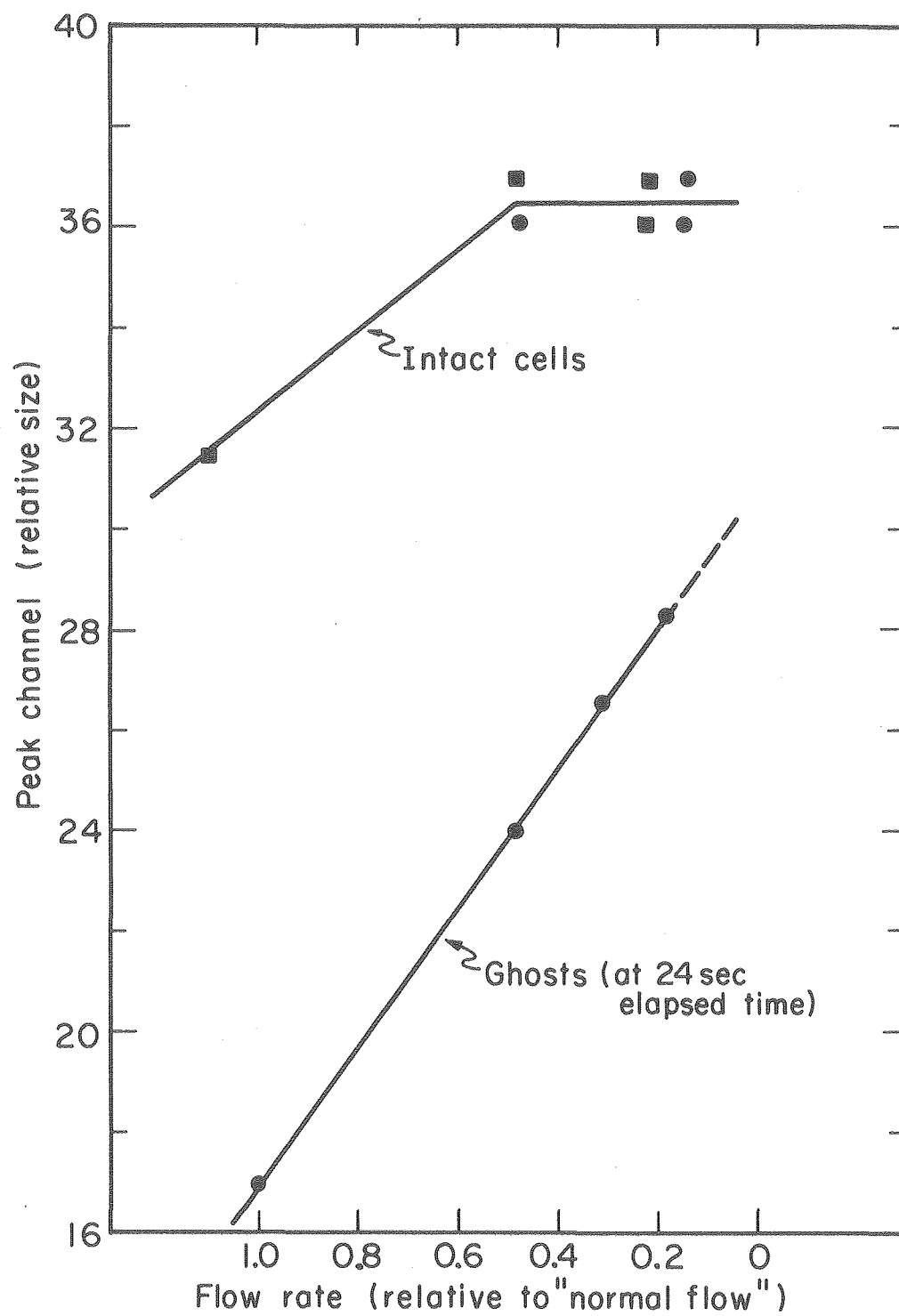
(b)
210 MOSM

Fig. 3
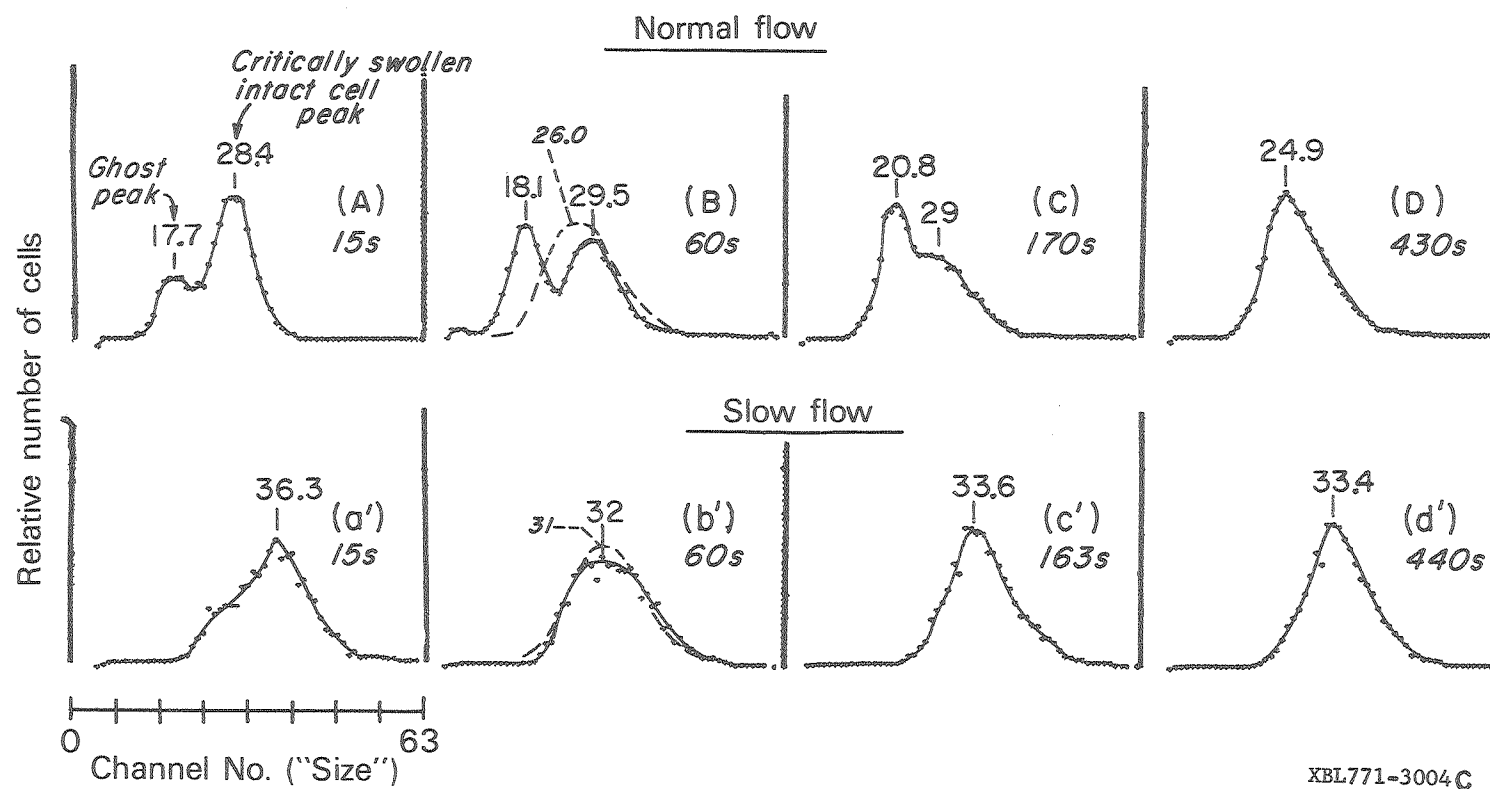
Fig. 4

Fig. 5

XBL782-2869A

Fig. 6

XBL782-2870A
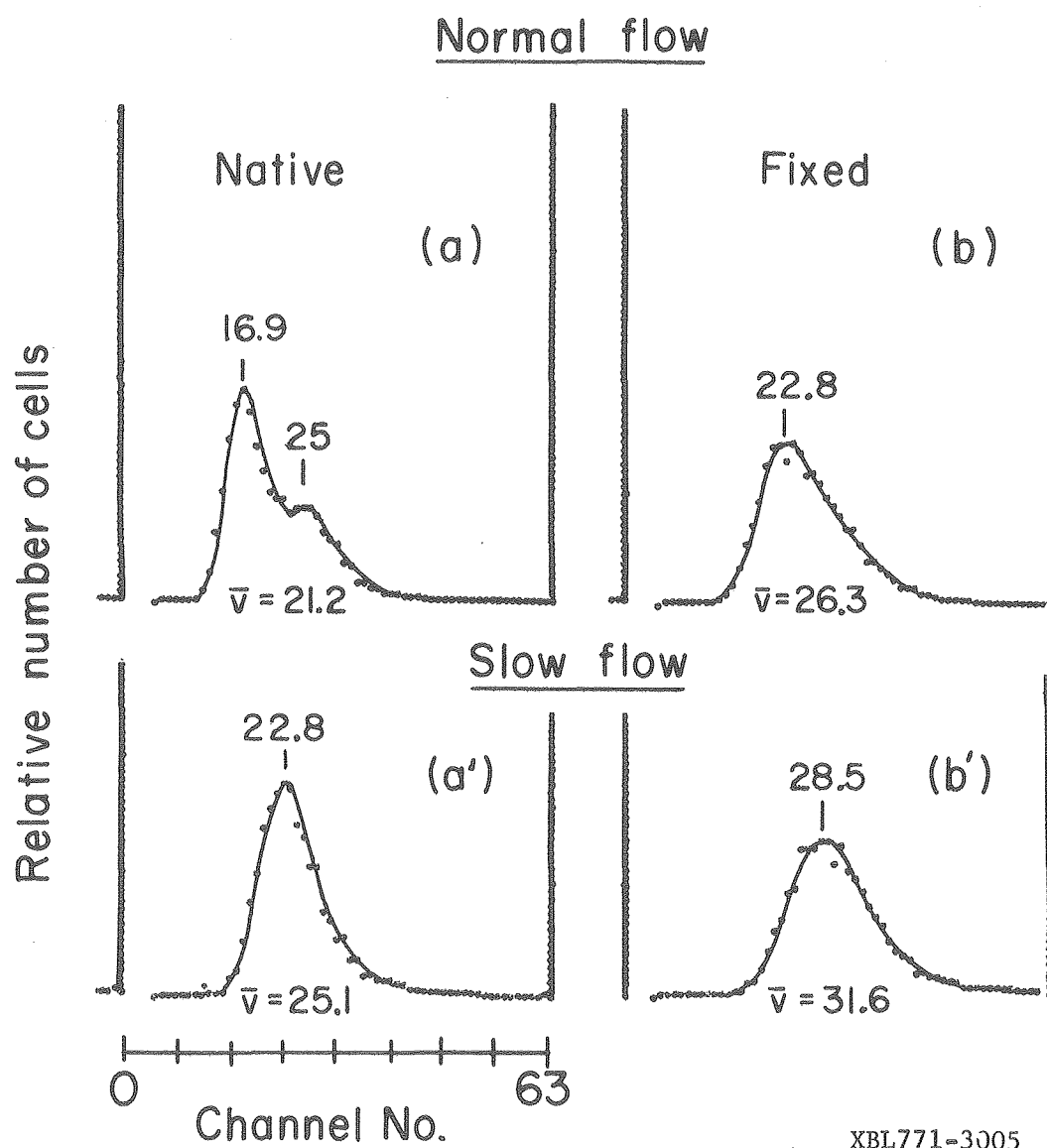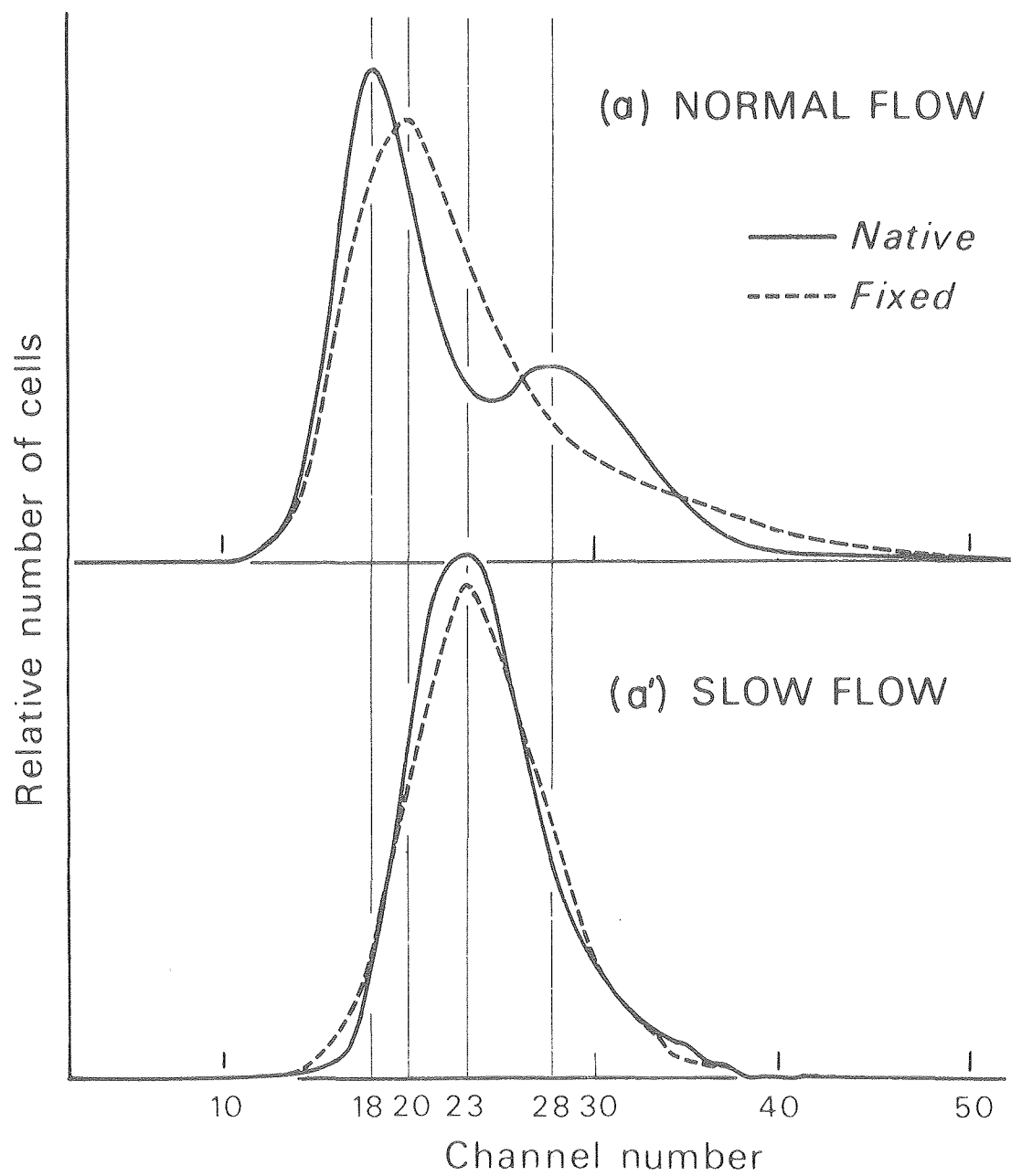
Fig. 7

XBL 782-2871A

Fig. 8A

Fig. 8B

XBL7812-12400

XBB 785-5962
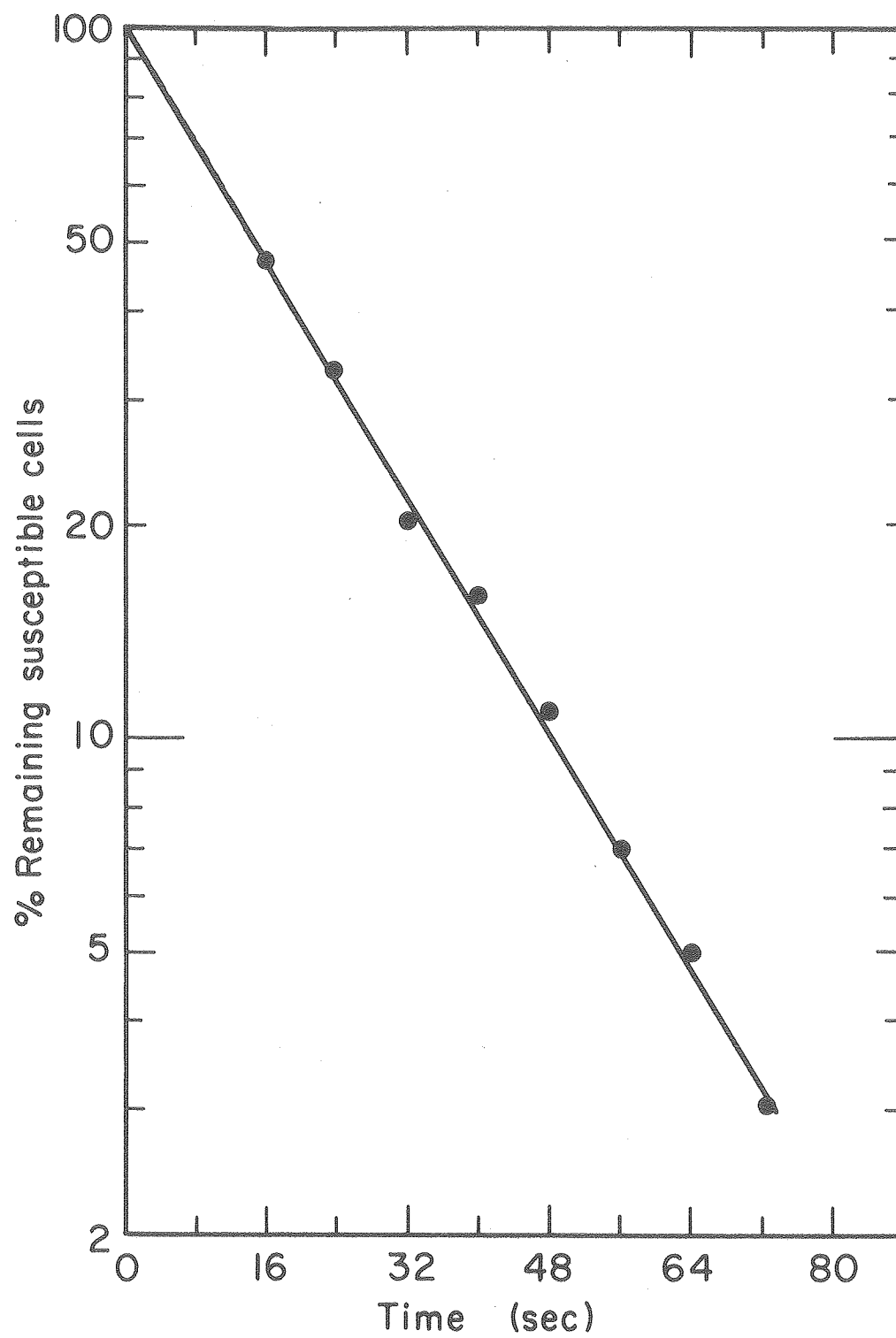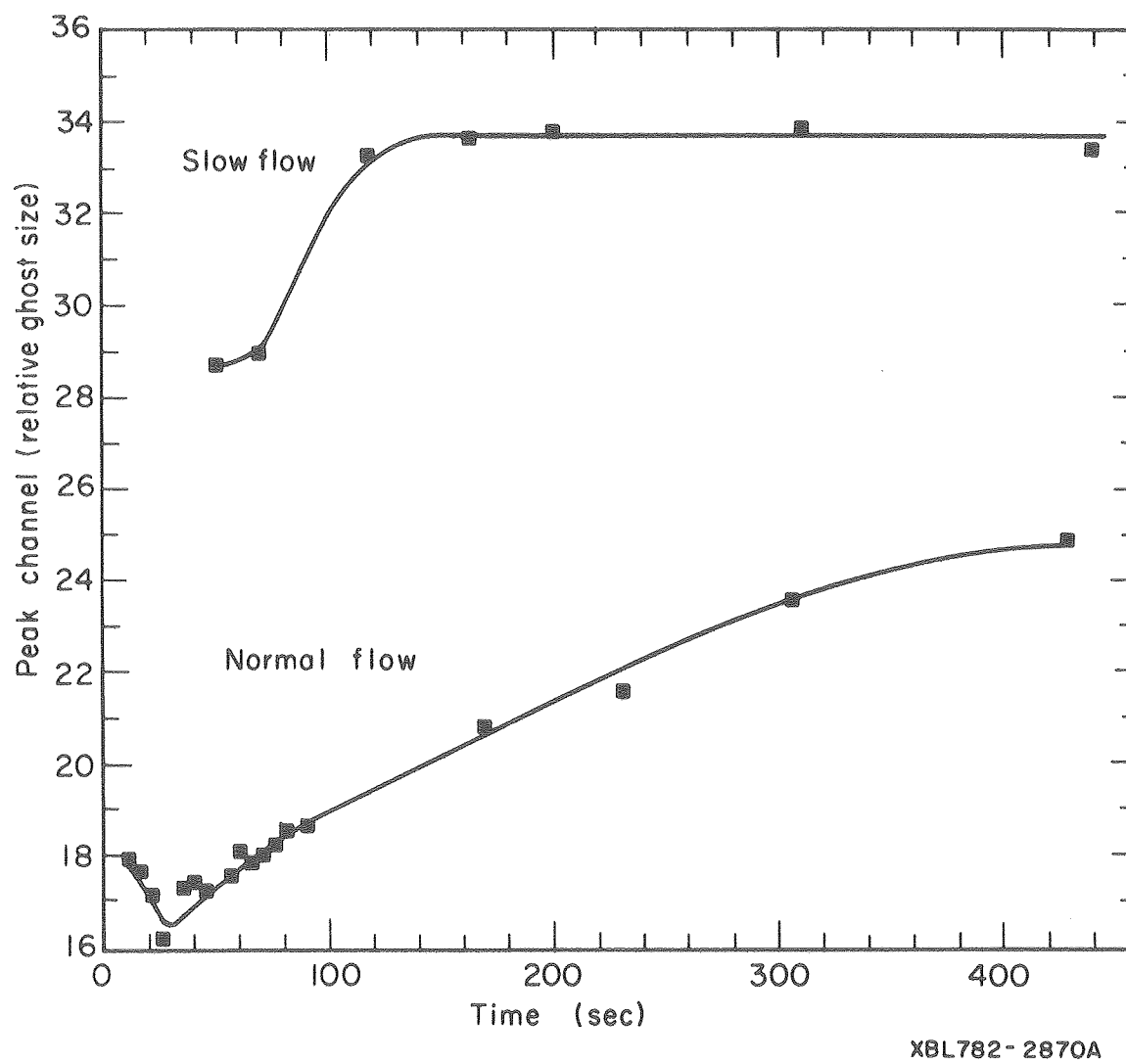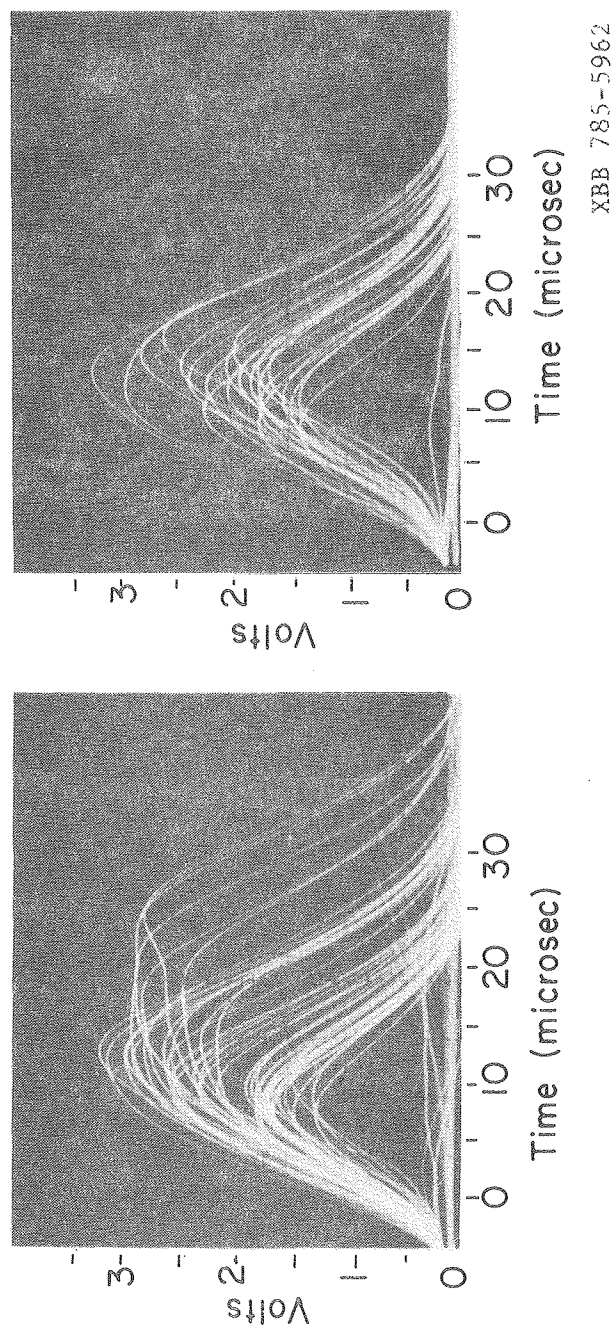
Fig. 9

CHAPTER 5

OUTLINE: CHLORPROMAZINE·HCl EFFECTS ON HUMAN ERYTHROCYTES

I. INTRODUCTION

    A. Morphological changes induced by chlorpromazine·HCl (CPZ·HCl).

        1. Stages of stomatocyte transition, related to volume.

        2. Changes of osmotic resistance with different concentrations of CPZ·HCl.

    B. RPS and electrophoretic mobility studies.

        1. Measure of changes in electrophoretic mobility with and without gross morphological changes; use of glutaraldehyde to preserve cell shape in fixed condition.

        2. RPS measure of changes in volume, shape and deformability of CPZ·HCl treated erythrocytes.

        3. RPS-"dynamic osmotic hemolysis" analysis of protective effects of CPZ·HCl.

II. MATERIALS AND METHODS

    A. Preparation of erythrocytes.

    B. Treatment with CPZ·HCl.

    C. Glutaraldehyde fixation.

    D. RPS system for study of volume, shape and deformability; dynamic osmotic hemolysis at 130 mosM PBS.

III. RESULTS

    A. Fig. 1: RPS – spectra of erythrocytes treated with CPZ·HCl, and following subsequent washing out and in of CPZ·HCl. (Normal-flow studies.)

    B. Table 1: Volume changes of CPZ·HCl treated cells compared to control: evaluation of shape factors associated with stomatocytes.

    C. Fig. 2: Dynamic osmotic hemolysis of CPZ·HCl protected erythrocytes: Representative RPS-spectra and tabulation of percentages of intact cells at selected "post-hemolysis" times.

IV. DISCUSSION

A. Interpretation of changes in RPS peak, mean, and bimodality characteristics with CPZ·HCl treatment.

B. Remarks on osmotic protectiveness of CPZ·HCl.

1. Evidence of change in maximal critical volume, ghost volume.

2. Rate of hemolysis and repair; rate of protective effects.

INTRODUCTION

The biconcave discocytic form of the human red cell can be made to assume various reversible conformations in vitro when exposed to chemical agents. Two basic groups of such agents, although not related to each other chemically, share the common property of having an amphiphilic molecular structure (1). The group of anionic and non-ionized compounds induces discocyte-echinocyte transformations, while the cationic compounds induce discocyte-stomatocyte transformations. Although it is difficult to find a substance which exists in both cationic and anionic forms, the phenothiazines exist in both anionic and cationic molecular forms, so that using the same basic structure, both types of shape transformations can be induced.

The cationic phenothiazine tranquilizer chlorpromazine·HCl (CPZ·HCl) is known to induce a change in erythrocyte morphology from the normal biconcave disk form (discocyte) to a cup shaped form (stomatocyte) (1, 2). The degree of morphological transformation has been quantitatively correlated with the concentration of CPZ·HCl in the suspending medium and the net cellular uptake of drug (2). Cells treated with CPZ·HCl in low concentrations have been demonstrated to have less sensitivity to osmotic hemolysis than have normal discocytes (3). At higher CPZ·HCl concentrations, stomatocytes attain a spherical shape and display an increased sensitivity to osmotic lysis, as compared with normal dis- cocytes (2, 3). As long as the transformation has not proceeded to a final spherical stage, the morphological transition from discocyte to stomatocyte can be completely reversed by removing CPZ·HCl from the medium (2).

The mechanism by which chlorpromazine·HCl leads to changes in erythrocyte shape and osmotic fragility is not yet well established. From studies on volume changes of ghosts exposed to CPZ·HCl, Seeman and associates (4, 5) concluded that this drug leads to a 1.5% - 3% expansion in membrane area. However, using an isotopic technique to quantitate drug binding, they found that the bulk volume occupied by membrane-bound CPZ·HCl could not account for the total calculated increase in area (6). These workers also demonstrated that the binding of CPZ·HCl to ghost membranes is an exothermic process, and they proposed that this is consistent with the site of drug binding being "at the immediate interface of the membrane-aquerous region" (6).

More recently, Sheetz and Singer (7) have discussed the localization of different CPZ devivatives. In their view CPZ·HCl binding occurs preferentially at the inner (cytoplasmic) membrane surface. That is, CPZ·HCl contains a teritary amine which exists in a partially uncharged state at physiological pH, which would thereby facilitate molecular diffusion across the membrane and intercalation of the drug at the interior membrane-water interface. On the other hand, they proposed that the quartinized cationic chlorpromazine derivative cannot diffuse across the membrane and gain access to the cytoplasmic membrane-water interface, and thus preferentially localizes at the outer membrane surface. Sheetz and Singer (7) suggest that it is the resulting expansion of the exterior half of the membrane bilayer which produces the echinocyte morphology. In their model, CPZ·HCl binding at the interior surface expands the cytoplasmic half of the membrane bilayer, and thereby produces the stomatocytic morphology.

Using the microscope method of cell electrophoresis (microelectro-phoresis) we have demonstrated several other aspects of CPZ-membrane interaction, namely: (a) that some CPZ·HCl binds quantitatively at the erythrocyte outer membrane surface, over a wide range of solution ionic strengths; and (b) that stomatocytes formed in the presence of CPZ·HCl have a reduced net negative surface charge density. In addition, we clarified the interrelationships between the CPZ·HCl induced change in morphology, and the effect of this drug on cellular surface charge (8). To this end, glutaraldehyde (GA) was used to fix erythrocytes in both non-deformable discocyte and in stomatocyte forms, thereby preventing the gross changes in morphology that accompany the addition or removal of CPZ·HCl from unfixed, deformable cells. Our microelectrophoretic studies on cells treated by these procedures showed that the reduction in surface charge is independent of the drug-induced shape change.

This chapter enlarges upon the previous RPS work and reports studies on changes in volume, shape, deformability and osmotic response pro-perties of erythrocytes treated with CPZ·HCl.

MATERIALS AND METHODS

Preparation of erythrocytes.

Fresh human blood from the same normal donor was used in all experiments. Several ml of blood were drawn quickly by venipuncture into a glass syringe without added anticoagulant, and immediately dis-pensed into approximately 30 vols. of Dulbecco phosphate-buffered

saline, pH 7.2, 290 mosM, (Grand Island Biological Co., Grand Island, New York). The erythrocytes were pelleted by centrifugation at 300 x g for 10 min, and the supernatant and buffy coat removed by aspiration. The cells were resuspended in phosphate buffered saline, washed once under the same centrifugal conditions and stored on ice as a concentrated stock suspension. They were then treated as described below and studied experimentally within a few hours following preparation of the stock cell suspension.

Treatment with chlorpromazine·HCl.

Chlorpromazine·HCl was obtained from Smith, Kline and French (Philadelphia, Pa.). Analysis indicated that the actual CPZ·HCl concentration was within 2% of the nominal value stated by the manufacturer, and that the concentrations of sulfoxide and sulfone contaminants were less than 0.1% of the total (8).

The washed erythrocytes were suspended in room temperature phosphate-buffered saline containing either 23 or 70μM CPZ·HCl at a cell concentration of approximately $5 \cdot 10^4$/ml. For each of these drug concentrations, a 100% conversion of discocytes to stomatocyte form occurred within approximately 5 min, as observed by phase contrast microscopy.

Glutaraldehyde fixation.

Erythrocytes were fixed for 20 min at room temperature with 0.25% (w/v) glutaraldehyde prepared in phosphate-buffered saline from an 8% solution (Polysciences, Englewood, N. J.). Sufficient NaCl was added to increase the osmolality of the fixative solution to 355 mosM/kg, under which condition it has been shown that no change in erythrocyte volume (relative to native cells in 306 mosM PBS) occurs during the fixative process (Chapter 3). After the fixation was completed, glutaraldehyde was removed by centrifugal washing, and the cells were resuspended in stock phosphate-buffered saline. When cells were fixed following incubation with CPZ·HCl, the same concentration of CPZ·HCl was added to both the fixative solution and the phosphate-buffered saline used as a resuspending medium.

Resistive Pulse Spectroscopy (RPS) studies of changes in volume, shape, deformability and osmotic resistance of chlorpromazine·HCl treated erythrocytes.

The RPS spectral "sizing" studies of CPZ·HCl effects employed a 48 micron diameter and length transducer aperture, a constant current source of 200 microamperes and normal flow rate of 0.008 ml/sec. The cell concentration in each case was about 5×10^5 cells/ml. Sequentia' data were collected in time intervals of 10 seconds per spectrum. RPS apparent size is reported in terms of channel number, corresponding to pulse height, with 64 channels in the absissca. Further technical details are given in Chapter 4.

RESULTS

RPS spectra of chlorpromazine·HCl treated erythrocytes.

Fresh stock erythrocytes were suspended in nominally isotonic phosphate buffered saline both with and without low concentrations of CPZ·HCl. Cells exposed to CPZ were subsequently washed with fresh stock PBS using a desk-top centrifuge and then reexamined by microelectrophoresis, light microscopy, and RPS. The RPS measured or apparent size distributions of the cells are summarized in Fig. 1.

Important features to be noted from Fig. 1 include: (1) the native discocytic erythrocytes have a characteristically distinct bimodal apparent size distribution, with the sample flow rate and geometric aperture employed; (2) spectra from cells incubated with $0.25 \mu M$ CPZ show a decrease in degree of "bimodality" (i.e., the two previously well discerned pulse subpopulations become less well separated); in addition, there is an increase in the peak channel number; (3) the above changes are reversible upon washing out the CPZ with a fresh PBS solution; and (4) the loss of spectral bimodality and increase in peak channel reoccur with the reintroduction of the previously washed cells into another $0.25 \mu M$ CPZ·HCl solution.

RPS measured "volume" change in CPZ treated erythrocytes.

The apparent volume changes of cells treated in varying sequences with glutaraldehyde and CPZ, are summarized in Table 2 (as measured by

RPS distributions, with slow sample flow rate, to optimally compare true size relationships).

TABLE 1

"Volume" Changes in CPZ Treated Cells

Cell Preparation	Mean[1] Volume (channel)	Volume[2] Ratio	Shape[3] Factor (γ)
a. Native cells (control)	28	1.0	1.2
b. GA-fixed, biconcave erythrocytes	28	1.0	1.2
c. 0.25 μM CPZ treated, stomatocytes	33	1.18	1.42
d. CPZ washed out: biconcave discoid cells	28-29	1.0 - 1.04	1.2
e. CPZ readded: stomatocytes	33.7	1.20	1.44
f. CPZ treated, then GA-fixed, then CPZ washed out	31.5	1.12	1.34
g. CPZ treated, GA-fixed, CPZ washed out, then CPZ washed in again	36.5	1.30	1.56

1. Using 48 μ aperture, slow flow rate (0.0025 ml/sec).

2. Normalized to mean volume of native cells.

3. Shape factor γ is calculated assuming no actual volume change in treated cells; $V \cdot (apparent) \simeq \gamma \cdot V (true)$. γ for discoidal cell assumed to be 1.2.

4. Mean volume was used since at slow flow mean $\simeq$ peak in symmetrical distribution.

The data in Table 1 show that: (1) CPZ·HCl treated erythrocytes have a mean "volume" increase relative to native cells; this increase is reversible with the washing out of the CPZ; (2) glutaraldehyde fixation tends to stabilize the cells against subsequent reduction in "volume," either prior to or after shape changes induced by CPZ (compare f. with c. and d.); (3) however, an increase in size can occur subsequent to the GA-treatment (g. vs. f.). The shape factor $\cancel{f}$, is estimated, based on assumption of a true "isovolume" stability of the cell despite the CPZ·HCl induced shape changes. This is further discussed below.

Changes in osmotic resistance with exposure to CPZ·HCl.

The effect of CPZ·HCl on the osmotic resistance of erythrocytes was investigated using the "dynamic osmotic hemolysis" technique described in Chapter 4. Erythrocytes were preincubated in nominally isotonic PBS solution with low concentrations of CPZ·HCl and subsequently transferred into hypotonic PBS solutions and observed by rapid sequence RPS spectral analysis. The results are summarized in Fig. 3. The two relatively discrete subpopulations in Fig. 3a are associated with ghosts and intact cells (9). The subfraction of remaining intact cells at any given time is estimated from the computer calculated integral of the upper subpopulation which corresponds to the intact cells; the percentage of remaining intact cells after 30 and 100 seconds exposure to the respective media is shown in Table 2.

TABLE 2

Percentage of Remaining Intact Cells

Time	CPZ·HCl in Preincubation & Lytic Med.	CPZ·HCl in Preincubation	No CPZ·HCl
30 s	43	24	34
100 s	36	16	27

Notes:

1. Time t = 0 s, is when cells were added from the isotonic pre-incubation medium into 130 mosM, lytic medium.

2. The rate of hemolysis (% lysis/sec) in the time interval between 30 and 100 s is calculated to be 0.21, 0.47 and 0.28, for the samples (a), (b) and (c) respectively.

From the data summarized in Fig. 3 and Table 2, it is surmised that: (1) the absolute percentage of intact cells is greatest and the rate of hemolysis least, for cells treated with CPZ·HCl in both the preincubation medium as well as the lytic medium; (2) cells exposed to CPZ·HCl in preincubation, but without CPZ·HCl in the hypotonic medium are significantly less osmotically resistant than control cells treated without any CPZ·HCl.

DISCUSSION

The interrelationships of several physico-chemical parameters of erythrocytes perturbed by the binding of CPZ·HCl at the membrane surface have been investigated. The previously reported drug induced electro-phoretic mobility change is independent of the gross shape change, but reflects a contribution of the membrane-bound CPZ·HCl molecule to the cellular surface charge density (8). Herein, RPS was used to explore some of the functional relationships betwen changes in cell shape, deformability and size associated with reversible CPZ·HCl binding.

The physical basis for the bimodal electronic "size" distributions of native deformable cells, when measured with a 48 X 48 micron aperture and a "normal flow rate" of about 0.008 ml/s has been given in Chapters 1 and 4. The RPS spectra in Fig. 1 for cells treated with CPZ·HCl show an apparent increase in modal and mean size of the cells as well as a decrease in spectral bimodality. Microscopic observations of the speci-mens reveal that the cells with CPZ·HCl present in the suspending medium are stomatocytes, and that these revert to discocytes upon washing out the CPZ·HCl with fresh PBS. Any explanation of the observed pattern of RPS spectral changes associated with CPZ exposure needs to encompass effects of the drug on all of the cell properties: shape, deformability and volume.

Shape change alone could account for the quantitative changes observed: the geometry of the stomatocyte results in a shape factor, γ, which is significantly larger than the shape factor of about 1.02 taken

for the deformed native cell. ($V_a = \gamma \cdot V_t$; V_a is the apparent, measured volume, and V_t the actual true volume.) If the stomatocyte were highly deformable under the shearing stress during passage through the aperture, and no intrinsic volume alteration was incurred, each signal, and hence the total RPS distributions measured should be identical to those of the native cells. Since, at normal flow, there is a loss of spectral bi-modality (and an increase in apparent size), a significant decrease in deformability must be associated with the transformation of native cell to the stomatocytic form. Intercomparisons of RPS results for specimens repeated at lower sample flow rates and with glutaraldehyde fixation of the cells reveal that the residual bimodality of the RPS spectra at normal flow is eliminated altogether at the decreased flow rate or with glutaraldehyde rigidification of the cells. This pattern suggests that there is significant residual deformability in the CPZ·HCl treated stomatocytes, and that shape and or volume changes are important factors in the observed increased peak and mean volumes of CPZ·HCl treated cells.

An independent method of measuring the cell volume changes is necessary to properly separate the contributions of changes in size and shape to the CPZ·HCl treated cell. Feo (9) has employed the micro-hematocrit technique with correction of trapped supernatant with radio-isotopic labels, and found no measurable change in cell volume for cell transformed to stomatocytes by low concentrations of chlorpromazine. Based on the assumption of an isovolumic shape change, we were able to calculate the effective shape factor of the stomatocyte relative to the

native deformable cell (Table 1). Interestingly, glutaraldehyde "fixed" cells were not fully stabilized against changes with the washing out or in of chlorpromazine as measured by RPS. This may be an indication that the physical effects of CPZ on the membrane are more powerful than the effects of fixation, at the concentrations of each agent employed. We note, however, that in correlated microscopic observations of the specimens, the glutaraldehyde fixed cells did not show any gross changes in shape subsequent to the fixation.

The effects of chlorpromazine on the osmotic resistance of erythrocytes were exemplified in Fig. 2. Our findings are consistent with previous reports of increased osmotic resistance in cells treated with low concentrations of CPZ·HCl (3). The RPS "dynamic osmotic hemolysis" technique provides a rapid, detailed, sensitive, and simple method of following not only the fraction of hemolysis at a given time, but the rate of hemolysis and recovery of ghosts, as well as monitoring the maximal critical volume. Interestingly, CPZ is required in the lytic solution as well as in the preincubating, isotonic medium in order to effect osmotic protection, further indicating that the membrane binding of CPZ·HCl is a rapidly reversible process. Further studies of the cationic CPZ·HCl described here in comparison with its anionic, amphiphilic derivative, CPZ·methiodide, which induces transformation to echinocytic forms, are in order.

REFERENCES

1. Deuticke, B., Transformation and restoration of biconcave shape of human erythrocytes induced by amphiphilic agents and changes in ionic environment, Biochem. Biophys. Acta., 163: 494-500, 1968.

2. Mohandas, N. and Feo, C., A quantitative study of the red cell shape changes produced by anionic and cationic derivatives of phenothiazine, Blood Cells, 1: 375-384, 1975.

3. Seeman, P., Kwant W. O., Membrane expansion of the erythrocyte by both the neutral and ionized forms of chlorpromazine, Biochem. Biophys. Acta., 183: 512-519, 1969.

4. Seeman, P., Kwant, W. O., and Sauks, T., Membrane expansion of erythrocyte ghosts by tranquilizers and anesthetics, Biochem. Biophys. Acta., 183: 499-511, 1969.

5. Seeman, P., Kwant, W. O., Sauks, T., and Argent W., Membrane expansion of intact erythrocytes by anesthetics, 183: 490-498, 1969.

6. Kwant, W. O., and Seeman, P., The membrane concentration of a local anesthetic (chlorpromazine), Biochem. Biophys. Acta., 183: 530-543, 1969.

7. Sheetz, M. P., Singer, S. J., Biological membranes as bilayer couples. A molecular mechanism of drug-erythrocyte interactions, Proc. Natl. Acad. Sci. (U.S.A.), 71: 4457-4461, 1975.

8. Tenforde, T. S., Yee, J. P., Mel, H. C., Electrophoretic detection of reversible chlorpromazine·HCl binding at the human erythrocyte surface, Biochem. Biophys. Acta., 511: 152-162, 1978.

9. Feo, C., Unpublished data; presented at Hematology-Oncology Conference, U.C. Moffitt Hospital, 1975.

Fig. 1 RPS - Spectra of Erythrocytes Treated With CPZ·HCl, and
Following Subsequent Washing Out and In of CPZ·HCl.   (Normal-flow studies).

Fig. 2 Dynamic Osmotic Hemolysis of CPZ·HCl Protected Erythrocytes:
Representative RPS-Spectra and Tabulation of Percentages of Intact Cells
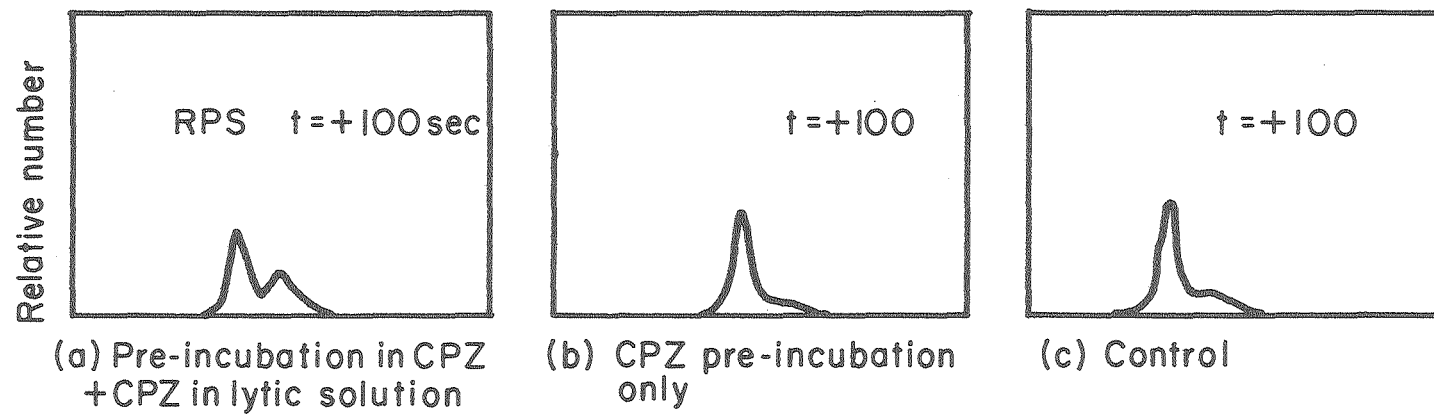at Selected "Post-Hemolysis" Times.
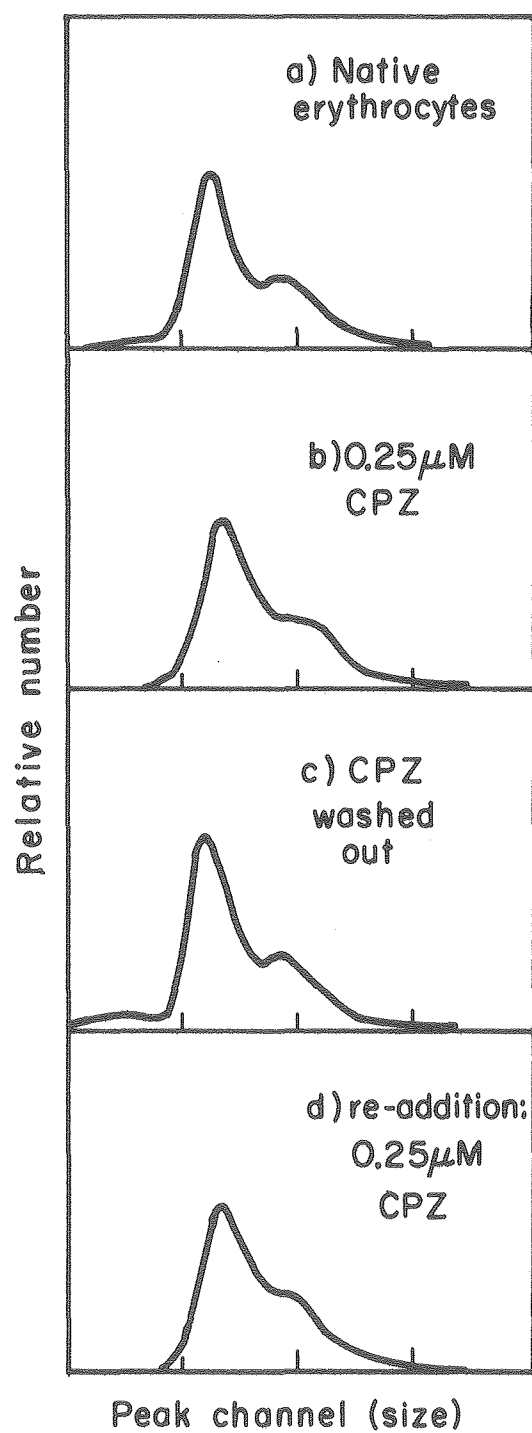
Fig. 1

XBL787-3315

CHLORPROMAZINE TREATED ERYTHROCYTES:
DYNAMIC OSMOTIC HEMOLYSIS

(a) Pre-incubation in CPZ +CPZ in lytic solution

(b) CPZ pre-incubation only

(c) Control

XBL787-3314A

Fig. 2

CHAPTER 6

OUTLINE: STUDIES ON CHOLESTEROL-FED GUINEA PIGS

I. INTRODUCTION

A. General remarks on previous studies on the effects of choles-
    terol on RBC membrane composition, function and gross mor-
    phology.

    1. Decrease in permeability to sodium and other solutes.

    2. Increase in viscosity of the lipid phase of the membrane.

B. Description of studies undertaken using RPS.

    1. RPS characterization of "dynamic osmotic hemolysis."

        a. Rate of hemolysis, apparent maximal critical volume,
            initial ghost size, and inferred rate of repair.

        b. Use of glutaraldehyde to "arrest" cells at specific
            stages of hemolysis and swelling.

        c. Simple sucrose density gradient separation of intact
            cells from lysed cells.

II. MATERIALS AND METHODS

A. Erythrocyte preparation and suspending media.

    1. Drawing of blood from guinea pigs.

    2. Phosphate buffered saline solutions and hypotonic dilu-
        tions.

B. Glutaraldehyde (GA) solutions.

    1. Timing and concentration of GA added to cell suspensions
        in order to arrest cells in different stages of swelling
        and hemolysis.

C. Methods employed in RPS "dynamic osmotic hemolysis" analysis.

D. Zeiss phase contrast microscopic observations of GA-arrested
    cells.

E. Separation of GA-fixed intact cells from ghosts using simple
    sucrose density layers.

III. RESULTS

A. Fig. 1: RPS "size" distributions of guinea pig erythrocytes: comparison of samples from a control and a 13 week, cholesterol dieted animal.

B. Fig. 2: Representative RPS spectra from a "dynamic osmotic hemolysis" series using 100 mosM PBS; blood from a cholesterol-fed guinea pig is compared with that of a control.

C. Fig. 3: A composite, summary curve representing the repair process in cholesterol-fed and control blood samples, plotting RPS-peak position vs. time elapsed.

D. Fig. 4: Micrographs showing GA-arrested red cells at different stages of swelling and lysis in 130 and 156 mosM PBS.

E. Fig. 5: Red cells at an early phase of swelling and hemolysis: arrested with GA-fixation. The relative number of intact cells and ghosts as discerned by phase contrast microscopy. Example of a sucrose density separation.

F. Table 1: Relative osmotic resistance of cholesterol-fed compared to control blood cells followed sequentially over a five day interval.

IV. DISCUSSION

A. Changes in membrane properties with increased cholesterol content: RPS spectral bimodality.

B. Interpretation of observed cell morphology (Fig. 4) and RPS-size (Fig. 2A and 2B).

   1. Changes of shape and deformability in isotonic PBS.

   2. Changes of shape and deformability in hypotonic PBS.

C. Interpretation of RPS-"DOH" results (Fig. 2, Fig. 3).

   1. Maximal critical volume, initial ghost volume, rate of lesion, repair.

   2. Correlation with microscopic observations.

D. Analysis of cell subpopulations separated by osmotic resistance (Fig. 5).

   1. Changes in osmotic resistance of red cells with cholesterol feeding (Table 1).

   2. Correlation with biochemical assay of cholesterol.

INTRODUCTION

Cholesterol is the most abundant sterol in the body and serves in numerous structural and functional roles including that as a basic component of all cell membranes, and as a precursor to steroidal hormones and bile acids. Several pathological conditions are associated with abnormal accumulations of the sterol, such as: (a) the formation of cholesterol calculi in the biliary tract; (b) the deposition of cholesterol-containing plaques in the intima of the aorta in atherosclerosis; and (c) hypercholesterolemia, which is a genetically transmitted disorder in the feedback control of cholesterol synthesis.

In disorders of familial lecithin-cholesterol acyl transferase (LCAT) deficiency, deficient enzyme results in an absence of esterfied cholesterol (1). Normally about two-thirds of the cholesterol in plasma is esterfied with fatty acids. With the deficiency in LCAT enzyme, there is an increased plasma concentration of lecithin and decreased amounts of lysolecithin. Clinically, a syndrome of an anemia with abnormal acanthocytic or "spur" red cell morphology, and with proteinuria is associated with the LCAT deficiency.

Ostwald and co-workers have shown that the guinea pig provides a useful model of the human disorder of LCAT deficiency because this animal accumulates cholesterol in its liver, plasma, and erythrocytes if it is given an elevated dietary source of the sterol (2). With an increasing duration on an elevated cholesterol diet, an increasing percentage of morphologically abnormal "spur" cells is observed. The

average cellular membrane content of cholesterol (C) is correlated to the number of spur cells observed (3). Normal red cells from control animals transform into spur forms after incubation in the plasma obtained from cholesterol fed animals. After about 12 consecutive weeks on a 1% C diet, a hemolytic anemia develops (4).

Measurement of changes in membrane mechanical and transport properties associated with increased cholesterol content or "loading" into the membrane provide evidence of the role of the sterol in the general fluid mosaic model of the cell membrane. The permeability of the C-loaded membrane to several non-electrolytes and to sodium ion is decreased (5). Decreases in both active and passive efflux suggested to Kroes and Ostwald that increased amounts of C in the membrane resulted in a tighter packing of the membrane lipids which in turn decreased the mobility of permeants through the membrane. Compression of the lipid phase of the membrane secondary to the increased C content has also been evidenced by electron-spin resonance studies showing a decrease in local viscosity of the membrane without detectable changes in protein interactions (6).

In this chapter, we focus on the early changes in the "dynamic osmotic hemolysis" of guinea pig red cells loaded with increasing amounts of cholesterol. The resistive pulse spectroscopy (RPS) method of measuring dynamic osmotic hemolysis (7), provides a rapid and sensitive measure of the kinetics of osmotic hemolysis. These studies provide information on the maximal critical volume, the ghost volume and inferred lesion size, and the apparent rate of membrane lesion repair.

The protein cross-linking agent glutaraldehyde (GA) is used to fix cells at specific stages of hemolysis such that the earlier hemolyzing cells are later separable from the remaining unhemolyzed cells. (These studies of the guinea pig by RPS were stimulated by and made possible through the ongoing investigations of guinea pig metabolism and biochemistry by R. Ostwald in the Department of Nutritional Sciences.)

MATERIALS AND METHODS

"Arrest" of red cells in early osmotic hemolysis, by glutaraldehyde (GA) fixation.

Fresh whole blood is drawn by capillary action into an unheparinized microhematocrit tube from a lancet wound of an ear vein of the guinea pig. This blood specimen is immediately diluted into an excess of hypotonic phosphate buffered saline (about 0.1 ml of blood is added to 10 ml of 130 mosM solution composed of Dulbecco's PBS diluted with distilled water). The suspension is gently mixed by inversion of the container for a total of 10 seconds before addition of 0.5 ml of 2.5% w/v glutaraldehyde to the mixture. The final concentration of glutaraldehyde is about 0.125%.

Microscopic observations of GA-treated cells.

Cell preparations were viewed in suspension in a hemacytometer with a Carl Zeiss Universal microscope (using 16 X (phase) and 40 X (phase)

objectives and a 10 X Peripan ocular lens). Photomicrographs were made
on Polaroid Polapan B-W 4 X5 Type 52 ASA 400 Film.

Guinea Pigs.

Guinea pigs were commercially supplied young albino, males gen-
erally weighing 200 to 400 grams during the span of the experiments. The
guinea pigs were fed a semi-synthetic diet with: (a) no cholesterol
added, (b) 0.1% , or (c) 1.0% cholesterol added to the chow. (The
animals were provided through the laboratory facilities of R. Ostwald.)

Separation of intact cells from ghosts.

The normal specific gravity of guinea pig erythrocytes is reported
to be 1.09 ± 0.1; this density should slightly decrease with osmotic
swelling and dilution of the intracellular contents. Glutaraldehyde
fixation also may perturb the natural density, but probably not more
than ± 0.1 (8). The density of ghosts is closer to 1.05 after the loss
of most of the intracellular hemoglobin. A sucrose layer of about 1.12
(nominal) specific gravity was prepared by mixing 30 g of sucrose into
100 ml of distilled water. This medium was found to be effective in the
following separation procedure: suspensions composed of GA-fixed intact
cells and ghosts were layered on top of the sucrose layer in a 15 ml
centrifuge tube (2 ml of cell suspension layered over 8 ml of sucrose
medium). The tube was then centrifuged at 300 x g for 10 minutes. The
resultant supernatant and sedimented cells were subsequently separated
for further studies.

Resistive pulse spectroscopy.

Details of the instrumentation are given in Chapters 1, 2 and 4. "Normal" sample flow rate is about 0.008 ml/s; "slow" flow rate is about 0.0025 ml/s.

RESULTS

Resistive pulse spectra "volume" distributions of cholesterol-fed guinea pigs.

The apparent size distributions for erythrocyte samples taken from cholesterol fed (1% C diet) and control guinea pigs are shown in Fig. 1. These RPS spectral forms for the control guinea pig red cells are qualitatively similar to the spectra for normal human erythrocytes; i.e., the spectrum for apparent size distribution is bimodal at the normal sample flow rate, and transforms to a unimodal distribution at the lower flow rate (7). In contrast, red cells taken from a guinea pig which has been on a 1% C diet for 13 weeks, give a RPS spectra which is significantly decreased in bimodal character at the normal sample flow rate. The bimodality index, i_1, (described in Chapter 2) quantitates the degree of "bimodality" to be 1.58 for native control guinea pig red cells and 0.34 for the cells from cholesterol fed guinea pigs. Microscopically, many "spur" morphological abnormalities are seen with the cholesterol-fed sample in comparison to the regular biconcave discoidal forms for the control cells. The "C-fed" red cells have a broader actual size range and larger mean volume than the control cells; this

is best observed by intercomparison of the "slow flow" spectra of each in Fig. 1.

Dynamic osmotic hemolysis of cholesterol-loaded red cells.

Erythrocytes were collected from cholesterol-fed and control guinea pigs for experiments on osmotic hemolysis as measured by sequential RPS spectra. Selected, representative spectra from these cell specimens are shown in Fig. 2.

The trend in RPS spectral peak position is qualitatively different between the C-fed and control red cells. At relatively early times after introduction of the native cells into the hypotonic hemolytic solution, the C-fed erythrocytes are relatively large in apparent size; with increasing elapsed time in the hemolytic medium, the RPS-measured size becomes smaller. A converse pattern occurs with the RPS size of control red cells. These start initially relatively small and become apparently larger with longer time after exposure. A more complete presentation of these contrasting, time-dependent RPS size relationships for cholesterol-fed and control red cells added to a hypotonic solution is given in Fig. 3.

The interpretation of the physical significance of the different RPS size behaviors observed in Fig. 3, is aided by light microscopic observations in the same time frame of selected, parallel red cell samples. Examples of representative optical observations are given in Fig. 4. The bright, highly refractile cells seen in Fig. 4 are intact,

swollen erythrocytes as verified by assessment of hemoglobin content by Soret band wavelength light absorption. The low contrast, poorly refractile particle are the red cell "ghosts." It is seen that the red cells from the cholesterol-fed guinea pig are much more resistant not only to lysis, but to swelling and shape change as well.

The evidence presented in Figs. 2, 3 and 4 needs to be considered together in order to arrive at a reasonable interpretation of the events. For control red cells, the initial small RPS size following exposure to the hypotonic solution is correlated with the microscopic observation of a large fraction of ghosts formed at an early time. In the case of native human cells, the relatively small RPS volume measured at early post-hemolytic times has been demonstrated to be the consequence of flow-induced deformation and volume expulsion of the intra-cellular contents through the hemolytic membrane lesion (7). The data presented here for native guinea pig red cells undergoing hemolysis are consistent with the results for the normal human red cells. It is thus postulated, as with the human red cell, that the guinea pig red cell under-goes the formation of a lytic lesion after maximal osmotic swelling, and the lesion then spontaneously undergoes a gradual resealing and repair. The electronically measured size, therefore, becomes larger with in-creasing elapsed time, as a result of the decreasing vulnerability of the post-hemolytic cell-membrane to deformation and volume expulsion as it passes through the sensing aperture.

The cholesterol-loaded cells, in contrast, have larger RPS size at the early times after exposure to the hypotonic medium, and microscopi-

cally, are large, swollen, intact cells. After about 100 s or more, the cells are seen to have undergone hemolysis. Interestingly, the formation of ghosts, as measured by the decreasing RPS peak volume with time, is more gradual and less clearly demarcated by a distinct pulse subpopulation of the type seen with human red cell ghosts, in comparison to the remaining intact cell subpopulation. Furthermore, the ghosts from C-fed animals do not tend to gradually increase in RPS size. This may reflect a loss of the ability for spontaneous repair of the membrane lesion which accounts for the upward size shift in post-hemolytic control cells (Fig. 3).

Separation of intact cells from ghosts.

A protocol for separating the later hemolysing intact cells from the earlier hemolysing cells was developed, taking advantage of the fixative properties of glutaraldehyde (Chapter 3). The addition of glutaraldehyde (GA) at a specific time after the initial cell sample has been mixed into the hypotonic, hemolytic medium, results in the arrest or stabilization of the remaining intact cells against further progression towards hemolysis (Chapter 4). After this GA fixation, the suspension of intact and ghost cells is layered over a sucrose medium for centrifugal separation (as detailed in MATERIALS AND METHODS). The simple single sucrose layer is adequate and effective for separating the GA fixed intact cells from the ghosts, in part because the fixation does not significantly alter the large difference in density between the intact and ghost cells. Examples of the results from this GA-fixed and separation protocol are displayed in Fig. 5.

Changes in osmotic resistance of red cells from cholesterol-fed
guinea pigs.

Red cell samples were taken from guinea pigs at selected times
after commencing cholesterol-enriched diets. Each specimen was treated
with a modification of the protocol of (hypotonic hemolysis)——→
(GA-fixation)—→(separation), as was described in MATERIALS AND METHODS.
Photomicrographs were taken of the resultant suspensions of GA fixed
cells and ghosts, and the percentages of intact cells were tabulated
from visual counts (Table 1). A significant change in osmotic resis-
tance compared with the control fraction was detected as early as 24
hours after initiating the cholesterol diet (1% C). The percentage of
resistant cells increased steadily over the 12-13 d of this study. In
contrast, cells from guinea pigs on 0.1% cholesterol and control diets
showed little or no change in osmotic resistance over the period of
study. These overall diet-associated trends were striking despite
considerable individual variation between animals on the same diet
regimens.

TABLE 1

Effects of Cholesterol Diet on Osmotic Resistance of
Guinea Pig Erythrocytes

Lowest % of Intact Cells, And
(Average % for 2 or 4 Animals)

Time on Diet	24 Hours	48 Hours	5 Days	13 Days
Control	5 (23)	3 (15)	5 (12)	5 (12)
0.1% Cholesterol	5 (8)	6 (7)	8 (8)	8 (8)
1.0% Cholesterol	12.5 (37)	23 (27)	50 (52)	58 (67)

Based on more than 100 counts/specimen.

DISCUSSION

Effects of increased cholesterol content on membrane properties.

Alterations of several membrane properties are associated with the increase of the guinea pig's dietary cholesterol which results in an increase in the content of cholesterol in the red cell membrane (5, 6). Here, "cholesterol-loaded" red cells were shown to have: (1) changes in RPS spectral bimodality characteristics, and (2) changes in osmotic resistance, rate of hemolysis, and apparent ability to repair or reseal the lytic lesion secondary to hemolysis.

Changes in RPS bimodality characteristics.

After 13 weeks on a 1% cholesterol diet, the guinea pig has developed "spurred" red cells. The RPS spectra for these cells display a decreased bimodality index. The physical significance of the loss in bimodality is interpreted as reflecting decreased cell-membrane deformability properties, and the associated loss of the native biconcave discodal shape of the cells. The argument for such an explanation is the same as that used on studies of human red cells and is detailed in Chapter 4. This explanation is consistent with findings by electron-spin label studies of decreased local membrane viscosity in membranes having an increased cholesterol content (5). In contrast, the control guinea pig red cells behave very much like native human red cells, when assessed by RPS flow-dependent spectral measurements (Fig. 1),

suggesting that the rheological properties of the red cells from these two species are very similar.

Dynamic osmotic hemolysis of guinea pig red cells.

The "dynamic osmotic hemolysis" characteristics of red cells from guinea pigs fed high cholesterol diets were studied by RPS techniques (7) including selected usage of glutaraldehyde. Using these methods, the C-loaded cells were detected to be more osmotically resistant than the control cells as early as 24 h after initiating the diet of 1% cholesterol. The RPS studies and associated microscopic observations showed that the C-loaded cells lyse much later than the control cells (Fig. 2-4).

Newly formed ghosts are highly deformed during passage at high velocity through the RPS sensing aperture, but gradually become less deformable, if an effective repair of the membrane lesion occurs (7). The C-loaded cells appear to lack the potential for spontaneous repair that is manifested by the control red cells (reflected by an increasing RPS peak channel with time for the control cells in Fig. 3). The loss of "repairability" by the cholesterol enriched cell membranes may be related to decreased membrane fluidity secondary to the tighter packing of the membrane lipids from the increased cholesterol content.

Previous reports (4) have correlated the fraction of cells having abnormal spur cell morphology with the average increase in cell membrane cholesterol content. However, it has been demonstrated here

(e.g. Fig. 5) that the total cell population is heterogeneous in its osmotic resistance properties. To facilitate comparison between cell types, we developed a simple method of separating the more "resistant" cells from the more "fragile," taking advantage of the GA fixation of the samples at a selected time. The GA fixed, intact cells are stable when subjected to centrifugal separation from the less dense ghosts. Glutaraldehyde does not significantly interfere with lipid extraction techniques because it is primarily a cross-linking agent of free amino groups of proteins. This renders feasible the assessment of the cholesterol content of the later hemolysing subfraction of cells. If an increase in osmotic resistance is attributable to increased cholesterol content, the measured cholesterol content for the more resistant subfraction may be considerably higher than values obtained from previous calculations based on the averaged cholesterol content of the whole cell population. Such a new result would be significant in understanding the role of cholesterol in the formation of spur cells, in a model of membrane interactions. Such biochemical assays of the cholesterol content of the separated more resistant cells are ongoing in the nutritional sciences laboratory of Professor R. Ostwald.

REFERENCES

1. Cooper, R. A., Lipids of human red cell membrane: normal composition and variability in disease. Seminars Hematol., 7: 296-322, 1970.

2. Ostwald, R., Yamanaka, W. and Light, M., The phospholipids of liver, plasma, and red cells in normal and cholesterol-fed anemic guinea pigs, Proc. Soc. Exp. Biol. and Med., 134: 814-820, 1970.

3. Sardet, C., Hansma, H., and Ostwald R., Effects of plasma lipoprotein from control and cholesterol-fed guinea pigs on red cell morphology and cholesterol content: an in vitro study, J. Lipid Res., 13: 705-715, 1972.

4. Ostwald, R., and Shannon, A., Composition of tissue lipids and anemia of guinea pigs in response to dietary cholesterol, Biochem. J., 91: 146-154, 1964.

5. Kroes, J. and Ostwald, M., Erythrocyte membranes - effect of increased cholesterol content on permeability, Biochem. Biophys. Acta., 249: 647-650, 1971.

6. Kroes, J., Ostwald, R., and Keith, A., Erythrocyte membranes - compression of lipid phases by increased cholesterol content, Biochem. Biophys. Acta., 274: 71-74, 1972.

7. Yee, J. P. and Mel, H. C., Cell-membrane and rheological mechanisms: dynamic osmotic hemolysis of human erythrocytes and repair of ghosts, as studied by resistive pulse spectroscopy. Biorheology, 15: 321-335, 1978.

8. Jay, A. W. L., Canham, P. B., Sedimentation of single human red blood cells. Differences between normal and glutaraldehyde fixed cells, J. Cell. Physiol., 80: 367-372, 1972.

Fig. 1. "Size" Distributions of Guinea Pig Erythrocytes. RPS sampling of erythrocyte suspensions was repeated at "normal" and "slow" flow rates using a 48 x 48 μ aperture.

Fig. 2. Erythrocytes Undergoing Osmotic Hemolysis and Subsequent Repair. RPS spectra from: (a) control red cells, and (b) red cells from a guinea pig after two weeks on a 1% cholesterol diet. The "size" distributions were collected over 10 s intervals at normal flow rate starting at the designated times (cells were added to the hypotonic solutions at t = 0 seconds).

Fig. 3. Dynamic Osmotic Hemolysis of Guinea Pig Red Cells. The relative size (distribution peak channel) is plotted against the time after initial exposure of cells to the hemolytic medium (normal sample flow rate).

Fig. 4. Morphology of Cells After Exposure to Hypotonic Hemolytic Solutions. Cells were fixed with 0.25% w/v glutaraldehyde added 10 seconds after the initial mixing of the cells into PBS solutions of 130 and 150 mosM. Control cells, at each of these osmolarities respectively, are seen in (a) and (b); "C-fed" cells are displayed in (c) and (d).

Fig. 5. Red Cells Treated With Glutaraldehyde During the Course of Osmotic Stress. Photomicrographs of red cells and ghosts: (a-c) prior to separation by sucrose layer centrifugation, and (d) the resuspended, sedimented, intact cells after removal of supernatant. Samples (c) and (d) are from a cholesterol-fed guinea pig.

RPS: CHOLESTEROL-FED GUINEA PIG
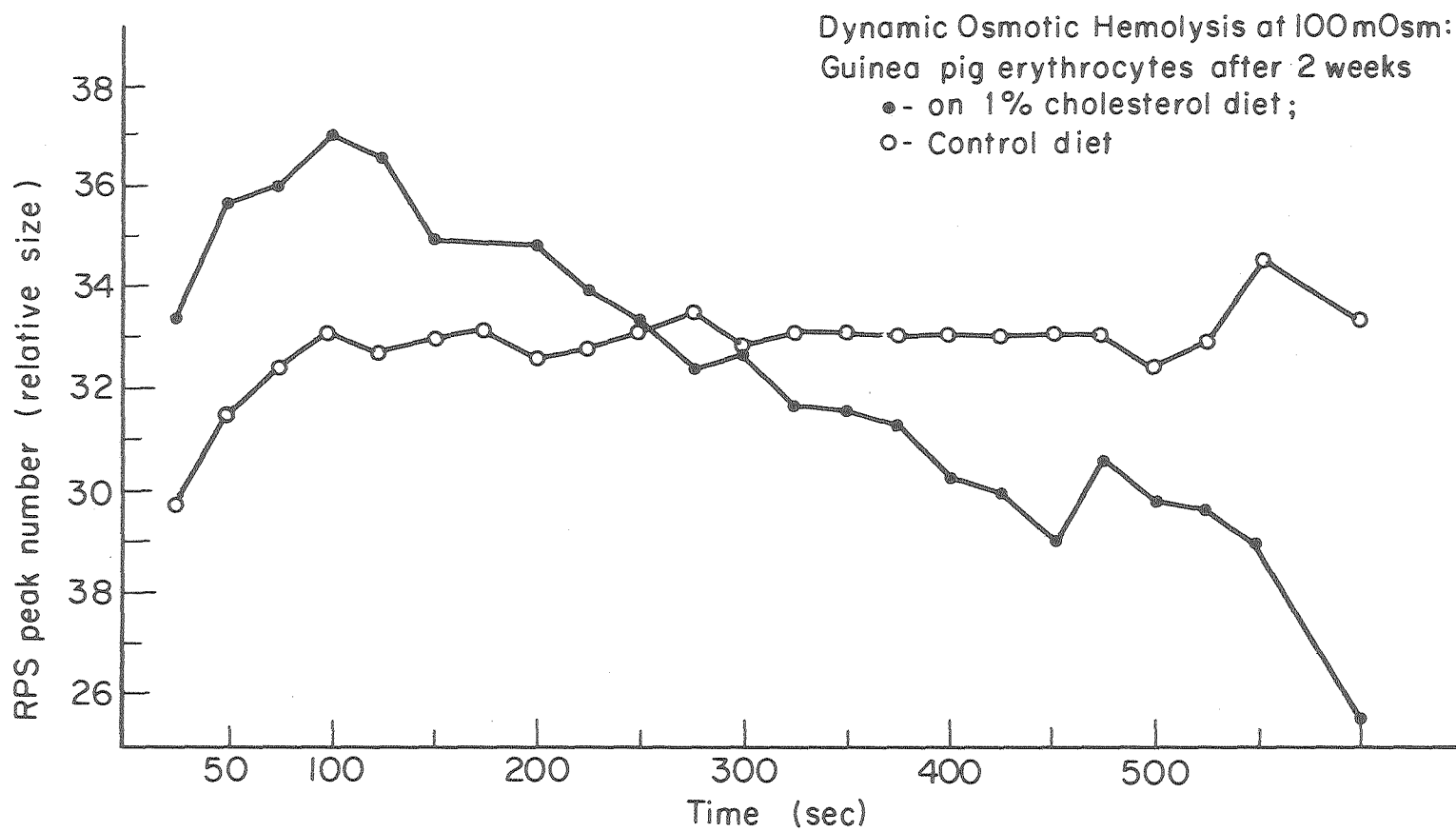
(Collab: Prof. R. Ostwald)

DBL 746-4798

Fig. 1

Fig. 2

XBL787-3316

Fig. 3

a) 156 mOsm, cholesterol

b) 156 mOsm, control

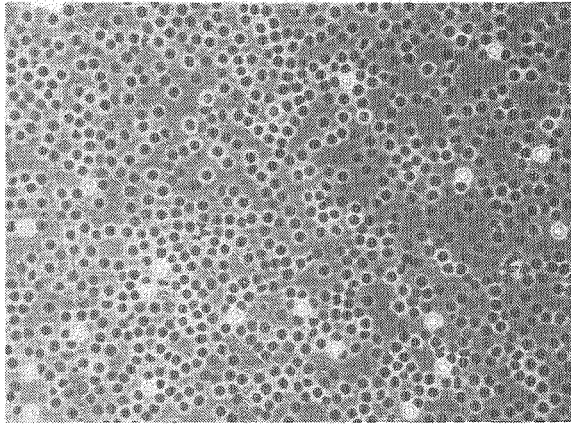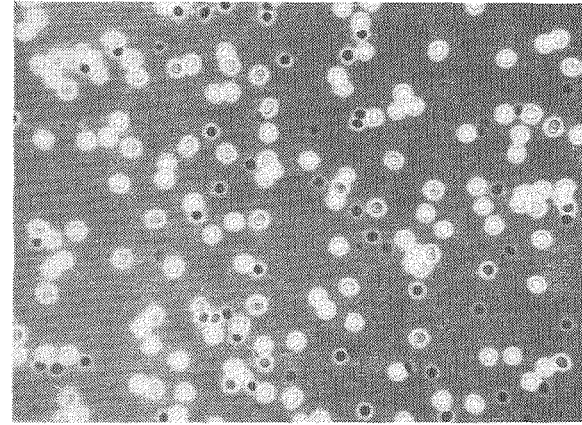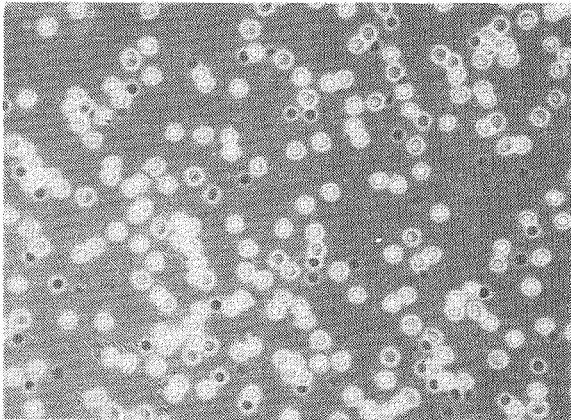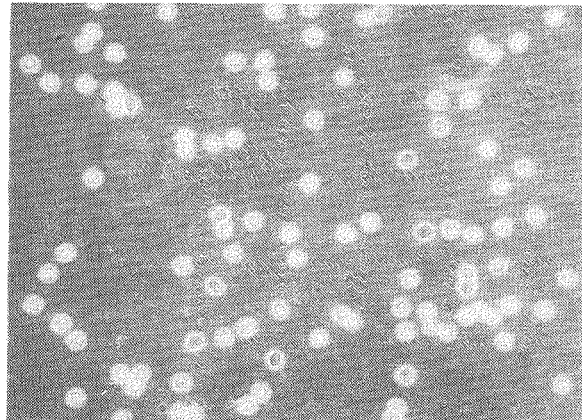c) 130 mOsm, cholesterol

d) 130 mOsm, control
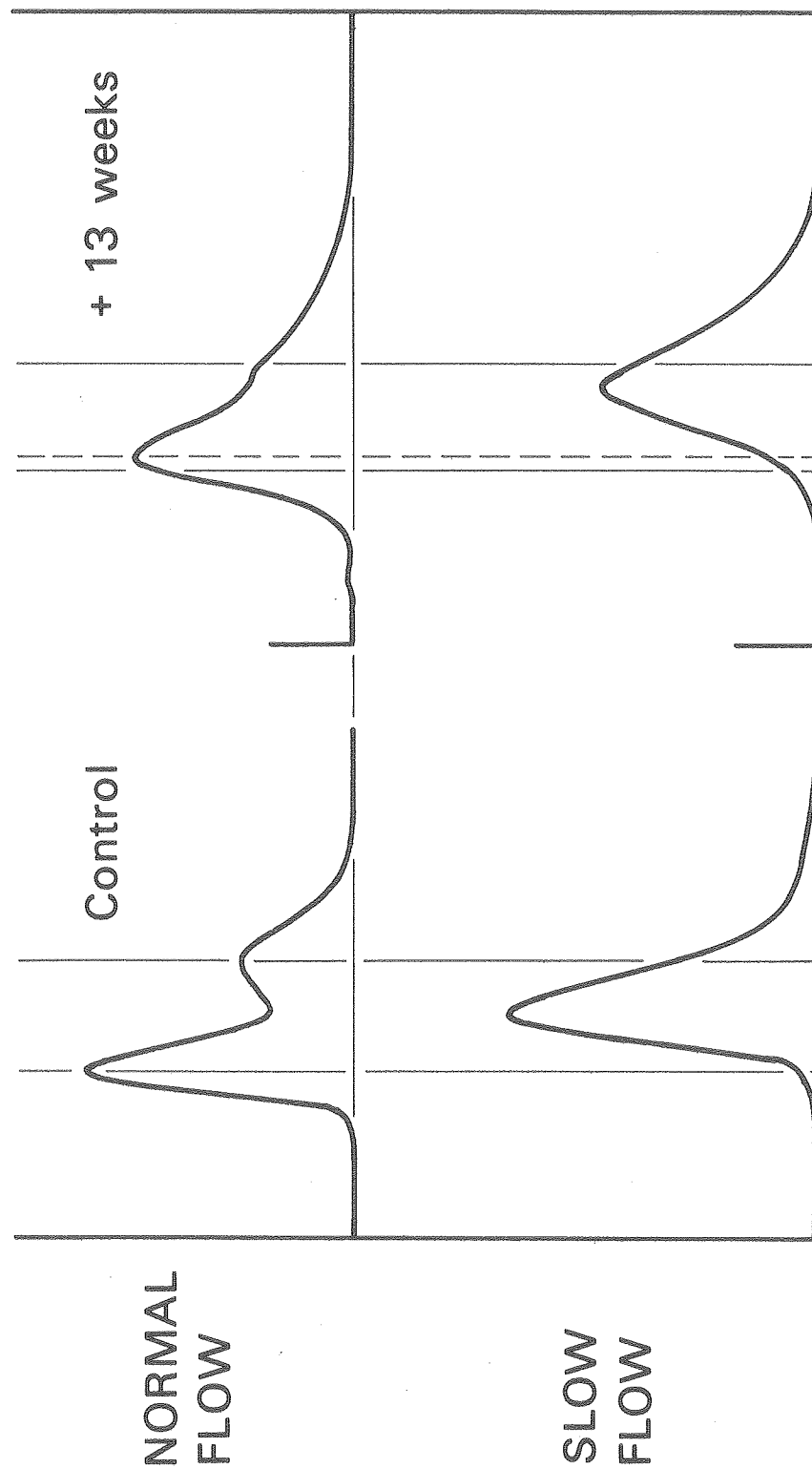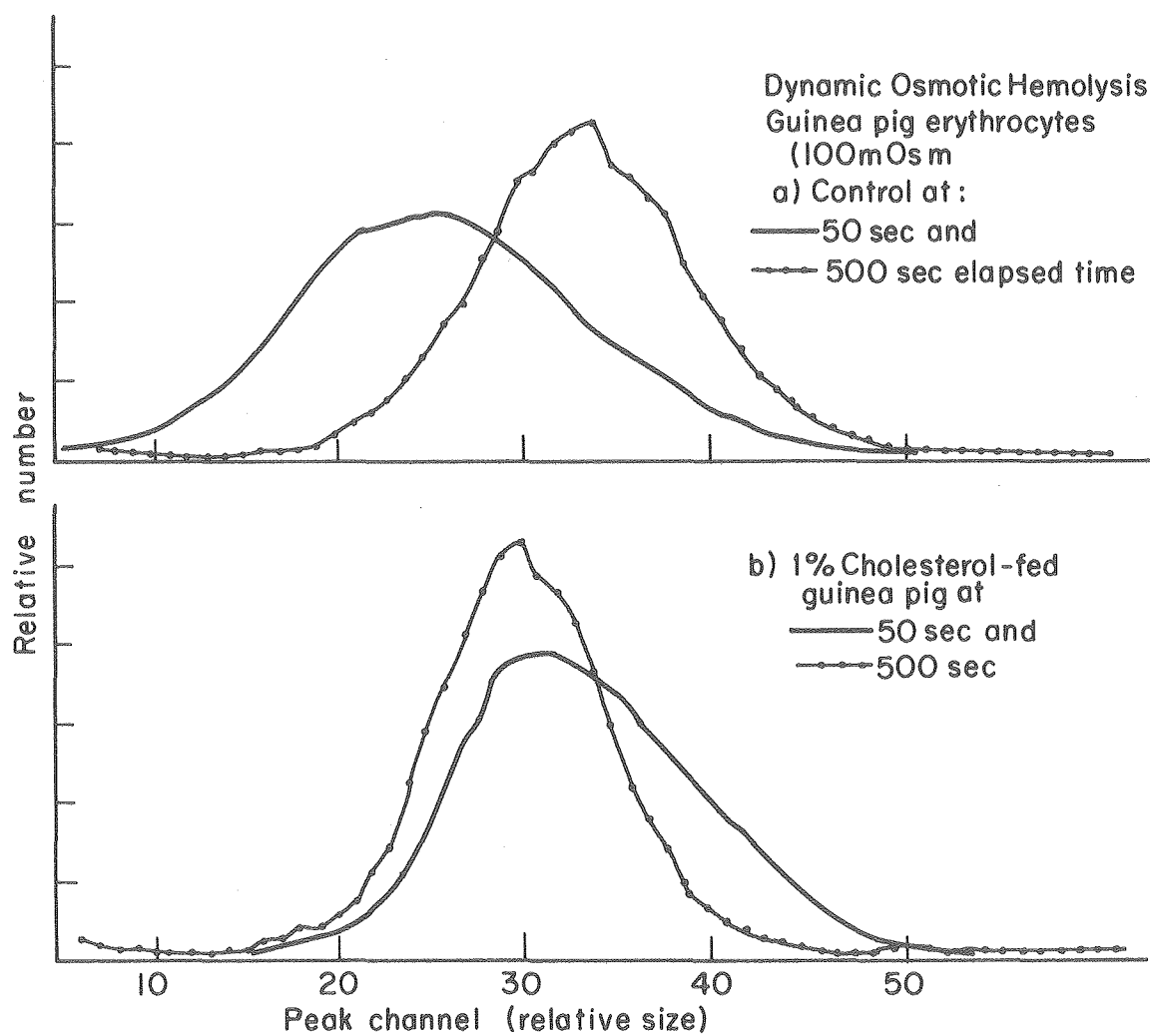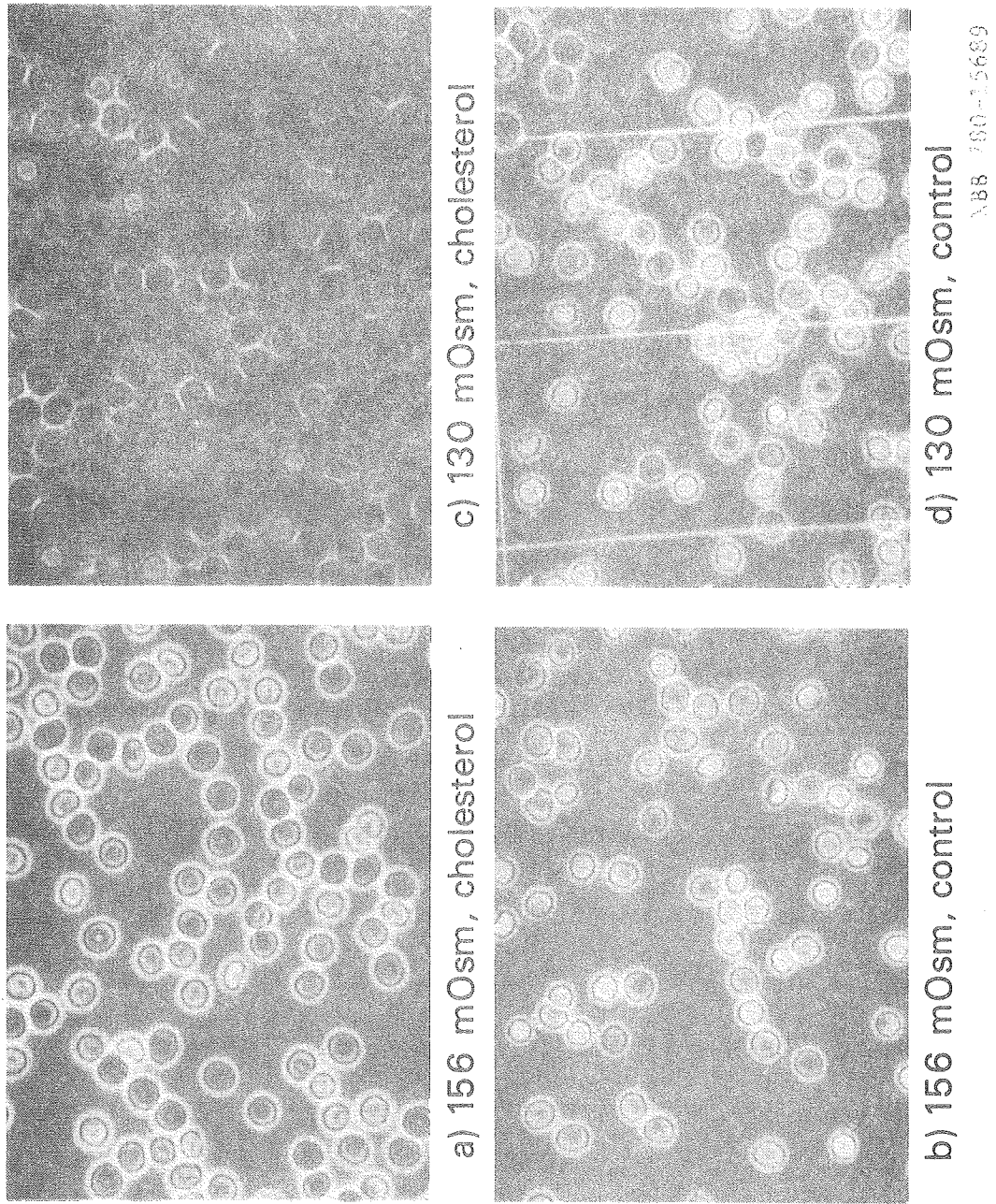
Fig. 4

a) Control

c) 1% Cholesterol, day 5

b) 1% Cholesterol, day 3

d) 1% Cholesterol, day 5
after separation

XBB 780-15690

Fig. 5

CHAPTER 7

OUTLINE: EXAMPLES OF RED CELL PATHOLOGIES

I.   INTRODUCTION

II. MIXTURE OF MATERNAL AND FETAL RED CELLS.

   A.   Fig. 1: RPS spectra of mixed blood at normal and slow flow
        rates.

III. PHENYLHYDRAZINE-INDUCED ANEMIA IN THE RAT.

   A.   Fig. 2: RPS spectra reflecting an erythropoietic response of
        immature large reticulocytes.

IV. IN VITRO AGING OF RED CELLS: CHANGES IN SPECTRAL BIMODALITY.

   A.   Fig. 3: Change in RPS volume plotted against RPS bimodality
        index for cells "aged" in vitro compared with fresh, hypo-
        tonically swollen red cells.

V.   HEREDITARY SPHEROCYTOSIS: RPS "DYNAMIC OSMOTIC HEMOLYSIS."

   A.   Fig. 4: Comparison of rate and percentage of lysis of
        (a) herditary spherocytes with (b) control, normal human
        red cells.

INTRODUCTION

In this final chapter, a few examples of previous and ongoing investigations of red cell-membrane pathologies are given in which the various modalities of resistive pulse spectroscopy described in the foregoing chapters were applied. These examples do not reflect the full range of applicability of the RPS method which has included "sizing" of lymphocytes, fibroblasts, platelets and polymorphonuclear leukocytes, in addition to erythrocytes from many different mamallian species. The cases here include (a) mixed adult and fetal red cells; (b) phenyl-hydrazine-induced anemia in the rat; (c) in vitro aging changes in red cell deformability, and (d) hereditary spherocytosis. These studies serve to exemplify many of the basic principles and pitfalls of electronic sizing that were elucidated in the other chapters of this dissertation. The methods are essentially the same as detailed in Chapters 1, 2, 3 and 4.

MIXTURES OF ADULT AND FETAL RED CELLS

The separation of maternal from fetal red cells is of practical importance in perinatal studies in which blood sampling of the placenta, amnionic fluid or cord may be contaminated by accidential mixing of fetal cells with maternal blood. The apparent volume distribution of a laboratory mixture of adult and fetal (cord) red cells is shown in Fig. 1. (These blood specimens were provided by Dr. Y. W. Kan, San Francisco General Hospital.)

Two major conclusions are derived: (a) spectral "bimodality" is not necessarily a manifestation of red cell deformability properties; in this case, as confirmed by the "slow flow" distribution, two real, overlapping, volume distributions corresponding to maternal and fetal cells exist; and (b) the resolution of actual volume distributions is improved at the "slow" flow rate. (The smaller of the two subpopulations corresponds to the adult cells, as established by RPS spectra of pure adult red cells.)

PHENYLHYDRAZINE-INDUCED ANEMIA IN THE RAT

Adult Sprague-Dawley rats were injected intramuscularly with a low dose of phenylhydrazine, and periodic blood samples were subsequently drawn. The RPS spectra for the samples are represented in Fig. 2. As was the case in the example of Fig. 1, the results for the phenylhydrazine treated rats again demonstrate that the RPS spectral distribution at a single, normal flow rate is inadequate to make any conclusions about cell volume or deformability. Here the RPS shoulder subpopulation (seen on day 4) is better resolved at the slow flow rate. By microscopic observation, this larger sized subpopulation seen with RPS, corresponds to unusually enlarged cells. These are premature reticulocytes released as part of the erythropoietic response to the phenylhydrazine induced anemia. It is also interesting that a partial loss of spectral bimodality is detectable almost immediately after administration of the phenylhydrazine (Fig. 2a).

IN VITRO AGING EFFECTS ON RPS BIMODALITY

Red cells were incubated at room temperature over a 24 hour period. At intervals of 8 hours, the cells were analyzed for RPS peak (modal) size and bimodality (index i_1). These results were plotted and compared with those from fresh red cells swollen with a series of hypotonic phosphate buffered saline solutions. The results (Fig. 3) clearly indicate that in vitro aged cells lose bimodality with a relatively small increase in volume. On the other hand, fresh cells may increase considerably in volume by osmotic swelling without losing so much bimodality.

It would be of interest to correlate these RPS observations with measurements of cellular calcium, ATP, and other biochemical parameters. The RPS "bimodality index" method of assessing deformability might be useful in studying the relative efficiency of different red cell preservation protocols.

HEREDITARY SPHEROCYTOSIS: RPS DYNAMIC OSMOTIC HEMOLYSIS

In this example, red cells were taken from a patient diagnosed by the usual clinical and laboratory criteria to have herditary spherocytosis. (The patient was a 36 year-old, white male with 4.22×10^9 red cells/cc, MCV = 87, MCH 31.9 and MCHC = 36.6, hematocrit = 37.1, and hemoglobin 13.5 g %.)

The cells were assessed by the RPS technique of measuring "dynamic osmotic hemolysis" as was described in Chapter 4. Here, cells were added to a 140 mosM, hypotonic PBS solution at t = 0 seconds. Representative spectra are displayed in Fig. 4.

The hereditary spherocytes show a marked increase in rate and percentage of hemolysis. This is reflected by the large number of pulses (corresponding to ghosts) in the lower (small channel size) subpopulation of pulses (Fig. 4a). In contrast, only a small fraction of normal cells lyse in the same time interval (Fig. 4b). Other details of maximal critical volume, rate of lesion repair, effects of in vitro storage, etc. may be obtained by more detailed analysis of similar RPS spectral series. RPS studies would probably be useful in following the effects of splenectomy in such a patient.

Fig. 1. Mixture of Adult and Fetal Red Blood Cells. RPS spectra at: (a) normal flow, and (b) slow flow. The smaller (lower channel) sized cells are adult cells, as determined by a pure sample study.

Fig. 2. Phenylhydrazine Induced Anemia and Erythropoietic Response in the Rat: RPS spectra at two time intervals after administering the drug.

Fig. 3. RPS Bimodality Index Plotted Against Peak (Channel) Size of (a) In Vitro Aged Cells, and (b) Fresh, Osmotically Swollen Cells.

Fig. 4. Hereditary Spherocytosis: Dynamic osmotic fragility by RPS at t = 10 and 90s of (a) hereditary spherocytes, and (b) normal control.

RPS: HUMAN MOTHER plus FETAL BLOOD - FIXED
(256 channel data)

NORMAL FLOW

SLOW FLOW

(Collab: Prof. Y. W. Kan)

DBL 746-4797

Fig. 1

RPS: PHENYLHYDRAZINE-TREATED RAT

NORMAL FLOW

SLOW FLOW

30 min

4 days

DBL 745-4791

Fig. 2

170

Fig. 3

XBL787-3318

(a) Hereditary spherocytosis   (b) Normal control

XBL787-3313

Fig. 4